POLITECNICO DI TORINO

Collegio di Ingegneria Chimica e dei Materiali

Corso di Laurea Magistrale
in Ingegneria Chimica e dei Processi Sostenibili

Tesi di Laurea Magistrale

Evaluation of pilot plant thermal profile effect on highly endothermic reactions

Relatore Accademico

Prof. Stefania Specchia

Relatori Industriali

PhD. Ing. Julien Gornay
PhD. Ing. Nicolas Aribert

Candidato

Gabriel Alejandro Ledezma Lopez

2018

Riassunto in Italiano

In questa tesi è studiato il problema di come profili termici che si formano lungo un reattore di un impianto pilota influenzano reazioni con elevato calore di reazione ed elevata energia di attivazione.

Per fare questo si ha:

- Programmato una simulazione del reattore per studiare la sensibilità de la conversione ai diversi parametri del sistema.
- Sviluppato un modello matematico per prevedere i valori della deviazione prodotta dai profili di temperatura.
- Verificato sperimentalmente le conclusioni de l'analisi di sensibilità in una impianta pilota.
- Confrontato la simulazione, il modello e i resultati esperimentali sono stati confrontati.
- Progettato strumento computazionale è stato avendo conto dei risultati del modello.

1. Il Problema

Un area di ingegneria chimica molto ampia e importante è IL controllo di processo. L'obiettivo del controllo di processo è garantire la qualità di un prodotto con la maggiore efficienza possibile. Tra i diversi parametri che devono essere controllati, uno dei più importanti è la temperatura di processo. La temperatura ha sempre una stretta correlazione con l'efficienza, la resa e la qualità dei prodotti chimici. Questo è il caso dei reattori chimici. Il controllo della temperatura deve essere effettuato rigorosamente in reattori chimici, con un grado di precisione che dipende dalla stabilità dei reattori e dalla sensibilità della reazione alla temperatura.

La sensibilità della reazione alla temperatura dipende dall'energia di attivazione e dalla costante di equilibrio. Se l'energia di attivazione è più elevata, la reazione diventa più sensibile, il che significa che con piccoli cambiamenti di temperatura, possono essere generati importanti cambiamenti sulla conversione, sulla distribuzione dei prodotti e sulla stabilità.

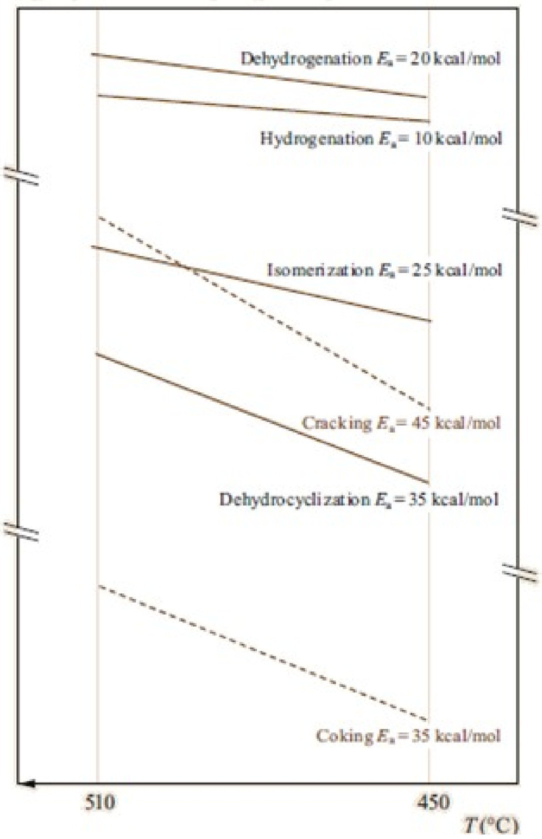

Figure 1.1. Relative Rate (V) of reaction versus the activation energy for different reactions (Hsu, 2017).

Man mano il calore di reazione è più elevato e la gamma dei vincoli di processo è più ristretta, la progettazione di un sistema di controllo diventa più difficile, poiché la sua efficienza può essere compromessa, dovuto al fatto che assorbe rilascia calore ad una velocità molto alta per compensare la quantità associata di energia alla stessa velocità

Per reattori tubolari imballati, una soluzione comune per facilitare il controllo della temperatura è quella di diluire il letto di catalizzatore con un solido inerte, con lo scopo di diminuire la velocità di reazione e quindi la velocità di assorbimento / rilascio del calore.

Di solito, i test cinetici vengono eseguiti in regime isotermico utilizzando reattori imballati. Quando queste reazioni sono molto esotermiche / endotermiche il controllo della temperatura può essere molto difficile ovvero non pratico.

Viene quindi presentata la presenza di profili termici nei test isotermici. Quando si effettuano test di questo tipo per reti di reazione che possono essere difficili da simulare o semplicemente sconosciute, può essere faticoso decidere quale sia un profilo accettabile. Questo al fine di catalogare il test come test isotermico.

La figura 1.2 mostra un test di reforming catalitico eseguito in reattori a letto impaccato con sofisticati sistemi di controllo della temperatura. Diversi test di reforming catalitico sono mostrati per diverse diluizioni del catalizzatore. Questa figura riflette diversi problemi associati a questo tipo di sistemi.

L'endotermicità della reazione è così elevata che la deviazione della temperatura impostata è compresa tra 5 e 20 ° C, producendo profili di temperatura molto notevoli.

La situazione migliora molto con la diluizione del catalizzatore. Tuttavia, determinare la diluzione adeguata rappresenta tempo, risorse umane e economiche per impostare il nuovo test nell'impianto pilota.

Nella direzione della conduzione degli esperimenti della divisione di sperimentazione di processo (R-15), questo è uno scenario di test comune.

Questa tesi cerca di rispondere alle seguenti domande:

- I profili sinusoidali della temperatura influiscono sulle prestazioni del test?

Figure 1.2. Experimental Thermal Profiles

- Quanto è permesso il massimo scostamento di temperatura per considerare il test ancora isotermico?
- In che modo i parametri operativi influenzano la deviazione risultante?
- Quali sono le possibili azioni da intraprendere per ridurre la deviazione?
- E 'possibile proporre un modello matematico per stimare la deviazione?

Per fare ciò, si è suddivisa come segue:

- Modellazione matematica e simulazione
- Verifica Esperimentale

Per facilitare lo studio del problema impostato, deve essere studiata una reazione chimica conveniente. Questa reazione deve essere:

1. Altamente endotermica.

2. Semplice e facile da seguire.

3. Una reazione ben nota. L'intenzione di questo lavoro non è quella di eseguire uno studio cinetico.

Le caratteristiche delle reazioni di reforming li hanno reso un perfetto esempio di valutazione per studiare l'effetto dei profili termici nella conversione dovuto al fatto di che l'elevata endotermicità che li caratterizza rende estremamente difficile il controllo della temperatura lungo i reattori. Data la complessità del test di reforming della nafta, si è deciso di puntare a una reazione aromatizzante chiave.

La reazione mirata per questo studio è la deidrogenazione del metilcicloesano, mostrato nella figura 1.3.

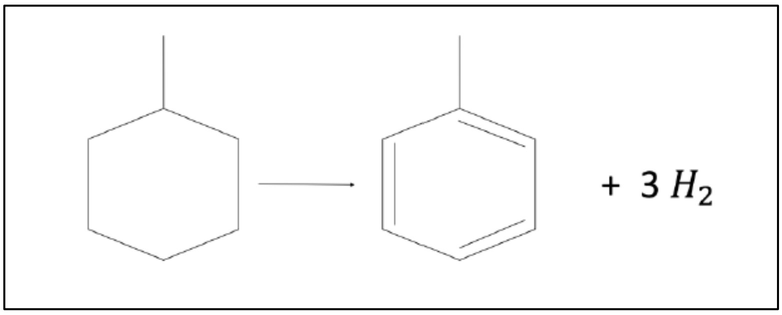

Figure 1.3. Deidrogenazione del metilcicloesano

Attraverso la deidrogenazione, il metilcicloesano è aromatizzato a toluene, producendo idrogeno come prodotto.

2. Valutazione dei fenomeni di trasporto

Per selezionare un tipo di modello per simulare il reattore di reforming sapendo quali sono le limitazioni di trasporto, è stata eseguita una valutazione di questi fenomeni.

Per la valutazione sono stati considerati la geometria del reattore pilota, le dimensioni del catalizzatore e le condizioni operative previste per il test sperimentale. La tabella 2.1 contiene i parametri più rilevanti. I dettagli sul catalizzatore rimangono confidenziali.

Tabella 2.1 Parametri più rilevanti per la valutazione del sistema

Parameter	unit	value
Reactor diameter (ID)	mm	4,75
Thermowell	mm	1,98
Reactor Length	mm	540
Reactor Length	mm	500
Catalyst	um	250-500
Inert material	um	210
Temperature	K	653
Pressure	Pa	1256
Volumetric Flow	$[m3/s\,]$	1,117E-06

La viscosità e la conduttività termica della miscela di gas (idrogeno, metilcicloesano e toluene) sono state calcolate attraverso il metodo Wilke (Fairbanks & Wilke, 1950) che rappresenta una semplificazione degli approcci rigorosi della teoria cinetica basati sulla legge di Chapman ed Enskog (Reid, Prausnitz , & Poling, 2001), testato per miscele di gas polare (Mathur, S., Saxena, 1966).

Le diverse diffusività binarie sono state calcolate seguendo il metodo Brokaw per miscele polari (Brokaw, 1969) basato sul potenziale Stockmayer. La diffusività molecolare del metilcicloesano in miscela è stata calcolata utilizzando l'equazione di Stefan-Maxwell (Reid et al., 2001). Per il calcolo della diffusione effettiva del metilcicloesano si è pensato di utilizzare sia la diffusione molecolare che quella di Knudsen secondo la formula di Caretto. (Caretto, 1963, Krishna & Wesselingh, 1997).

Il coefficiente di dispersione radiale di massa è stato calcolato utilizzando le correlazioni empiriche proposte da Delgado nel 2005 e 2007 in cui studiano la dispersione in mezzi porosi e la sua correlazione con i numeri di Smith e Reynolds (De Carvalho & Delgado, 2005; Delgado, 2007). Al valore ottenuto è stato applicatà una correzione per la variazione del numero di Peclet radiale. (Kulkarni e Doraiswamy, 1980).

Il regime fluidodinamico secondo questa correlazione sembra essere proprio nel limite tra il regime di diffusione pura e il regime di dispersione meccanica.

Il coefficiente di dispersione assiale di massa è stato calcolato utilizzando il modello proposto da Tsotsas & Schlünder nel 1988, nel quale l'effetto della dispersione assiale nei reattori a letto impaccato e lo correlano con diverse scale di flusso (Evangelos Tsotsas & Schlünder, 1988).

I fattori di trasferimento J-h e J-m, introdotti da Colburn (Colburn, 1933) e esteso al trasferimento di massa di McCune (McCune & Wilhelm, 1949), sono stati calcolati attraverso le correlazioni per letto impaccato sviluppate da Wakao et al. (Yagi, Kunii e Wakao, 1960) per il caso di trasporto di calore e Dwivedi (Dwlvedi e Upadhyay, 1977) per il trasporto di massa. Con questi fattori di trasferimento sono stati ottenuti i coefficienti di trasferimento e i numeri adimensionali.

Poiché il modello di calore 1D è adatto a questo caso, il coefficiente di trasporto di calore effettivo è stato calcolato utilizzando la correlazione sviluppata da Tsotsas et al. (E. Tsotsas & Schlünder, 1990).

Il profilo di porosità radiale è stato calcolato tenendo conto della presenza del pozzetto termometrico, a causa del fatto che occupa una sezione importante della zona del reattore interno utilizzando la correlazione sviluppata da Mueller et al. è stata usata (Mueller, 1999). Per la perdita di carico è stata utilizzata l'equazione di Ergun classica (Ergun e Orning, 1949).

Per valori maggiori del numero di Reynolds in questo sistema, il numero di Peclet praticamente non cambia fino alla dispersione meccanica pura. È ovviamente desiderabile fissare le condizioni di prova per avere la minore dispersione possibile nel sistema per semplificare il modello.

Il valore del Peclet radiale di massa è circa 2 e quello assiale è circa 11 (entrambi per la particella), che indica un flusso quasi completamente sviluppato e una dispersione assiale e radiale praticamente irrilevante (Aris & Amundson, 1957; James J Carberry, 1958; McHenry & Wilhelm, 1957).

Il criterio di dispersione assiale è soddisfatto poiché il valore calcolato per il sistema è molto superiore al valore minimo. La dispersione assiale può essere trascurata (Mears, 1971b). (Vedere la Tabella 2.2)

Dovuto a che non c'è alcuna evidenza di limiti di trasporto di alcun tipo, è stato selezionato il modello flusso pistone per simulare il reattore ed eseguire lo studio.

3. Studio dell'effetto dei profili termici sulla conversione

La deviazione causata al sistema dai profili termici è stata quantificata in termini di conversione. La conversione che sarebbe stata ottenuta in un test isotermo ideale è stata confrontata con la conversione ottenuta nel caso dell'esistenza dei profili termici.

In base al numero di gusci di riscaldamento, il sistema di controllo può essere programmato per controllare la temperatura utilizzando i sensori in uno o più gusci particolari.

Sui documenti di ricerca interni, sono riportati rapporti in cui viene sottolineata la presenza di profili termici molto sottili nelle prove con reattori vuoti con un limite massimo di 2 ° C di deviazione che suggeriscono chiaramente che la prominenza del profilo termico è influenzata anche dall'elemento del sistema di controllo e probabilmente dalla composizione non omogenea dei materiali dei gusci.

In base al numero di gusci di riscaldamento, il sistema di controllo può essere programmato per controllare la temperatura utilizzando i sensori in uno o più gusci particolari.

Se si osserva il punto in cui il profilo termico attraversa la temperatura operativa impostata, si può vedere che in quel stesso punto si trova un sensore di temperatura. Tenendo presente questa osservazione, il comportamento di questi profili può essere descritto come segue:

- All'ingresso del letto, la temperatura all'interno cade in modo significativo, a causa della quale il sistema di controllo aumenta la potenza di riscaldamento.
- La potenza verrà aumentata fino a quando la temperatura del sensore coincide con la temperatura operativa impostata.
- Come risultato dell'incremento di potenza, la temperatura nel guscio successivo è chiaramente molto superiore alla temperatura operativa impostata e il sistema di controllo agisce abbassando la potenza fino a quando la temperatura nel punto in cui è posizionato il sensore corrisponde al valore di temperatura preimpostato.

Quindi, i profili hanno un comportamento sinusoidale con lunghezza d'onda costante (distanza tra i sensori) e ampiezza decrescente.

Avendo abbastanza informazione qualitativa, è stato deciso di imporre il profilo termico assiale nella simulazione, il modello matematico e gli sperimenti invece di prevederlo.

Le caratteristiche desiderabili in funzione matematica per simulare la forma di questi profili in modo realistico e vantaggioso sono:

- Comportamento ondulatorio
- La forma dell'onda facilmente e tecnicamente deformabile.
- Area normalizzata

Le funzioni matematiche che hanno già due di queste tre caratteristiche sono le distribuzioni statistiche. La sezione inferiore dell'onda può essere ottenuta moltiplicando per un operatore negativo la funzione.

$$f(x) = \frac{\Gamma(\alpha+\beta)}{\Gamma(\alpha)+\Gamma(\beta)} x^{\alpha-1}(1-x)^{\beta-1} \qquad \alpha \geq 0 \qquad \beta \geq 0 \tag{3.2}$$

Dopo di considerare diverse distribuzioni statistiche, quella scelta è la distribuzione beta. La distribuzione beta viene applicata per modellare il comportamento di variabili casuali limitate ad intervalli di lunghezza finita. Cambiando α e β è possibile modificare in modo estremamente semplice la forma.

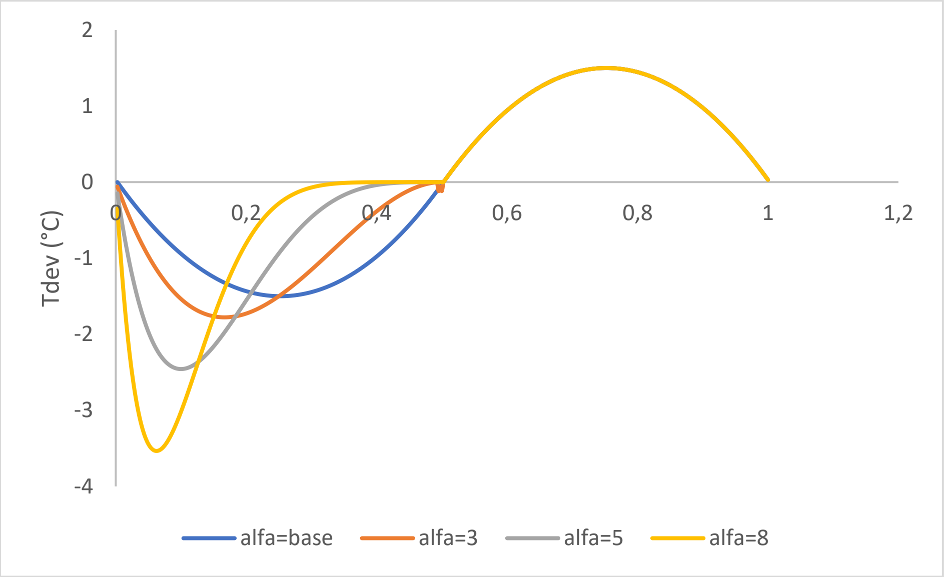

Figure 2.19. Diversi profili termici modellati utilizzando la distribuzione beta

Per far corrispondere ogni punto del profilo simulato ad una posizione lungo il reattore, la lunghezza del reattore è stata normalizzata.

La deviazione nella conversione è influenzata da due variabili intrinseche ai profili termici. Il valore di deviazione della temperatura e l'estensione del reattore lungo la quale quella temperatura persiste. Di solito, questo viene affrontato dal punto di vista del calcolo integrale. Tuttavia, sul campo, non esiste ancora la possibilità di misurare continuamente tutto il profilo di temperatura.

L'effetto di un overshoot è esponenzialmente più grande dell'effetto di undershoot dovuto alla relazione tra la temperatura e la velocità di reazione.

Nella figura, viene mostrato un grafico 3D che mostra come la deviazione varia in base alle diverse zone di overshoot e undershoot per un insieme di condizioni. Una pendenza più pronunciata è il prodotto dell'intersezione tra la superficie e un piano generico con una direzione perpendicolare all'asse Aov. Inoltre, quando Aun diminuisce, la pendenza aumenta, il che dimostra che in quelle condizioni la deviazione aumenta più rapidamente con il cambio di Aov.

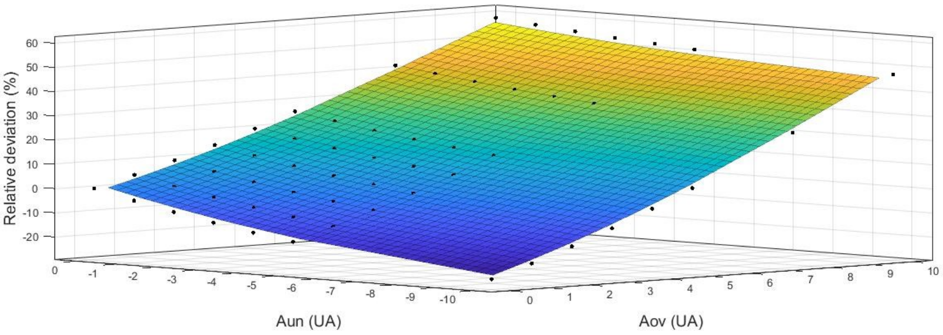

Figure 2.21 Effecto dell'overshoot e l'undershoot sulla deviazione relativa

Ciò indica chiaramente che non esiste un rapporto tra i due per avere una deviazione uguale a zero o qualsiasi altro valore di deviazione fissa.

La figura 2.22 mostra una vista laterale della superficie generata, che presenta un grado di contorsione corrispondente chiaramente alla variazione della velocità di reazione quando il termine di Arrhenius aumenta; nel caso della Fig. 2.22, a causa dell'incremento nell'energia di attivazione.

Un'analisi di sensibilità normalizzata è stata fatta per studiare la deviazione (d'ora in poi, il nome deviazione sarà usato esclusivamente per parlare della deviazione relativa della conversione causata dai profili rispetto alla conversione isotermica) causata da diversi livelli di undershoot in quanto l'overshoot varia per un valore di conversione isotermica fisso di X= 0,5.

Una deviazione negativa significa che il profilo termico provoca una conversione sotto la conversione isotermica e una positiva che la conversione causata dal profilo è al di sopra della conversione isotermica.

La presenza di profili termici può influire notevolmente sulla conversione all'uscita del reattore quando la reazione ha un'elevata energia di attivazione. Per questo motivo, occorre fare attenzione a questo fattore quando anche il calore di reazione è elevato.La sensibilità della deviazione relativa aumenta principalmente con la temperatura operativa, la pressione e l'energia di attivazione. Nel frattempo, la velocità spaziale e il rapporto

H / HC giocano un ruolo secondario in quanto la deviazione è meno sensibile a questi parametri, il che non significa che non sia influenzato da loro.

Tutte le variabili operative studiate influenzano la deviazione, principalmente la temperatura e la pressione.

L'effetto della pressione è importante perché la reazione viene eseguita in fase gas, quindi la pressione è legata alla concentrazione.

L'energia di attivazione, come è stato sempre affermato, definisce il livello di sensibilità della velocità di reazione alla temperatura, che influisce direttamente sulla deviazione associata ai profili di temperatura.

La valutazione della sensibilità lungo l'intera gamma di conversioni consente di vedere anche le sue implicazioni sulla deviazione.

La conversione è legata alle variabili studiate come è già noto in letteratura. Proprio per chiarire, poiché l'energia di attivazione, la pressione, il rapporto H / HC o il tempo spaziale aumentano, anche la conversione lo fa. Se la temperatura aumenta, anche la conversione lo fa.

Sono state fatte numerose simulazioni facendo variare due parametri più la deviazione relativa all'estesa volta.

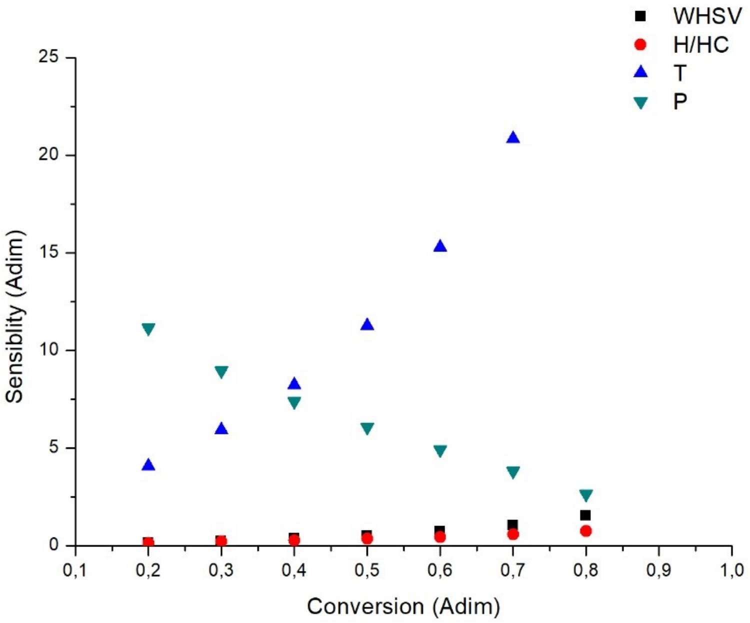

Figure 6 Sensibilità della deviazione ai diversi parametri testati

4. Modello matematico

Il modello matematico è stato sviluppato sulla base del concetto di area. L'utilizzo delle aree come input consentirà di effettuare una stima rapida sul campo.

$$\delta = a + b * \alpha + c * \beta + Ln\left(\frac{\frac{H}{HC}^{D} * whsv^{e} * P^{f} * Ea^{g}}{RT}\right) \tag{2.59}$$

Dove:

δ Deviazione relativa [%]

α Area totale dell’undershoot

β Area totale dell’overshoot

Table 3.1: Statistical parameters

Utilizzando il modello è facile generare grafici che indicano le zone operative consigliate, basate su tutti i diversi parametri.

Le peggiori condizioni per operare sono:

- Pressioni elevate: X / X_{equi} inferiore a 0,8.
- Bassa temperatura: X / X_{equi} inferiore a 0,8.
- Aov / Aun> 0,9
- Aov / Aun <0,1
- Coperture basse (X <0,4).

- La proporzione raccomandata di Aov / Aun è 0,5.

La figura 2.29 illustra le zone operative a fine di ottenere una deviazione entro un certo limite. Questo grafico è estremamente utile, poiché consente di stimare la forma che il profilo termico deve avere per ottenere una certa deviazione.

Queste curve offronno tre vantaggi:

- Stimare quantitativamente se il profilo termico del test genererà una deviazione entro la tolleranza accettabile.
- Progettare l'esperimento in un modo più accurato.
- Salvare le risorse necessarie che sarebbero necessarie per ripetere il test fino a ottenere una condizione qualitativa accettabile.

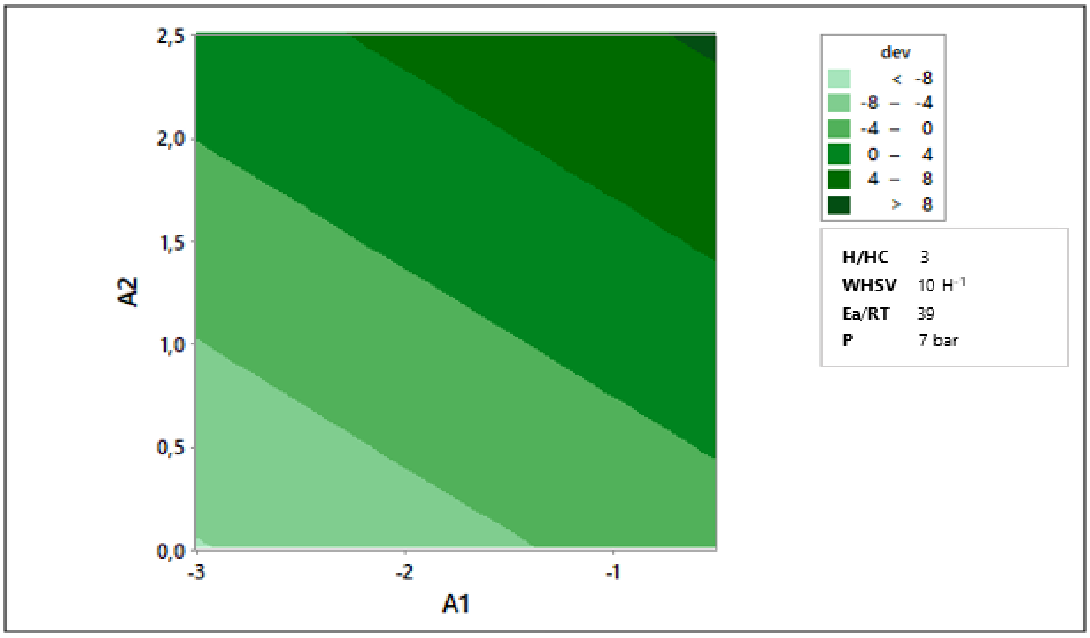

Figure2.30. Curva di contorno per identificare la zona favorevole per il test dev@(Aov,Aun).

5. Prove sperimentali

Per verificare le precedenti analisi sulla sensibilità del sistema, sono stati condotti diversi test in un'unità di impianto pilota. Allo stesso tempo, sono stati testati la veracità e l'utilità del modello.

Per il test è stato utilizzato un piccolo impianto pilota preparato meccanicamente e attrezzato per le reazioni in fase gassosa. Questa unità è stata rinnovata nell'ambito di questo lavoro per svolgere le reazioni di riforma.

Nella prima sezione, il liquido caricato viene alimentato in un recipiente di acciaio inossidabile a tenuta, da dove viene pompato al sistema di reazione tramite pompa HPLC. L'alimentazione dell'idrogeno proviene dalla rete di utilities della sala.

La sezione di reazione è composta da un reattore tubolare coperto da un sistema di riscaldamento conformato da otto anelli indipendenti e smontabili disposti lungo la lunghezza del reattore. Questi anelli coprono 80% della superficie esterna del reattore. L'intero sistema di reazione è isolato attraverso una scatola isolante. La potenza di riscaldamento esercitata dagli anelli viene controllata attraverso un sistema di controllo SCADA e monitorata a distanza.

Il reattore è attraversato longitudinalmente da un piccolo pozzetto termometrico. La gassificazione della miscela di reazione viene effettuata nella sezione iniziale del reattore, dopodiché la miscela reattiva entra nella sezione catalitica dove si verificano le reazioni.

La miscela di gas all'uscita del reattore, va attraverso una linea isolata riscaldata direttamente al gascromatografo, il quale è dotato di un rivelatore FID. Dopo l'analisi, la miscela di gas entra in un separatore di gas liquido dove vengono rimossi i non condensabili e la frazione condensabile può essere recuperata per fare il bilancio di massa. Il sistema conta su diversi livelli di sicurezza ed è totalmente automatizzato. L'intero processo e le variabili di sistema possono essere monitorati e modificati a distanza dalla sala di controllo. L'unità funziona 24 ore su 24 con operatori di sicurezza notturni.

La pressione nell'unità è regolata mediante una valvola di regolazione di contropressione mesa prima della sezione di analisi del gas.

Per una reazione altamente endotermica, la velocità di energia consumata può essere superiore alla velocità di energia fornita dal sistema di riscaldamento. Inoltre, esiste il caso in cui il sistema di riscaldamento eroga un'enorme quantità di energia in un particolare punto nel reattore causando il surriscaldamento del reattore a valle.

Sono stati eseguiti diversi test termici per analizzare:

- Il tempo di stabilizzazione della temperatura lungo il reattore.
- La precisione con la quale il reattore adotta la temperatura imposta dal sistema di controllo senza reazione.
- Come si comporta il sistema quando una perturbazione è causata per una reazione endotermica (limiti fisici).
- La stabilità della temperatura lungo il reattore.

Essere totalmente consapevole di come la sezione di reazione interagisce con il sistema di controllo ha un'importanza fondamentale poiché si intende imporre il profilo termico all'interno del reattore. Con questi risultati verrà definita la strategia di controllo da adottare durante il test.

Come è stato menzionato nella formulazione del problema, a causa dell'elevato calore di reazione è molto difficile controllare la temperatura lungo il reattore. Infine, è stato testato il sistema di controllo e le considerazioni sul comportamento termico del sistema meccanico. Vengono imposti quattro tipi di forme di profilo generale.

Nella figura 3.9 si ottiene il profilo più vicino alle condizioni isotermiche raggiunte per un test a 380 ° C. La deviazione di temperatura massima lungo il profilo non supera +/- 2 ° C. La conversione sperimentale ottenuta quando questo profilo termico è stato imposto è considerata come la conversione isotermica sperimentale per il gruppo di condizioni operative impiegato. La stessa metodologia viene applicata tutti i set.

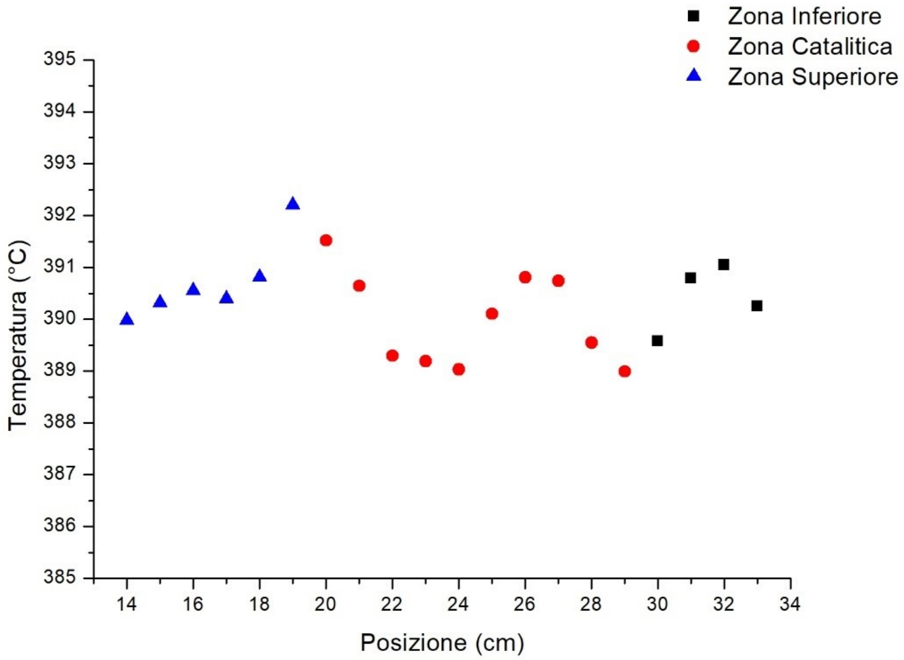

Figure 3.9. Profilo termico per 390 °C come temperatura di operazione. Numero di identificazione #141253

Nella figura 3.9 è anche possibile distinguere tra la temperatura nella zona catalitica (riscaldata dall'anello 3 e dall'anello 4) e la temperatura nella zona superiore e inferiore.

Il secondo tipo di geometria del profilo è mostrato nella figura 3.10. In questo caso, viene studiato solo l'effetto del undershoot, ottenendo diversi valori sperimentali

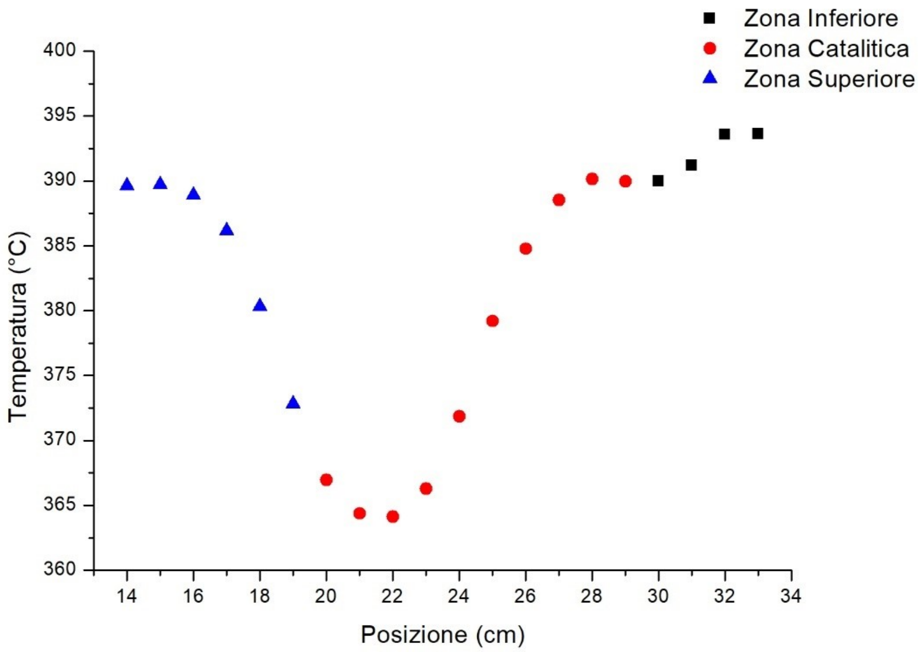

Figure 3.10. Profilo termico per 390 °C come temperatura di operazione. Numero di identificazion#151033

Il terzo tipo è fatto per testare l'effetto sulla deviazione del overshoot e del undershoot contemporaneamente come mostrato in figura 3.11 .

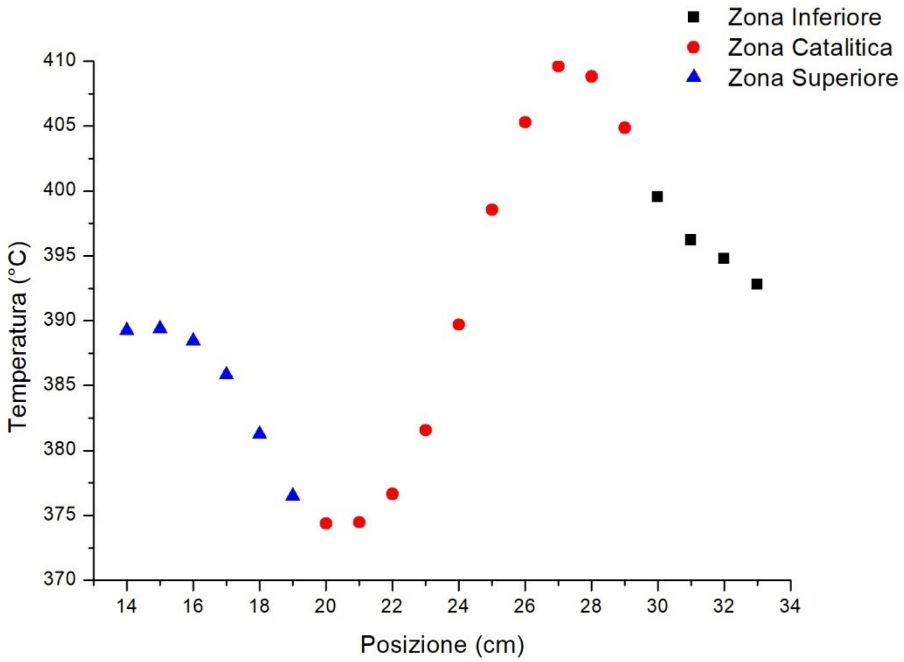

Figure 3.11. Profilo termico per 390 °C come temperatura di operazione. Numero di identificazion#151552.

L'ultimo tipo viene eseguito per verificare che il modello possa prevedere la deviazione causata da profili irregolari con diversi picchi.

Nella tabella 3.5, vengono raccolti risultati chiave. Diverse conclusioni possono essere indicate al guardare questa tabella. (Il termine errore relativo viene utilizzato per parlare dell'errore nella previsione del valore sperimentale).

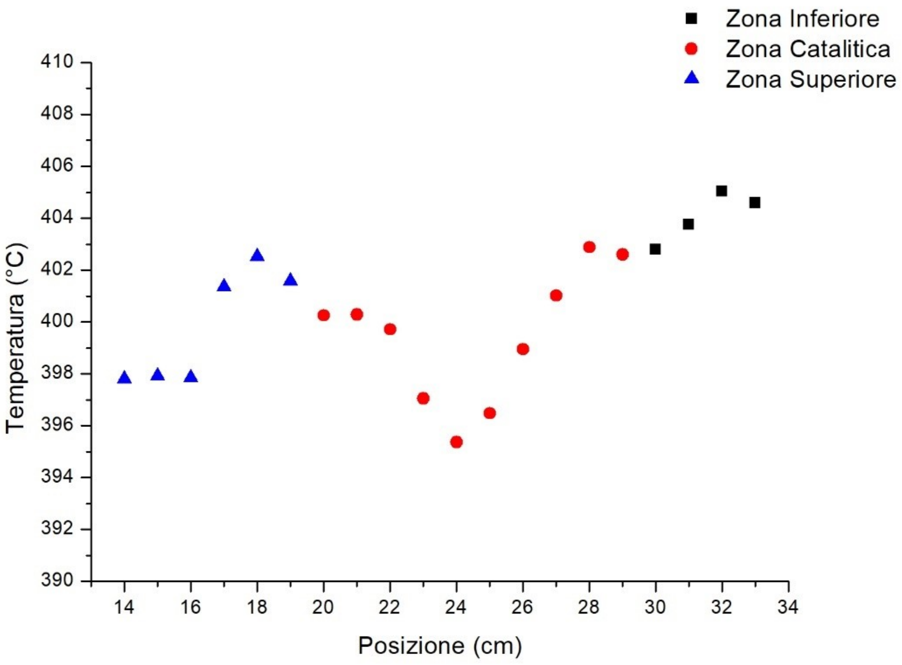

Figure 3.12. Profilo termico per 400 °C come temperatura di operazione. Numero di identificazion #210930

Tabella 3.5: Comparazione tra la simulazione, il modello e i risultati esperimentali.

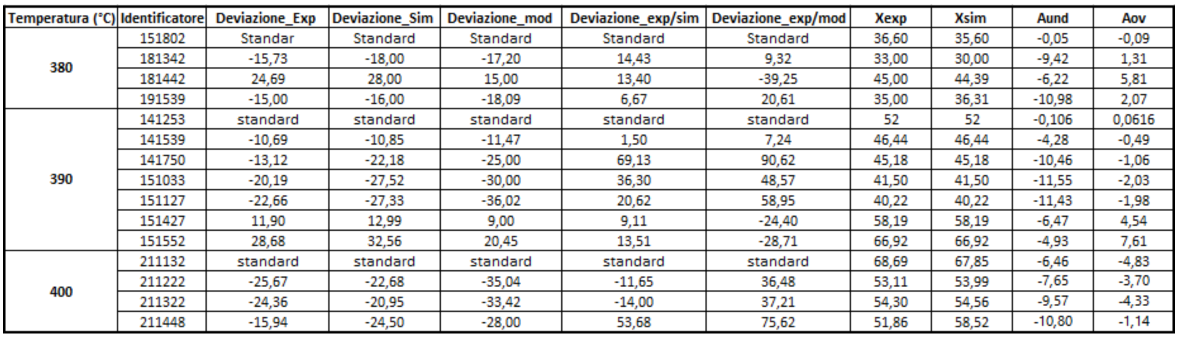

Temperatura (°C)	Identificatore	Deviazione_Exp	Deviazione_Sim	Deviazione_mod	Deviazione_exp/sim	Deviazione_exp/mod	Xexp	Xsim	Aund	Aov
380	151802	Standar	Standard	Standard	Standard	Standard	36,60	35,60	-0,05	-0,09
	181342	-15,73	-18,00	-17,20	14,43	9,32	33,00	30,00	-9,42	1,31
	181442	24,69	28,00	15,00	13,40	-39,25	45,00	44,39	-6,22	5,81
	191539	-15,00	-16,00	-18,09	6,67	20,61	35,00	36,31	-10,98	2,07
390	141253	standard	standard	standard	standard	standard	52	52	-0,106	0,0616
	141539	-10,69	-10,85	-11,47	1,50	7,24	46,44	46,44	-4,28	-0,49
	141750	-13,12	-22,18	-25,00	69,13	90,62	45,18	45,18	-10,46	-1,06
	151033	-20,19	-27,52	-30,00	36,30	48,57	41,50	41,50	-11,55	-2,03
	151127	-22,66	-27,33	-36,02	20,62	58,95	40,22	40,22	-11,43	-1,98
	151427	11,90	12,99	9,00	9,11	-24,40	58,19	58,19	-6,47	4,54
	151552	28,68	32,56	20,45	13,51	-28,71	66,92	66,92	-4,93	7,61
400	211132	standard	standard	standard	standard	standard	68,69	67,85	-6,46	-4,83
	211222	-25,67	-22,68	-35,04	-11,65	36,48	53,11	53,99	-7,65	-3,70
	211322	-24,36	-20,95	-33,42	-14,00	37,21	54,30	54,56	-9,57	-4,33
	211448	-15,94	-24,50	-28,00	53,68	75,62	51,86	58,52	-10,80	-1,14

6. Sviluppo di uno strumento computazionale di calcolo

L'obiettivo di sviluppare un modello del tipo prodotto era quello di consentire agli ingegneri e ai tecnici di eseguire rapide stime quantitative per progettare un test catalitico o per verificare se il test poteva essere considerato come isotermico.

Per rendere questo compito più semplice, lo strumento di calcolo è stato sviluppato utilizzando un compilatore commerciale per programmare il modello e una HMI per ottenere facile e velocemente i risultati desiderati. Lo strumento è stato chiamato Thermal Oriented Reaction Simulator -TORS V 1.0

4. Conclusioni

Per la verifica dell'analisi di sensibilità

- La presenza di profili termici può influire sulla conversione all'uscita del reattore quando la reazione ha un'elevata energia di attivazione. Per questo motivo, occorre prestare attenzione a questo fattore quando anche il calore di reazione è elevato.
- L'effetto di un overshoot è esponenzialmente più grande dell'effetto di undershoot dovuto alla relazione tra la temperatura e la velocità di reazione. Questo indica chiaramente che non esiste un rapporto di correzione tra i due per avere una deviazione uguale a zero o qualsiasi altro valore di deviazione fissa.

- La presenza di un undershoot profondamente marcato può mettere in atto l'effetto dell'equilibrio, provocando gravi deviazioni, motivo per cui è consigliabile considerare il tipo di equilibrio di reazione.

- Tutte le variabili studiate influenzano la deviazione, principalmente la temperatura e la pressione.

- Una deviazione relativa più grande sarà ottenuta alla conversione più bassa. È possibile attribuirlo a due ragioni:

  Numerica: dato che il valore di conversione isotermico è inferiore, piccole variazioni sul valore target causano errori relativi importanti.
  Deviazione assoluta: la deviazione assoluta è maggiore alle conversioni basse ed alte, generando un minimo per le conversioni medie. Una deviazione assoluta elevata ad alta conversione è dovuta all'effetto di equilibrio.

- Per diversi livelli di energia di attivazione “PV”, al crescere di questa variabile, aumenta sempre la deviazione (per tutte le variabili considerate). Invece di quando la temperatura e la pressione sono considerate come “PV”, poiché entrambe aumentano, la deviazione diminuisce.

- L'esistenza di overshoot nel profilo deve essere considerata molto più attentamente rispetto all'esistenza di undershoot nella temperatura. L'effetto di overshoot sulla deviazione è maggiore in grandezza rispetto all'effetto di undershoot.

- Il rapporto di compensazione Aov /Aun sarà sempre compreso tra 0 e 1. Inoltre, in genere, questo valore sarà compreso tra 0,4 e 0,8.

- All'aumentare dell'energia di attivazione (PV), l'area di overshoot per portare la deviazione a zero aumenterà sempre. Lo stesso scenario è stato fondato per il rapporto H / HC.

- Se si studia un sistema con Aov fisso e anche con una deviazione negativa, al crescere della temperatura operativa, la deviazione negativa diminuisce avvicinandosi allo zero. Ma, se si desidera aumentare Aov fino a raggiungere una deviazione zero, all'aumentare della temperatura, l'Aov richiesto per la compensazione sarà più alto. Una volta raggiunta la deviazione zero, con l'aumento di Aov, la deviazione aumenterà più rapidamente quando la temperatura operativa sarà maggiore.

- Per la pressione fissata come, PV, poiché il livello di pressione è più alto, la frazione richiesta per la compensazione sarà inferiore. Questa situazione ha un limite evidente, l'equilibrio. All'aumentare della pressione, il sistema ha conversioni più vicine all'equilibrio. In questo scenario, un overshoot può spingere oltre il limite di equilibrio causando una deviazione positiva.

- Il WABT non rappresenta necessariamente una buona approssimazione alla temperatura isotermica del test. Potrebbe essere utile in termini di diluizione del catalizzatore ma non per quantificare l'impatto del profilo di temperatura sulla conversione di reazioni chimiche con elevato calore di reazione. Il motivo è che la formula WABT non considera la deviazione in base all'ampiezza della del profilo di temperatura, ma solo in termini di massa del catalizzatore in una sezione.

Le peggiori condizioni per operare sono:

- a-) Pressioni elevate: X / Xequi inferiore a 0,8.
- b-) Bassa temperatura: X / Xequi inferiore a 0,8.
- c-) Aov / Aund > 0.9

d-) Aov / Aund < 0,1
e-) Conversioni basse (X <0,4).
f-) La proporzione raccomandata di Aov / Aund è 0,5.

Per la verifica dell'analisi di sensibilità effettuato nella prima parte di questo lavoro.

- All'aumentare della temperatura del test, la deviazione relativa diminuisce.
- All'aumentare della temperatura del test, aumenta la temperatura richiesta per compensare l'effetto di undershoot.
- Poiché l'effetto del undershoot inizia a essere trascurabile rispetto all'effetto di overshoot, la deviazione relativa inizia a crescere più velocemente in senso positivo.
- Un rapporto Aov / Even superiore a 0.9 deve essere evitato.
- All'aumentare della pressione, la deviazione relativa diminuisce.

Confronto tra la deviazione prevista dal modello e la simulazione con i risultati sperimentali.

- I risultati della simulazione sono accurati in termini di conversione, che è inferiore al 5% di errore relativo.
- La deviazione prevista dalla simulazione ha un errore relativo di circa il 15% in media.
- La deviazione prevista dal modello ha un 5% di errore relativo in media per aree inferiori a 3 UA.
- Per valori elevati di Even (meno di -10) il modello sopra stima l'impatto del undershoot.
- Per valori elevati di Aov (inferiore a 10) il modello sottostima l'impatto del overshoot
- Il modello funziona bene anche per profili non simmetrici

Per lavori futuri

- Dovrebbe essere fatto un modello per tenere conto della diluizione nel letto catalitico.

- Simulazioni e prove sperimentale dovrebbero essere fatti per capire quante sono le misure minime che devono essere fatte per avere una migliore approssimazione della temperatura media lungo un letto catalitico.

- Un modello sotto le stesse considerazioni può essere fatto per cariche e reazioni più complesse.

- Dovrebbero essere eseguiti più esperimenti per comprendere il comportamento della deviazione a conversioni alte e basse.

Table of contents

List of Figures

List of Tables

List of Symbols

Symbol	Definition	Units
a_v	Specific external surface area of one pellet	[m^2/m^3]
$Aun=A1$	Undershoot Area	UA
$Aov=A2$	Overdershoot Area	UA
b	Volume of inert material as fraction of total solids	[m^3-inert / m^3-total]
Bi_w	Biot number at the reactor wall	Adim
Bo	Bodenstein number for axial mass transport:	Adim
$c_{p,G}$	Heat capacity gas	[J/mol K]
$c_{p,L}$	Heat capacity liquid	[J/kg K]
$C_{A,b}$	Concentration of A in bulk	[mol/m^3]
$C_{A,s}$	Concentration of A at external catalyst surface	[mol/m^3]
Ca	Carberry number	Adim
d_p	Pellet diameter	[m]
d_t	Bed diameter (internal tube diameter)	[m]
$D_{A,m}$	Molecular diffusivity A in mixture	[m^2/s]
D_o	Reduced molecular diffusivity of A in mixture	[m^2/s]
$D_{A,eff}$	Effective diffusivity of A in the pellet	[m^2/s]
$D_{A,k}$	Knudsen diffusivity A in the pores	[m^2/s]
$D_{A,ax}$	Axial dispersion coefficient	[m^2/s]
D_{er}	Radial dispersion coefficient	[m^2/s]
$D_{o\ rad\ ,A}$	Standard radial dispersion coefficient for component A	[m^2/s]
E_a	Activation energy (apparent)	[kJ/mol]
f_A	Film factor (for component A)	Adim
$f_{A,app}$	Approximate film factor (for component A)	Adim
F_0	Feed molar flow	[mol/s]
$F_{in\ v}$	Feed volumetric flow (at reactor conditions)	[m^3/s]
$\square_r H$	Reaction enthalpy	[kJ/mol]
k_f	Mass transfer coefficient between pellet and fluid bulk	[m/s]
$k_{w,A}$	Rate coefficient	[mol-A/kg-cat s]
L	Bed length or height	[m]
M_{av}	Molar mass	[kg/mol]
n	Reaction order	Adim

Nu	Nusselt number	Adim
p_A	Partial pressure	(A) [kPa]
$p_{A,0}$	Partial pressure of A at reactor entrance	[kPa]
Pe	Péclet number	Adim
Pe'	Modified Péclet number	Adim
$Pe_{m,r}$	Radial mass Péclet number	Adim
$Pe_{m,a}$	Axial mass Péclet number	Adim
Pr	Prandtl number	Adim
$R_{v,A}$ =	Volumetric reaction rate per unit of catalyst pellet	[mol-A/m3-catpellet s]
$R_{obs\ v,A}$	Observed volumetric reaction rate per unit of catalyst pellet volume	[mol-A/m^3-catpellet s]
$R_{w,A}$	Reaction rate per unit of catalyst mass (observed)	[mol-A/kg-cat s]
Re	Reynolds' number	
S_p	Specific internal surface area	[m^2/kg-cat]
Sc	Schmidt's number	Adim
Sh	Sherwood's number	Adim
T_f	Temperature of the fluid in the bed	[K]
T_{ad}	Adiabatic temperature change	[K]
u_0	Superficial fluid velocity	[m/s]
W	Amount of catalyst	[kg]
X_A	Conversion of A.	Adim
y_A	Molar fraction of A	Adim

List of Greek Symbols

Symbol	Definition	Units
α_p	Heat transfer coefficient between pellet and gas bulk	[W/m^2K]
α_w	Heat transfer coefficient at reactor wall	[W/m^2K]
α_0	Heat transfer coefficient at reactor wall at zero fluid velocity	[W/m^2K]
δ	Relative experimental error	adim
ε_b	Bed porosity	adim
ε_p	Pellet porosity	[m^3-pore/m^3-pellet]
ϕ	Thiele modulus	adim
Φ	Weisz modulus	adim
Φ_{ij}	Contribution factor	adim
η	Catalyst effectiveness	adim
λ_d	Diluting inert pellets thermal conductivity	[W/m K]
λ_{er}	Effective radial bed thermal conductivity	[W/m K]
λ_f	Fluid thermal conductivity	[W/m K]
λ_p	Catalyst pellet heat conductivity;	[W/m K]

λ_{ps}	Catalyst pellet solid phase thermal conductivity	[W/m K]
λ_{s}	Average pellets thermal conductivity	[W/m K]
μ_{f}	Dynamic fluid viscosity	[kg / m s]
ν_{i}	Stoichiometric coefficient of component i	adim
ρ_{f}	Fluid density	[kg/m^3]
$\rho_{s,p}$	Solid density of catalyst pellets (density of catalyst material without pores)	[kg/m^3]
ρ_{p}	Density of catalyst pellets (density of the catalyst including the pores)	[kg/m^3]
ρ_{b}	Catalyst bulk density (density of a catalyst bed, thus including the pores and the bed porosity)	[kg/m^3]
$\rho_{s,d}$	Solid density of diluting pellets	[kg/m^3]
τ	Real residence time in catalyst bed	[s]
τ_{p}	Correction factor for the tortuosity of the pores	adim

1. Introduction

1.1 Problem Statement

One very wide and important chemical engineering area is process control. Process control objective is to grant the targeted quality of a product with the higher possible efficiency. Among the different parameters that need to be controlled in a chemical plant, the temperature of the process is an important one. Temperature have always a tight correlation with the efficiency, yield and quality of chemical products. This is the case for chemical reactors.

Temperature control must be carry out strictly in chemical reactors, with a precision grade that depends on the reactors stability and sensibility of the reaction to temperature.

The reaction sensibility to temperature fundamentally relies on the activation energy and the equilibrium constant. As the activation energy is higher, the reaction brings to be more sensible to the temperature, which means that with small changes in temperature, important changes on the conversion, distribution of products and stability can be generated.

As the reaction heat is higher and the process constraints range are narrower the design of a control system can be challenging since its efficiency can be compromised. Since the reaction absorb/release energy at a very high rate to compensate the associated amount of energy in a short time it can be very difficult..

One of the most studied cases is the reactor stability when highly exothermic reactions take place.

If the reactor, and the control system are not designed to operate in the desired stable point, the effects on yield, conversion and product distribution can be important.

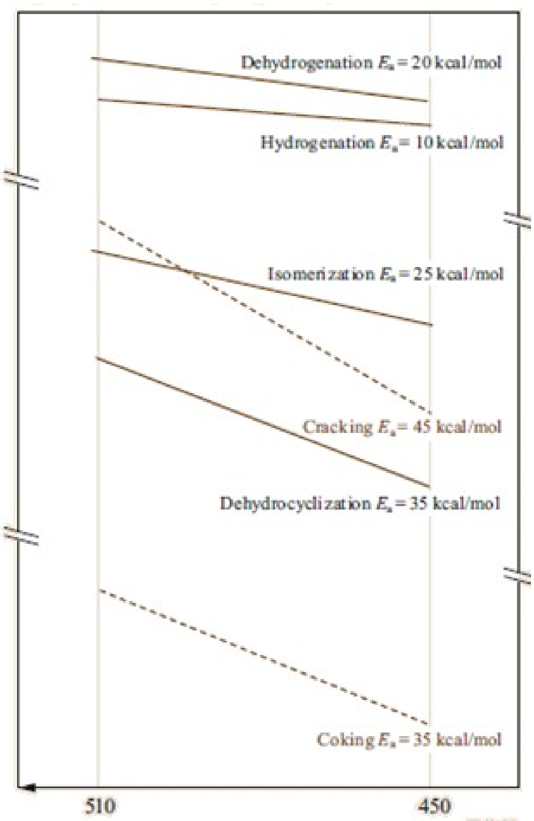

Figure 1.1. Relative Rate (V) of reaction versus the activation energy for different reactions (Hsu, 2017)

For packed tubular reactors, a common solution to make easier the temperature control is to dilute the catalyst bed with an inert solid. It decrease the reaction rate and so the heat absorption/releasing rate.

Usually, kinetic and performance catalytic test are done in isothermal regime using packed reactors. When these reactions have very exothermic/ endothermic character, the temperature control to generate an isothermal profile can be difficult if not unpractical.

. When test of this kind are done for reaction networks that can be difficult to simulate or are simply unknown, it is difficult to decide what to consider an acceptable profile in order to catalog the test as an isothermal test.

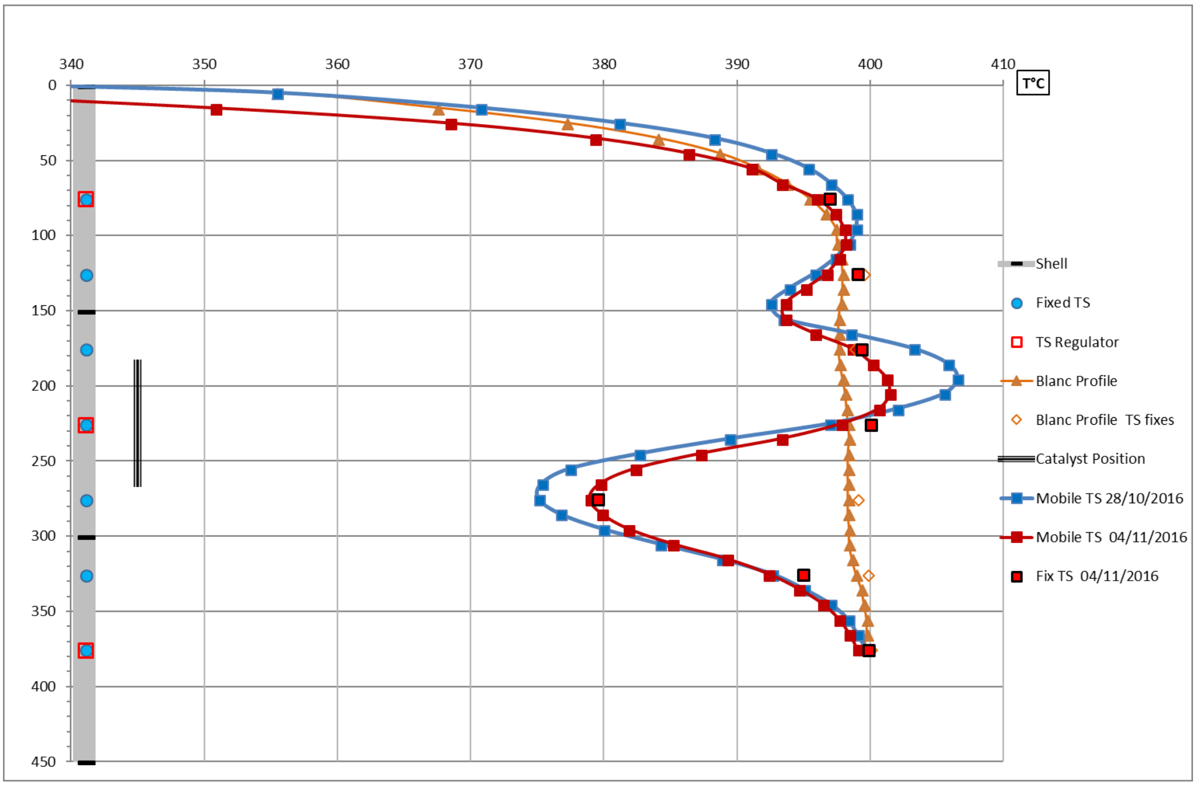

Figure 1.2. Experimental Thermal Profiles

The figure 1.2 shows a catalytic reforming test done in packed bed reactors with sophisticated temperature control systems.

Catalytic reforming is one very common industrial process that is very endothermic due to aromatizing reactions.

In figure 1.2, several catalytic reforming test are showed for different catalyst dilutions. This figure reflects several problem associated to this kind of systems.

The endothermicity of the reaction is so high that the temperature undershoot is between 5 and 20 °C, producing marked temperature profiles.

The situation on figure 1.2. improves a lot with the dilution of the catalyst. However, it represented time, human and economic resources to set in the pilot plant the new test. The is not a criteria to discard or approve a thermal profile.

In the direction of Conduction of Experiments of the Process Experimentation Division (R-15), this is a common test scenario.

This thesis looks to answer to the following questions:

- Do temperature sinusoidal profiles affects the test performance?
- How much is the maximum temperature deviation allowed to still consider the test as isothermal?
- How the operation parameters influence the resulting deviation?
- Which are the possible actions to take in order to reduce the deviation?
- Is it possible to propose a mathematical model to estimate the deviation?

1.2 Targeted chemical reaction

To make easier the study of the stated problem, a convenient chemical reaction must be targeted. The following characteristic are desiderables:

1. High reaction heat
2. Simple and easy to follow.
3. A well know reaction. The intention of this work is not to perform a kinetic study, because of which must exist enough information about the reaction.

The characteristics of the reforming reactions made them a perfect evaluation example to study the effect of thermal profiles in the conversion since the high endothermicity that characterize them made difficult the temperature control along pilot reactors. Given the complexity of testing the reforming of naphtha, it was decided target a key aromatizing reaction.

The reaction targeted for this study is the dehydrogenation of the methylcyclohexane showed in the figure 1.3.

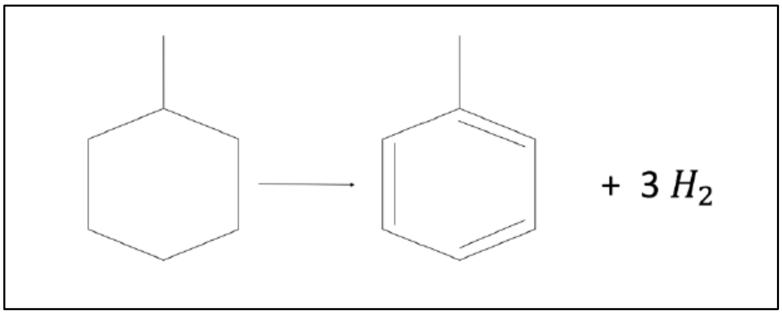

Figure 1.3. Dehydrogenation of methylcyclohexane scheme

Through dehydrogenation, the methylcyclohexane is aromatized to toluene, producing hydrogen as by product.

In 1997 Vestraette did a Kinetic study about the catalytic reforming of naphtha over a Pt-Sn / Al_2O_3 catalyst (J., 1997). In his work, he considers different possible mechanism for methylcyclohexane reforming. At IFP, in 2015 Oliveira (Oliveira, 2016), picked up two of these mechanisms and determined experimentally which one adapts better to experimental data.

$$MCH + l \rightleftharpoons MCH - l$$

$$MCH - l \rightleftharpoons MCH^{=} - l + H_2$$

$$MCH^{=} - l \rightleftharpoons MCH^{2=} - l + H_2$$

$$MCH^{2=} - l \rightleftharpoons Tol - l + H_2$$

$$Tol - l \rightleftharpoons Tol + l$$

Figure 2. Single site surface reactions according to an Eley-Rideal mechanism (J., 1997)

In his work he determined experimentally that the best model was based in the single site surface reaction with the generation of the second hydrogen molecule as the controlling step mechanism (Eq. 1.1) . This is an Eley-Rideal mechanism type.

$$\boldsymbol{r = \frac{k_o e^{\frac{E_a}{R}\left(\frac{1}{T_o}-\frac{1}{T}\right)}\left(P_{MCH}-P_{TOL}P_{H_2}{}^{3}\right)}{P_{H_2}\left(1+K_{MCH}P_{MCH}+K_{TOL}P_{TOL}\right)}} \qquad \textbf{(1.1)}$$

Table 1.1: Reforming of Methylcyclohexane kinetics parameters (Oliveira, 2016)

Parameter	**Value**	**Lower Limit**	**Upper Limit**	**t-value**
ko	5,52E-01	4,981E-0,1	6,06E-01	20,52
Ea	2,00E+05	1,92E+05	2,084+E05	47,62
KMCH	4,20E+00	3,60E+00	4,81E+00	1,39E+01
Ktol	1,36E+00	7,67E-01	1,95E+00	4,60E+00

2. Evaluation of the thermal profiles effect on the final conversion

2.1 Reforming Reactions

2.1.1 Reforming fundamentals

Petroleum is the backbone of the world market. It is the main actual energy source and its derivates are the basis of the chemical industry.

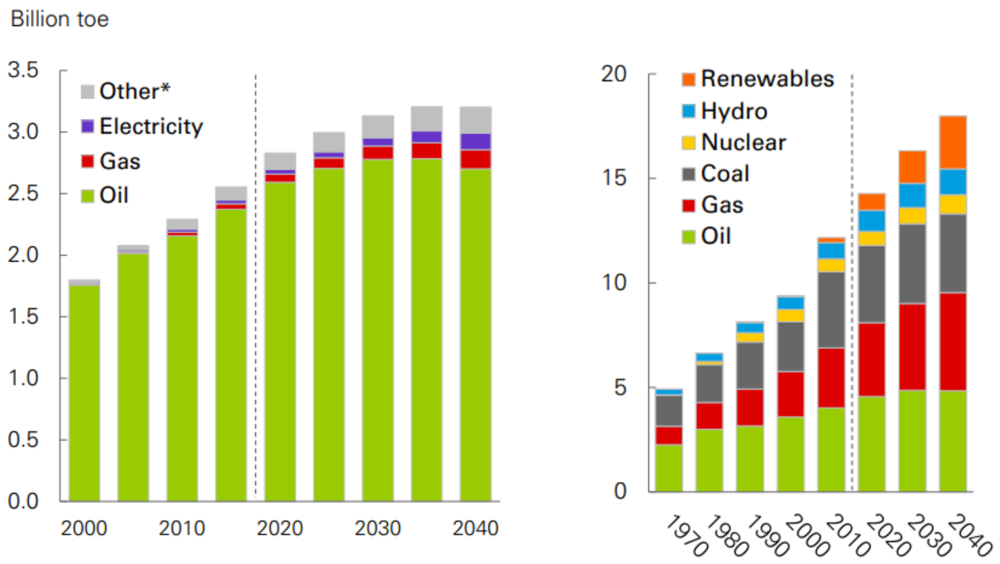

Figure 2.1 Primary energy consumption by fuel, transport energy consumption by fuel type (BP, 2017)

The oil is extracted, refined and converted according with the market configuration to fulfill the different products demand.

The conversion of some oil fraction into another more valuables or strategically needed is a vital petrochemical operation. One of the main processes that allow such conversion is the reforming. It consists into transform paraffins and/or olefins into monocyclic aromatics. The aromatic are heavy chemical compounds characterized by the presence of cyclic carbon structures, high boiling point and an elevate octane number (Speight, 2014). Light aromatics are used as an additive to increase naphtha's octane number and as chemical reactive for consumer goods production. Reforming reactions are very endothermic and possess a high activation energy.

There are two ways in which catalytic reforming may be used. One option is to process the heavy fractions of straight run naphtha in order to increase their octane rating by 40–50 units. The other way is to process a narrow fraction of gasoline such as C6-C8 or C7-C8. From the obtained reformate (called in this case BTX) are then separated the aromatic hydrocarbons (mainly benzene, toluene and xylenes), for the petrochemical industry. This second process is also called aromatization. Both processing options are performed in the same units working under similar operative conditions.

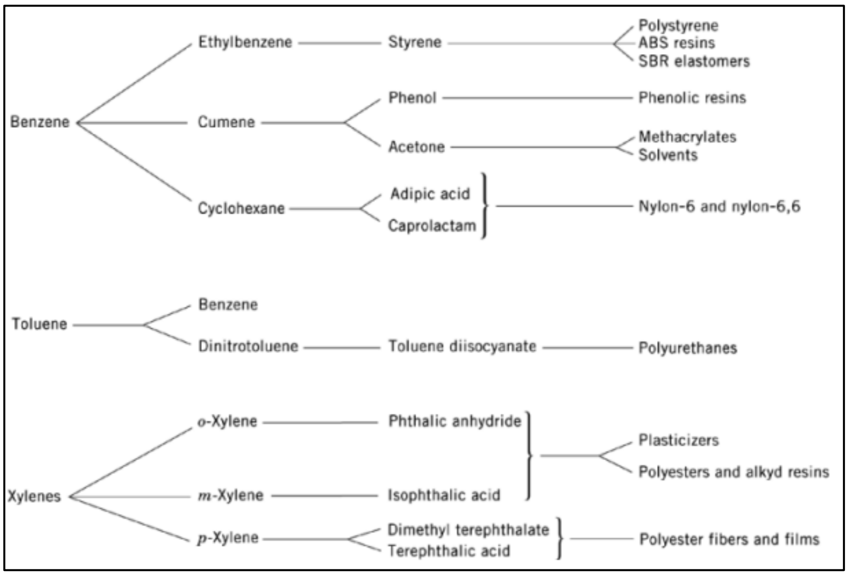

Figure 2.2. Chemistry of BTX

Molecular hydrogen/hydrocarbons ratios of between 2 to 10 are used to decrease the rate of coking of the catalyst. Since hydrogen is a product of the aromatization reactions, its presence in the feed to the reactor affects the thermodynamic equilibrium.

2.1.2 Catalyst

The catalyst used for reforming are the bifunctional type. On the acidic sites the hydrocracking and isomerization is made meanwhile on the metallic sites is dehydrogenation that takes place. The acidic/metallic sites ratio affects deeply the yield and the stability of the catalyst. A reforming catalyst performance is evaluated according its activity, selectivity and stability (Speight, 2014)

Since 1940, platinum is the most common metal used to prepared reforming catalyst (Hsu, 2017)With time, it was discovered that the use of some other metals as Iridium, Palladium, Germanium and Rhenium as promoters can increase the activity and the stability of the catalyst (EM Blue, GD Gould, CJ Egan, 1975; JP Frank, 1994; Vo¨ lter, G Lietz, 1981). For example, Iridium has a higher hydrogenating activity than the platinum, which decrease the amount of coke on the catalyst active surface, increasing the stability. The quantity of Platinum is usually about 0.2-0.6 % w/w. The most used support is alumina and the acid level required is reached using hydrofluoric or hydrochloric acid.

The level of dispersion of the catalyst and the size of the crystal are important parameters for the catalyst performance (KR Murthy, N Sharma, 1995; Little, 1985).

In the catalytic reforming process, excess of water reduces the availability of the acid sites for the reaction. Small quantities of hydrochloric acid are continuously injected into the reactors to maintain the acidity level of the catalyst and the proportion must be carefully balanced to maintain the yield and the selectivity (BC Gates, JR Katzer, 1979; Little, 1985)Reforming feed must be lower than 5 ppm in water content.

Sulphur can also poison severely the catalyst due to the interaction between sulfur and platinum, which decreases the number of metallic active sites. The sulfur content into the feed usually must be under 0.5 ppm (Raseev, 2003). Other poisoning component for the catalyst are coke, nitrogen and metals. Coke production is controlled through hydrogen recirculation while nitrogen and metals must be retired previously from the feedstock as the sulfur and water.

2.1.3 Industrial Process

All catalytic reforming units normally have 3 or 4 adiabatic reactors with intermediate heating stages due to the endothermicity of the aromatization figure 2.3. The process takes place in gas phase and the temperature through the reactors varies between 400 and 550 °C. The pressure level change considerably according to the type of technology used.

The reforming processes can be classified in non-regenerative, semi-regenerative and regenerative type, which is also the chronological order into which these processes were developed, been the most effective the last type. The technological improvement in the reforming process followed the necessity to perform the reactions at lower pressure and with lower hydrogen/hydrocarbon ratio to increase the aromatic yield (Hsu, 2017; Speight, 2014). These two process constrains have as consequence an increment in the coke yield which brought along the necessity to regenerate in a shorter interval of time the catalyst.

In a typical old conventional fixed bed process, dehydrogenation reactions of the alkylcyclohexanes take place mainly in the first reactor, while the reactions of dehydroisomerization of alkylcyclopentanes just start. The high rates of these reactions and their strong endothermic character cause a temperature drop by approximately 50 °C when the naphtha have gone through 10–14% of the total amount of catalyst (Elia, 2013).

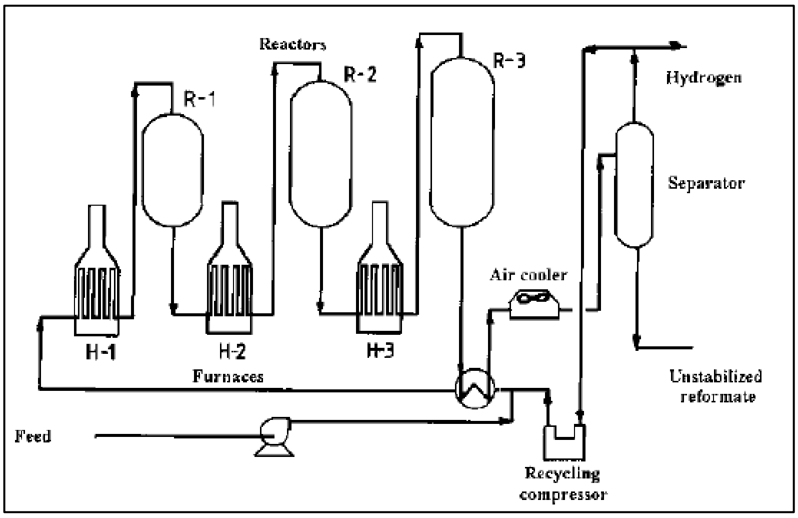

Figure 2.3 Process flow diagram of a fixed bed catalytic reformer (Raseev, 2003).

The thermodynamic conditions reached at this point are not favorable for aromatization. At the lowered temperature obtained, the reaction rate is low and would require reactor dimensions that would be uneconomical. Therefore, the reaction mixture is reheated in a furnace (Raseev, 2003).

The dehydroisomerization reactions are completed in the second reactor. This is the stage where dehydrocyclization reactions take place and hydrocracking begins. The quantity of catalyst affected by these reactions represents approximately 35% of the total catalyst in the system, and the temperature drop is lower than in the first step (Speight, 2014).

.

The reactions of dehydrocyclization and hydrocracking take place in the last reactor. The exothermic character of the latter reaction compensates almost fully the endothermic character of the reformer. The temperature drop in this step is only a few degrees and it is used as a criterion for the correct control of the process (Hsu, 2017; Speight, 2014).

The most modern and efficient regenerative processes are moving-bed systems that allow the continuous regeneration of catalyst.

Three processes technologies for continuous regeneration systems design by IFPEN are dual forming, dual forming plus and Octanizing. The Dual Forming and Dual Forming Plus processes are designed for revamping old fixed bed technology adding a reactor with moving-bed catalyst system and a regeneration unit. The Octanizing process is an integral circulation of catalyst process to which the catalyst is conveyed through all the reactors.

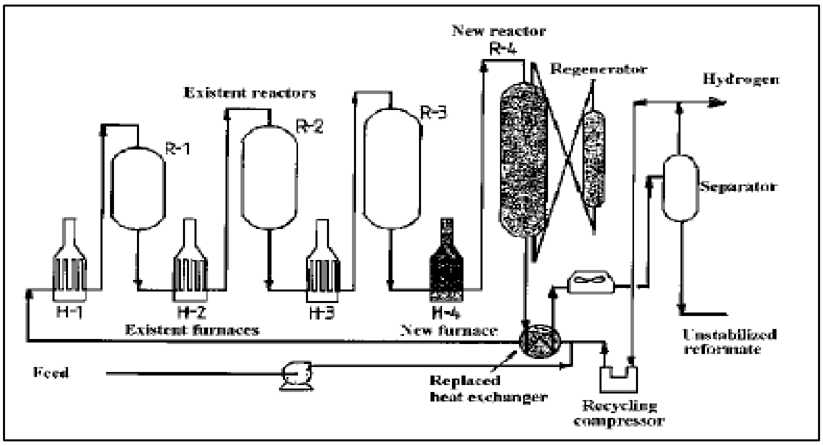

Figure 2.4 Dual Forming Technology (Raseev, 2003)

In the Table 1, for the same capacity it is possible to see how from process to process the pressure decrease, hydrogen/hydrocarbon ratio feed to the reactor decreases, the catalyst life before the regeneration change, the RON increase and the profits also increase.

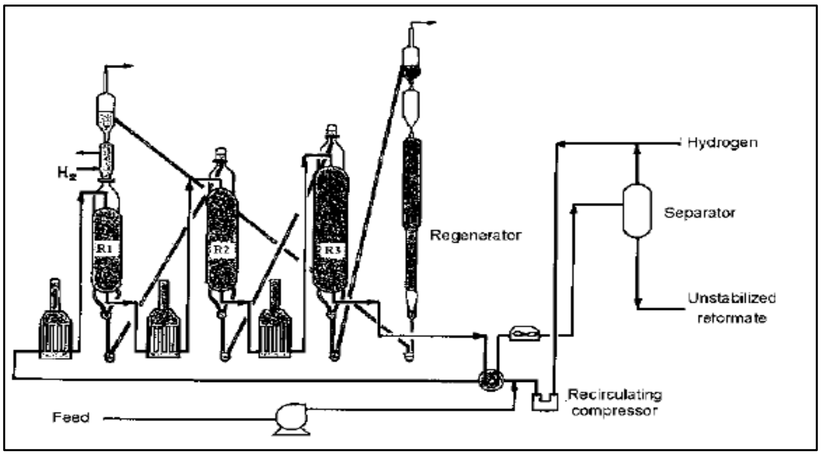

Figure 2.5 Octanizing Technology (Raseev, 2003)

According with the product mix required and the feed composition these processes are modified. Catalyst, separation technology and number of units vary from one type of process to another. Also, process parameter as temperature, pressure and hydrocarbon ratio varies. Cyclar, RZ Platforming, Isomar, Parex and Tatoray are some examples design for particular feed compositions and to maxime yield in some direction. Usually, what it is find in petrochemical complexes is the integration of this different process technologies.

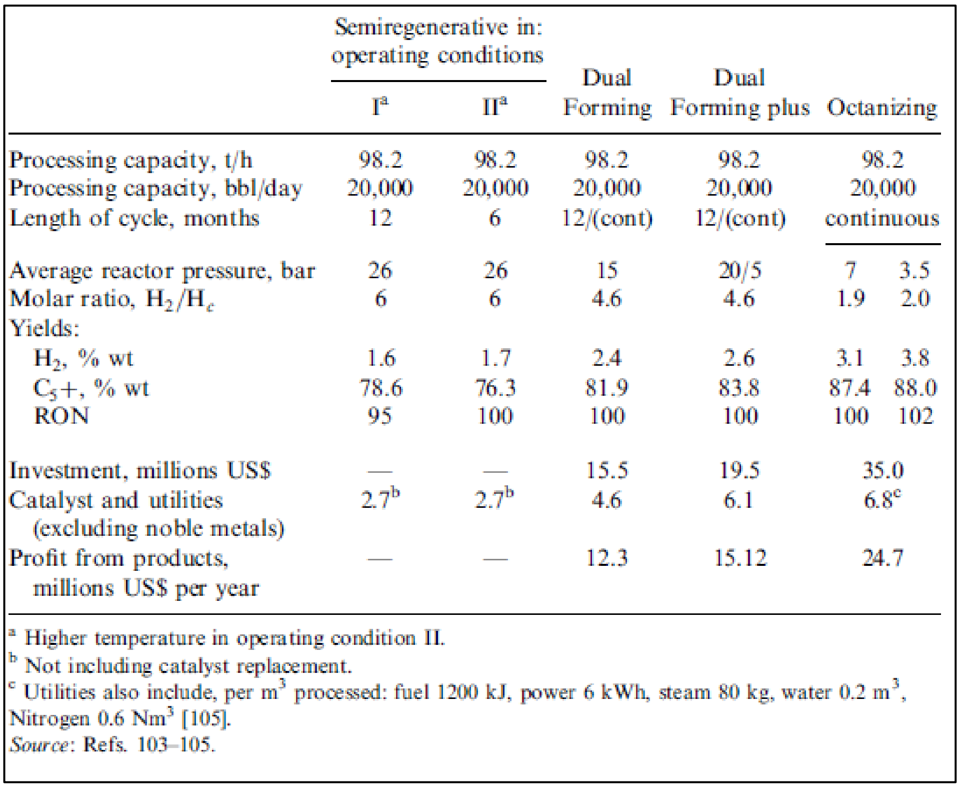

	Semiregenerative in: operating conditions		Dual	Dual		
	I[a]	II[a]	Forming	Forming plus	Octanizing	
Processing capacity, t/h	98.2	98.2	98.2	98.2	98.2	
Processing capacity, bbl/day	20,000	20,000	20,000	20,000	20,000	
Length of cycle, months	12	6	12/(cont)	12/(cont)	continuous	
Average reactor pressure, bar	26	26	15	20/5	7	3.5
Molar ratio, H_2/H_c	6	6	4.6	4.6	1.9	2.0
Yields:						
H_2, % wt	1.6	1.7	2.4	2.6	3.1	3.8
C_5+, % wt	78.6	76.3	81.9	83.8	87.4	88.0
RON	95	100	100	100	100	102
Investment, millions US$	—	—	15.5	19.5	35.0	
Catalyst and utilities (excluding noble metals)	2.7[b]	2.7[b]	4.6	6.1	6.8[c]	
Profit from products, millions US$ per year	—	—	12.3	15.12	24.7	

[a] Higher temperature in operating condition II.
[b] Not including catalyst replacement.
[c] Utilities also include, per m^3 processed: fuel 1200 kJ, power 6 kWh, steam 80 kg, water 0.2 m^3, Nitrogen 0.6 Nm^3 [105].
Source: Refs. 103–105.

Figure 2.6 Process Parameters for the Semi regenerative Systems, Revamped Units and IFP Units (Speight, 2014)

2.1.4 Modeling

According with the literature, the first kinetics models for catalytic reforming was proposed by Smith (Speight, 2014)taking as typical reactions for the process the dehydrogenation of cycloalkanes, the dehydrocyclization of cycloalkanes and hydrocracking of alkanes and cycloalkanes. Krane (HG Krane, BA Groth, LB Schulman, 1959) created a more complex kinetic network with 53 differential equations to describe the reactions taking place in the process and using n-heptane as typical for the catalytical reforming process; the model considerate the process as isothermal and the kinetic constant were valid at 21 bar.

The equation general form was:

$$\frac{dW_k}{d\left(\frac{A_c}{w}\right)} = \sum W_{k,i} \qquad (2.1)$$

Henningen (H Henningen, 1970) developed a more complex model that discriminate between cycloalkanes with five and six carbon atom and between normal and iso alkanes. Jenkins and Stephens (JH Jenkins, 1980) improved the model creating an extension to recalculate the values of the kinetics constants at different pressures. Ancheyta-Juarez and Anguilar-Rodriguez (Juarez & Aguilar-Rodriguez, 1994)added a temperature correction to the pressure corrective equation included by Jenkins.

$$k_i = k_i^0 \left(\frac{p}{21}\right)^{\propto} exp[\frac{E_i}{R}\left(\frac{1}{T_0} - \frac{1}{T}\right) \qquad \mathbf{(2.2)}$$

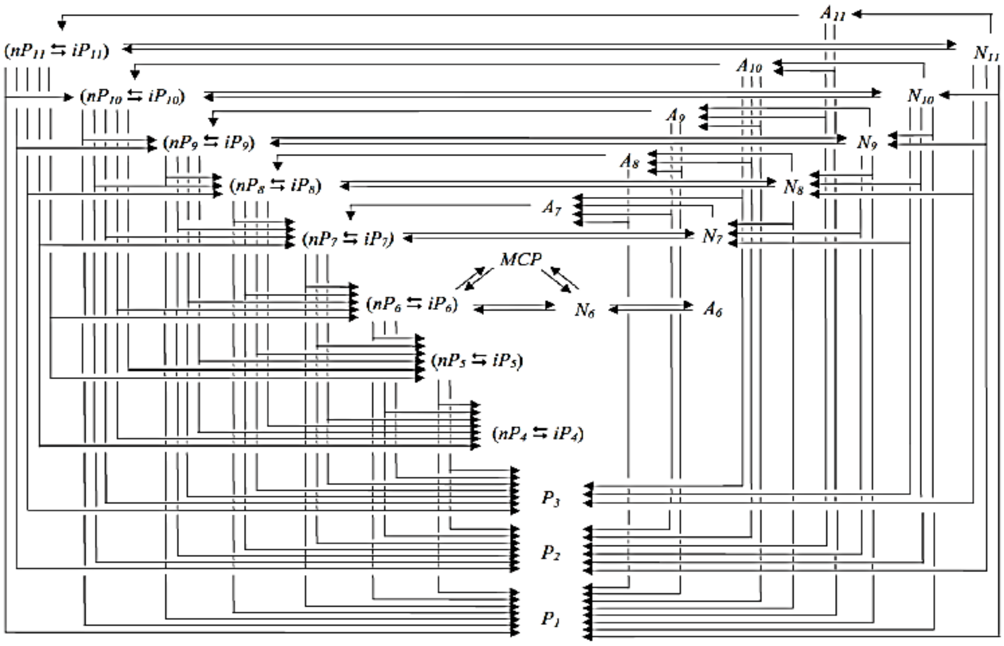

*Figure 2.*7 Reaction Network proposed by Ancheyta for catalytic reforming of naphtha (Juarez & Aguilar-Rodriguez, 1994)

Normally, the reforming kinetics models are adjusted according to the characteristics of the feedstock used for the process. Which means, that according with the catalyst and the feedstocks characteristics these models need to be modified or adjusted through experimentation; this models model are of the pseudo-homogeneous models type.

2.2 Transfer Phenomena in Packed Bed Reactor Modelling

2.2.1 Packed Bed Reactors

The packed bed tubular reactor is a continuous reactor type widely used in the chemical industry to determine intrinsic and non-intrinsic kinetics, chemical reactors scaling-up and Industrial production. Since the beginning of the XX century a lot of R&D have been made to understand more about the phenomena and mechanism that play an important role into the PBR design (Beek, 1962; James J Carberry & Wendel, n.d.; Castañeda-López et al., 2001; Hickman, Degenstein, & Ribeiro, 2016; Westerink, Koster, Reaction, & Laboratories, 1990). Heat, mass and momentum transfer play a fundamental role in this kind of reactor design/study. The next scheme roughly describes the different transfer phenomena between the main elements that are present in a PBR system.

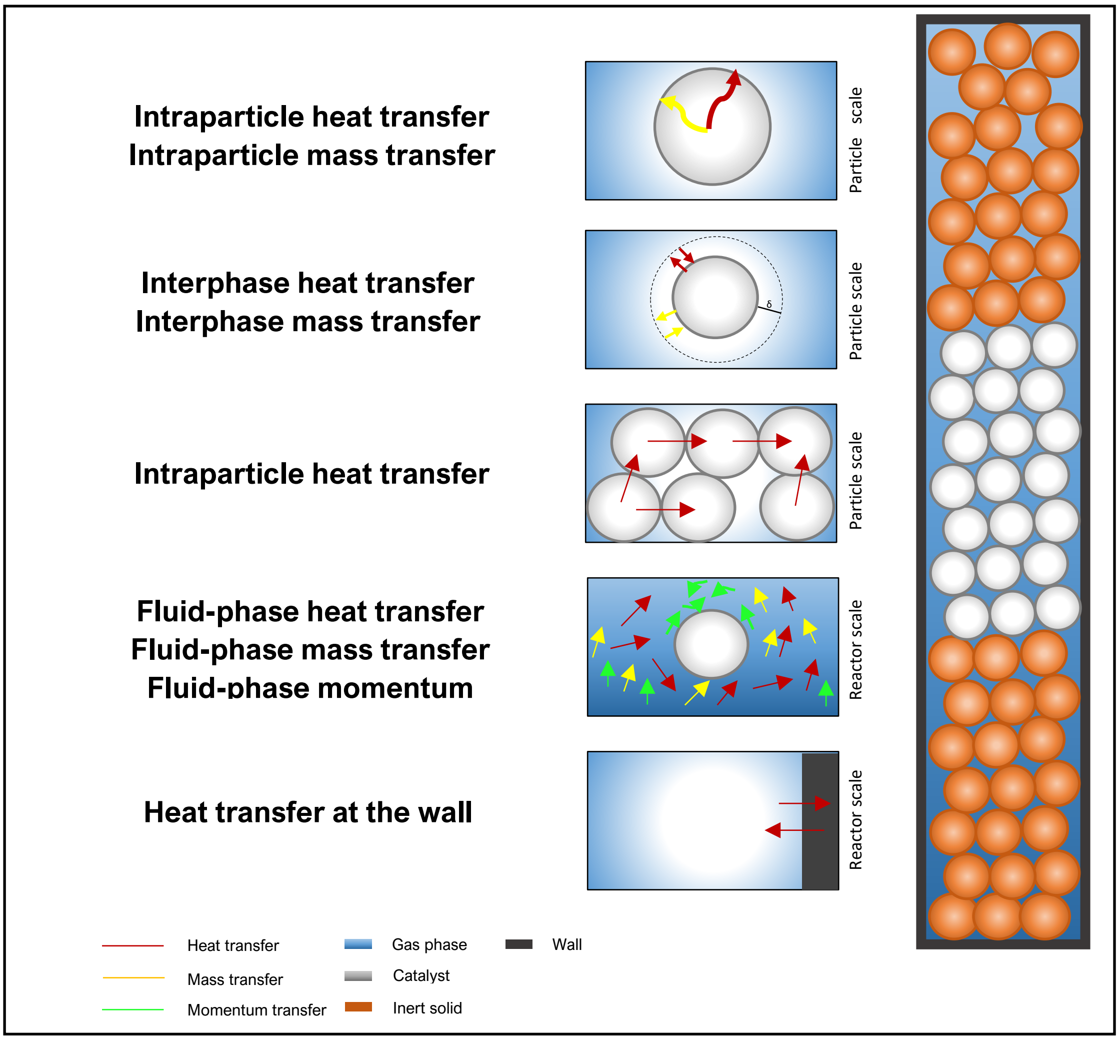

Figure 2.8 Transfer phenomena inside a catalytic packed bed reactor

In the Figure 2.8 can be seen the phenomena at different scales considered in the PBR modelling. For the momentum transfer, the scale and the phenomena showed can be considered an over simplification. The problem in modeling relies into decide which ones of these mechanism must be considered and which ones do not. There are very important additional considerations such as reaction kinetics and reactor's stability.

The conventional approaches used to model chemical reactors are based on mass, heat and moment balance equations (Eq. 1-3) (Bird, R., Stewart. W., Light, 1960).

$$\boldsymbol{\phi} = \boldsymbol{\rho v v} + \boldsymbol{\pi} = \boldsymbol{\rho v v} + \boldsymbol{p \delta} + \boldsymbol{\tau} \tag{2.3}$$

$$\boldsymbol{e} = \rho\left(\hat{\mathrm{H}} + \frac{1}{2}v^2\right)\boldsymbol{v} + \boldsymbol{q} + [\boldsymbol{\pi}\cdot\boldsymbol{v}] \tag{2.4}$$

$$n_A = \rho\omega_A\boldsymbol{v} + \boldsymbol{j_A} \tag{2.5}$$

Given its complexity (Eq. 1-3)., those equations can be conveniently simplified and overlaid according to the reactor system conditions

The mass and heat balance must be written for every phase considered into the reactor and the equivalents mass/heat balance into each phase are linked between them through border conditions. In some approaches, one of the phases can be lumped, reducing the number of equations.

According with the author opinion, considering that packing in tubular reactors can strongly affect the flow pattern of the fluid phase, for packed reactors the great majority of the existent models can be classified into three groups.

1. Ideal flow pattern models.
2. Non-ideal flow pattern models Type I. Into which are included those that consider implicitly the non-ideality of the flow pattern (as dispersion, for example).
3. Non-ideal flow pattern models Type II. Into which the fluid field is explicitly considered, and into which it is possible reach a more rigorous level of reactor modelling.

All of three can be classified as **pseudo-homogeneous** models and **heterogeneous models** (Levenspiel & Chemical, 2009)**.**

In the pseudo-homogeneous models, the solid phased is lumped and its effect (hydrodynamic effects) on the system are accounted modifying some coefficients values.

In heterogeneous models, the solid phase in considered and modelled explicitly (fully or partially effects are accounted).

The heterogeneous models are used when the solid phase must be considered due to the existence of important mass and heat gradients on the catalyst surface and within it. This is very common in industrial size catalytic reactors but can be also present in smaller scales (Duarte, Ferretti, & Lemcoff, 1984; Gilbert F Froment, Juray De Wilde, 2011). When these gradients are considered, heat and mass transfer coefficients are used to describe the transport through them. The transfer mechanism suits to the diffusion law (and the heat analogous).

When temperature gradients are present, it opens the possibility to have multiple stationary states, because of which it is important take care of the reactor is designed for the right stationary state (Elia, 2013; McGuire & Lapidus, 1965; Varma & Amundson, 1973).

Also, non-conventional models can be created using Residence Time Distribution analysis in order to predict the conversion. (figure 2.9)

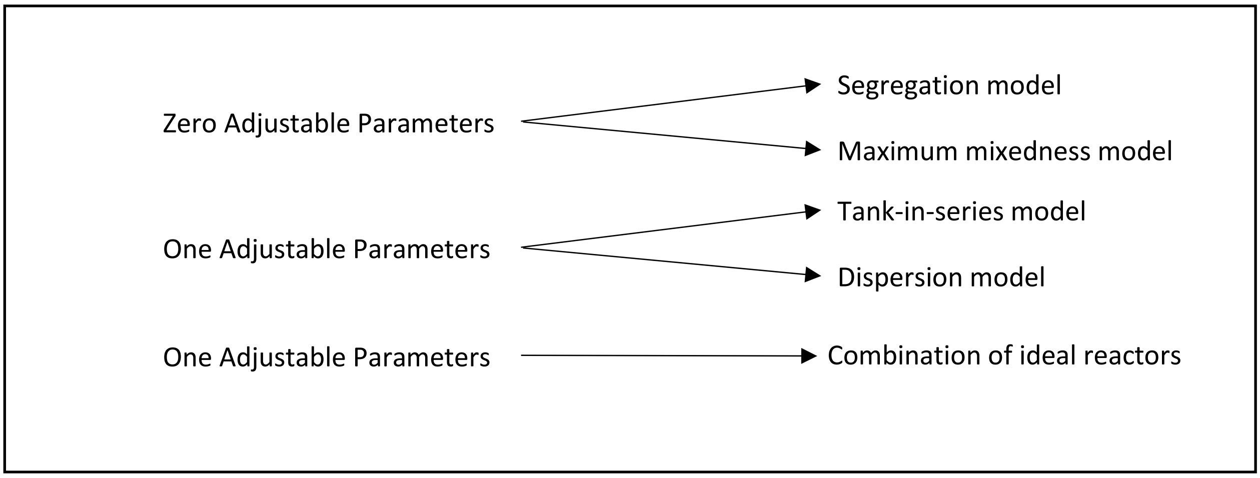

Figure 2.9 Residence Time Distribution analysis models based

The plug flow model

The system under study can be strongly affected by the flow pattern that governs the system. Through the years, the most common approach to simplify the complexity of the models and their respective calculation is based them on the hypothesis of an ideal flow pattern called plug flow.

In this perfectly ordered flow model:

- There is no mixing of the stream lines (those are always parallel) and have a uniform velocity.
- Every reactor slice, perpendicular to the flow along the reactor has uniform temperature and composition.
- The plug flow is the only mass transfer mechanism explicitly considered (intrinsic/extrinsic kinetics).

The plug flow model can be understood as a succession of infinite perfectly mixed reactors, every of which is represented as a cross differential section of the reactor (Figure 2.10). In this fluid model, the concentration gradient is clearly in the axial direction (Eq. 4-5).

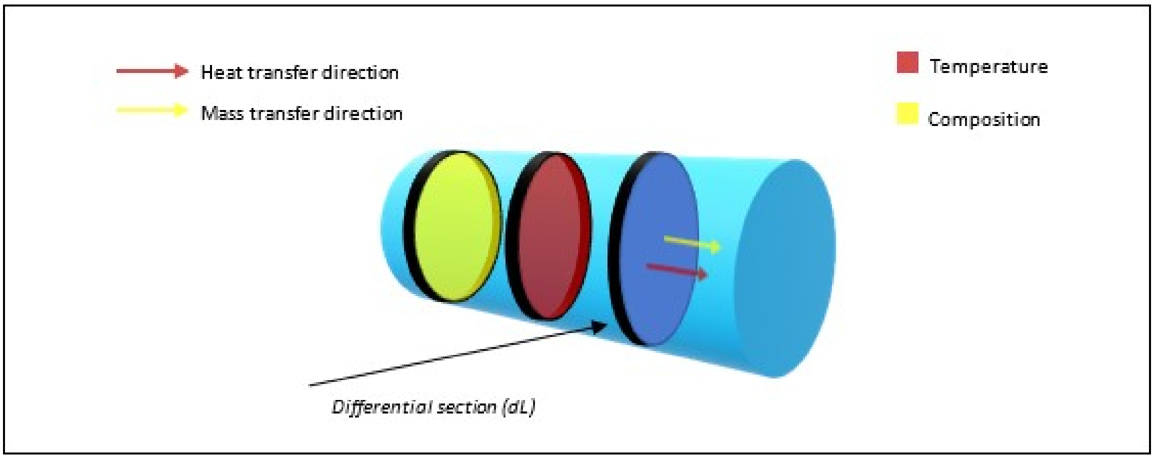

Figure 2.10 Plug Flow Reactor Model

This fluid model represents a good over simplification that must be carefully used (mainly in the case of packed reactors). On the practice, important deviation can be seen associated to the phenomenological intrinsic transfer behavior inside the system which is associated to operative and design variables. Also, technological problems (as fluid shortcuts and heat transfer equipment limitations) can also affect.

$$F_A - (F_A + dF_A) = r_A \mathrm{dV} \qquad (2.6)$$

$$(-\Delta H)r_A - 4\frac{U}{d_t}(T - T_r) = u_s \rho_g c_P \frac{\partial T}{\partial z} \qquad (2.7)$$

$$\frac{dp_t}{dz} = f\frac{\rho_B\, u_s^2}{d_p} \qquad (2.8)$$

To take the non-ideality of the flow pattern into account and to produce models that can express in a more accurate and logical way the phenomena occurring inside the reactor, effective transfer coefficients and statistical terms are added to this ideal model. This means overlay on the ideal model whit additional flow considerations and creating pseudo-plug flow models . (Castañeda-López et al., 2001; de Wasch & Froment, 1972; Wakao, Kaguei, & Funazkri, 1979)

With the raising computational calculation capacities is every year easier to couple mass, heat and kinetic models with flow field equations, which allows to reduce the number of experiments that are needed to evaluate a technology. It is pointed to decrease the R&D that are spent.

2.2.2 Axial **Dispersion** effect

The catalyst presence can cause axial mixing and the convective diffusion can became important. The axial mixing buffers the axial mass gradient and decrease the conversion. The Residence Time Distribution Analysis (RTD) is an experimental technique that allows to study the flow model inside a chemical reactor. It allows to determine deviations from the plug flow model due to different causes. Based on this technique, on figure 2.11 it is observed that as the retention time distribution becomes wider the dispersion effect come along to be more important. $D_{A,ax}$ represent the effective dispersion coefficient in the axial direction and the group $\frac{D_{A,ax}}{uL}$ is the inverse of the Axial Peclet's number for mass transfer ($Pe_{m,ax}$) (that for a particle is also equal to the Bodestein's number (Bo)). The Peclet number is strongly correlated to the Reynolds number and the reactor diameter to particle ratio. When the ${Pe_{m,ax}}^{-1}$ tends to zero, its means negligible dispersion, hence plug flow. When the ${Pe_{m,ax}}^{-1}$tends to infinite, its means large dispersion, hence mixed flow.

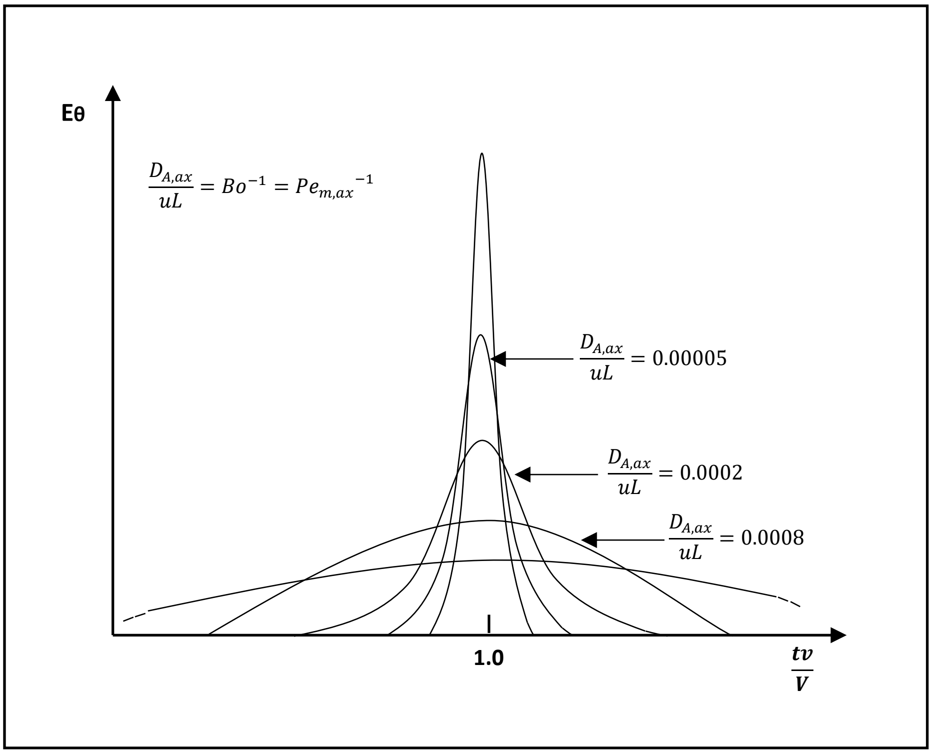

Figure 2.11 Example of different retention time distributions associated to tubular packed reactor.(Levenspiel & Chemical, 2009)

To consider the axial dispersion effect, bearing in mind that the description of the dispersion phenomena suits to the Fick Diffusion Law, it is just necessary add to the plug flow model the diffusive transport term of the equation 1.1 and transform the diffusion coefficient in an effective diffusion coefficient term (for this case called effective axial diffusion coefficient) that is the sum of the molecular diffusion and the dispersion (also called convective or turbulent diffusion coefficient) coefficients, in this way, the interest's flux will be considered (J. J. Carberry & Bretton, 1958; Mears, 1971b; Wakao et al., 1979).

Border conditions

$$(\varepsilon D_{ea})_s \left(\frac{\partial^2 C}{\partial z^2}\right) - u_s \frac{\partial C_A}{\partial z} - \rho_B r_A = 0 \qquad (2.9)$$

$$u_s(C_{A0} - C_A) = (\varepsilon D_{ea})_s \left(\frac{\partial C}{\partial Z}\right) \quad \text{for z=0}$$

$$\lambda_{ea}\left(\frac{\partial^2 T}{\partial z^2}\right) - u_s \rho_g c_P \frac{\partial T}{\partial z} + \rho_B\,(-\Delta H) r_A - 4\frac{U}{d_t}(T - T_r) = 0 \qquad (2.10)$$

$$u_s \rho_g c_P (T_0 - T) = -\lambda_{ea}\left(\frac{\partial T}{\partial z}\right) \quad \text{for z=L}$$
$$\frac{\partial C}{\partial z} = \frac{\partial T}{\partial z} = 0$$

2.2.3 Radial Dispersion

As in the axial direction, in the radial one the flux is superposed on transport by overall convection, which is of the plug flow type (Gilbert F Froment, Juray De Wilde, 2011). Effective transport coefficients are used, in this case to model the radial transport, using radial effective heat transfer coefficient and a radial effective mass transfer coefficient. These two coefficients are mainly affected by the fluid velocity and the radial effective heat transfer coefficient is highly dependent of the diffusion term.

Given the non-isotropic nature of diffusivity in packed beds, the radial effective diffusion coefficient is different from the axial one.

Border conditions

$$(D_{er})_s\left(\frac{\partial^2 C}{\partial r^2} + \frac{1}{r}\frac{\partial C}{\partial r}\right) - u_s \frac{\partial C}{\partial z} - \rho_B r_A = 0 \qquad (2.11)$$

$$\lambda_{er}\left(\frac{\partial^2 T}{\partial r^2} + \frac{1}{r}\frac{\partial T}{\partial r}\right) - u_s \rho_g c_P \frac{\partial T}{\partial z} - \rho_B\,(-\Delta H) r_A = 0 \qquad (2.12)$$

$$C = C_0 \quad \text{at } z = 0 \quad 0 \le r \le R_t$$
$$T = T_0$$
$$\frac{\partial C}{\partial r} = 0 \ \text{ at } r = 0 \quad r = R_t$$
$$\frac{\partial T}{\partial r} = 0 \ \text{ at } r = 0 \quad Z \ge 0$$

The radial effective heat transfer coefficient is dependent of the radial position and decrease importantly close to the wall due to velocity decay caused by the viscous stresses. Thus, there are two treatments that can be given to this coefficient, one option is to treat it as an average value along the cross section; the second one is summing the bulk and the wall heat transfer coefficients to form an effective one. The coefficient that belongs to the bulk section is dependent at the same time of a static and a dynamic contribution (R. Berger & Kapteijn, 2007; Borkink & K.R., 1994; Yagi & Wakao, 1959).

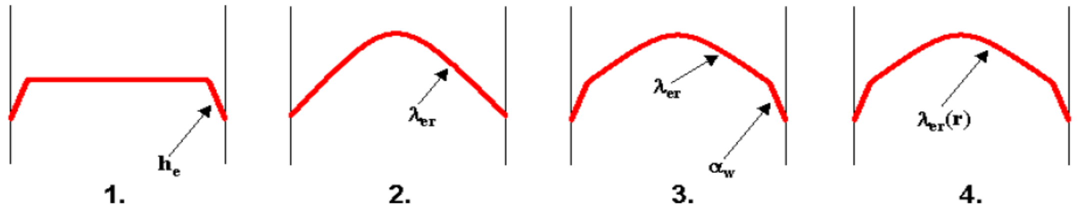

Figure 1. Radial T-profiles for cases 1. – 4. above

1. 1D model with overall heat transfer coefficient h_e;
2. 2D model with one constant parameter (l_{er})
3. 2D model with two parameters: effective radial thermal conductivity (l_{er}) for the bed and a heat transfer coefficient at the wall (a_w)
4. 2D model with one parameter for every radial coordinate ($l_{er}(r)$).

Figure 2.12 Radial effective heat transfer coefficient examples. (M. Maestri, Tronconi, Berger, Kapteijn, & Moulijn, n.d.) (modified)

2.2.4 Interphase Transfer Phenomena

Mass transport in a packed bed is the resultant of molecular and turbulent phenomena: it is postulated that an effective dispersion parameter can incorporate the sum of both the molecular diffusion and turbulent (or mechanical) contributions. As in the case of the effective thermal conductivity, different dispersions apply in the radial and axial direction (F. Maestri & Rota, 2005).
The radial effective dispersion *Der* is associated with random walk transport, while dispersion in the direction of flow (axial), characterized by *Dea*, can be regarded as a diffusion-like process superimposed to bulk fluid flow.

The magnitude of superficial gradients on solid catalyst is influenced by the geometry of the catalyst, the reaction's kinetic, the fluid velocity (mixing) and the fluid intrinsic properties.

Usually on industrial reactors, the velocity is so high that the interphase gradients are not very significant (de Wasch & Froment, 1972; Levenspiel & Chemical, 2009)

As was state before, to consider a phase explicitly, balances on that phase must be done. The most common transfer model used to represent the transfer between the gas and solid phases is the stagnant film model. In this model it is stablished that the catalyst pellet is surrounded by a stagnant film made of gas, through which the mass and heat diffuses. This is a logical assumption since due to the friction, the velocity in a very narrowed region close to the catalyst surface is close to zero.

For the fluid phase

$$u_s \frac{dC}{dZ} = k_g a_v (C - C_s^s) \tag{2.13}$$

$$u_s \rho_g C_p \frac{dT}{dz} = h_f a_v (T_s^s - T) - 4\frac{U}{d_t}(T - T_r) \tag{2.14}$$

For the interphase

$$\rho_B r_A = k_g a_v (C - C_s^s) \tag{2.15}$$

$$(\Delta H)\rho_B r_A = h_f a_v (T_s^s - T) \tag{2.16}$$

With the boundary conditions

$C = C_0$ at $z = 0$ $C = C_0$ at $z = 0$ $T = T_0$

The temperature gradient can become significant when the reaction is very endothermic or very exothermic. When there is an interphase heat transfer gradient the problem of the determination of the stables states of the reactor can get complicate.

2..2.5 Intraparticle transfer phenomena

According with Maestri (F. Maestri & Rota, 2005)The diffusion inside a porous matrix can be modeled according three types of diffusion mechanism.

a) Free molecular diffusion
b) Knudsen diffusion
c) Surface diffusion of adsorbed molecular species along the pore wall surface.

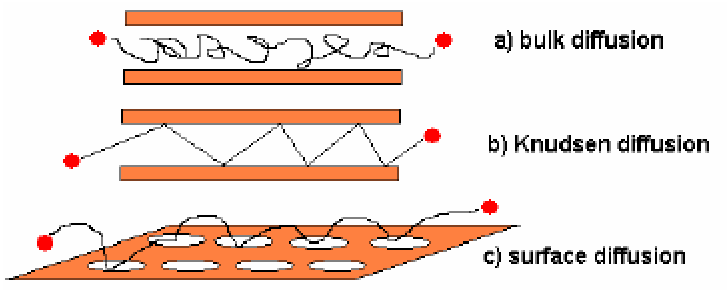

Figure 2.13 Pore diffusion types (F. Maestri & Rota, 2005).

It was showed that a catalytic reaction could be strongly affected by diffusion within the catalyst pores. Intraparticle mass gradients can be important when the reaction rate is slower than diffusion rate through the pores, which can be due to several reasons. It brings as consequence that over certain dimension of the catalyst's particle just a fraction of itself is effectively used, which cause a drop in the observed reaction rate and in the apparent activation energy (Levenspiel & Chemical, 2009; Thiele, 1939)To consider the diffusion inside the catalyst porous, terms for the quantification of the flux that diffuses a reacts inside the particle are added (Eq. 2.17-2.20).

-

For the fluid phase

$$-u_s \frac{dC}{dz} = k_g a_v \left(C - C_S^S\right) \tag{2.17}$$

$$u_s \rho_s c_p \frac{dT}{dz} = h_f a_v \left(T_S^S - T\right) - \frac{4U}{d_t} - (T - T_r) \tag{2.18}$$

For the solid phase

$$\frac{D_e}{\xi'^2} \frac{d}{d\xi'} \left(\xi'^2 \frac{dC_s}{d\xi'}\right) - \rho_s r_A (C_s, T_s) = 0 \tag{2.19}$$

$$\frac{\lambda_e}{\xi'^2} \frac{d}{d\xi'} \left(\xi'^2 \frac{dT_s}{d\xi'}\right) - \rho_s (-\Delta H) r_A (C_s, T_s) = 0 \tag{2.20}$$

Boundary conditions

$C = C_0$

at z=0

$T = T_0$

$\frac{dC_s}{d\xi'} = \frac{dT_s}{d\xi'} = 0$ at $\xi' = 0$

$k_g a_v (C - C_S^S) = -D_e \left(\frac{dC_s}{d\xi'}\right)$ at $\xi' = \frac{d_p}{2}$

$h_f a_v (T_S^S - T) = -\lambda_e \left(\frac{dT_s}{d\xi'}\right)$ at $\xi' = \frac{d_p}{2}$

Considering the diffusive interparticle limitations, Levenspiel introduced a parameter that allows to compare the diffusion and the reaction rate (the so-called Thiele's modulus) and an efficiency factor (Eq.21-22) which express the fraction of the catalyst which is effectively used. It is calculated as the ratio between the reaction rate with limited by the diffusion effect and the reaction rate at the surface of the catalyst. Froment (de Wasch & Froment, 1972) introduced a generalized version (generic expression) of Thiele modulus.

$$\psi' = \frac{V_P}{A_P} \frac{-R_{Ai}}{[2D_e \int_0^{C_{Ai}} (-R_A) dC_A]^{\frac{1}{2}}} \tag{2.21}$$

$$\eta = \frac{< R_A >}{R_{Ai}} = \frac{\int_0^{C_{Ai}} (-R_A) dC_A}{R_{Ai} V_P} \tag{2.22}$$

The efficiency parameter is widely used in catalytic reactors models because it allows to consider the effect of the intraparticle diffusion on the reaction rate which is as helpful in modelling as in design.

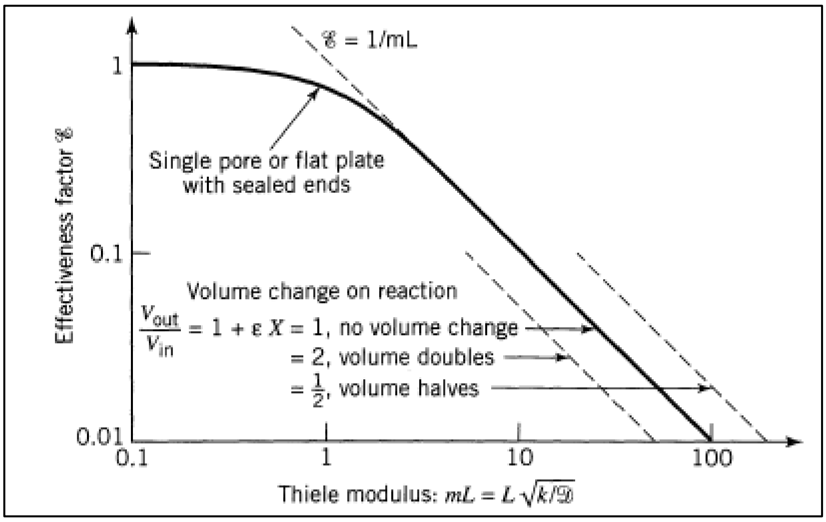

Figure 2.14 The effectiveness factor as a function of the Thiele modulus (here represented ad mL) [Aris 1957] [Thiele1939]

As the Thiele modulus increase (higher diffusive limitation within the pores) the efficiency decreases.

For strongly exothermic/endothermic reactions the particle is usually in isothermal, but the conductivity of the pellet should be always considered. The main resistance inside the pellet tend to be to the mass transfer and the main resistance in the film surrounding the particle use to be to the heat transfer [Weisz and Hicks, 1962; Carberry, 1961, Froment]. To face the non-isothermally condition of the pellet, the efficiency factor can be calculating for the different temperature values along the pellet.

Based in Thiel's work, the intraparticle diffusion effect on the product distribution (Weisz, 1955) and the effect of the temperature profile inside the catalytic particle (J. J. Carberry, 1961) have been also studied. The figure 2.15 shows how the efficiency can be higher than 1 (exothermic reactions) the it is heavily affected by the reaction activation energy and the reaction heat. Diffusion limitations can affect heavily the product distribution.

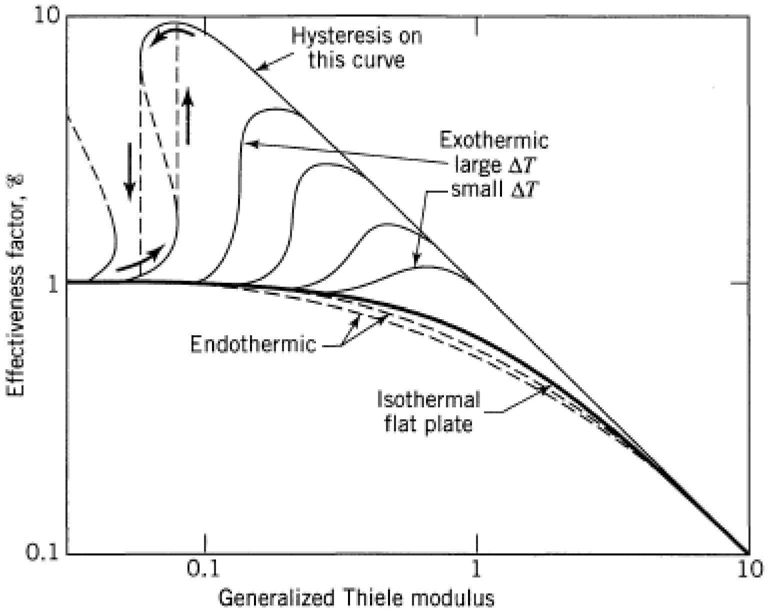

Figure 2.15 Non-isothermal effectiveness factor curve for temperature variation within the particle [Jura][Bischoff 1967].

For non-isothermal conditions the efficiency needs to be calculated for every point into the catalyst which complicates the calculation.

2.3 Packed Bed Reactor Criteria

To identify the conditions in which the different phenomena acting on the system have a relevant effect on its behavior, several criteria are been developed which are useful in a very wide range of conditions. It is necessary keep in mind that as much more simple and efficient the model is, much less calculation resources a time are required.

2.3.1 Intraparticle transfer phenomena criteria

- Internal Diffusion limitation

The Weisz-Prater criterion (**Froment & Bischoff [9], Anderson & Pratt [10])**

$$\phi = \frac{n+1}{2} \frac{R_{v,A}^{obs}\left(\frac{d_p}{6}\right)^2}{D_{A,eff} C_{A,s}} \qquad \begin{matrix} < 0.33 \; if \; n = 0 \\ < 0.08 \; if \; n \geq 0.5 \end{matrix} \qquad (2.23)$$

The Weisz modulus (ϕ) relates the observed reaction rate with the diffusion rate through the catalyst pellet. The value of $C_{A,s}$ can be calculated through the Carberry number (C_a)

and under some circumstances the use of the value of concentration within the bulk can be considerate as acceptable (F. Maestri & Rota, 2005).

- Heat transfer limitation

Mears in 1995 stablish that in order of neglect the temperature gradient inside the pellet the temperature difference between the pellet surface and the average temperature within it must be less than 1 K (Tajbl D.G., Simons J.B., 1966).

$$\Delta T = \frac{R_{v,A}^{obs}|\Delta H_r|{d_p}^2}{60\lambda_p} < \frac{0.05\,R{T_f}^2}{E_a} \qquad < 1\,K \qquad (2.24)$$

2.3.2 Interparticle transfer phenomena criteria

- Interphase mass transfer limitation

The criterion is that the resistance due to external mass transfer must be less than 5% of the resistance due to chemical reaction. For a first-order reaction, the efficiency follows as:

$$\eta = 1 - Ca \qquad (2.25)$$

$$Ca = \frac{R_{v,A}^{obs}}{k_f a_v C_{A,b}} = \frac{C_{A,b} - C_{A,s}}{C_{A,b}} < \frac{0.05}{n} \qquad n > 0 \qquad (2.26)$$

- External Heat Transfer limitation

Assuming in arbitrarily that the critical deviation between two extremes of the film should is 5%, Tajbl developed the following criteria criteria (Tajbl D.G., Simons J.B., 1966):

$$\Delta T(film) = \frac{R_{v,A}^{obs}|\Delta H_r|d_p}{6\alpha_p} < \frac{0.05RT_f^2}{E_a} \qquad (2.27)$$

2.3.3 Fluid-phase transfer phenomena

Mass transfer axial dispersion effect

According to Mears (Mears, 1976)

$$\frac{L}{d_p} > \frac{8}{Bo} nLn\left(\frac{1}{1-X_A}\right) \tag{2.28}$$

The axial dispersion effects become particularly important in short fixed beds (J. J. Carberry & Bretton, 1958)

- - Mass transfer radial dispersion effect

According to Mears (Mears, 1971a, 1976)

$$\frac{d_t}{d_p} > 8 \tag{2.29}$$

Assuming plug flow behavior, Berger developed a criterium taking in to account the porosity and velocity profiles, in order to measure intrinsic kinetics directly from the observed kinetic data. The criterium goes as follow:

$$Ln\left(\frac{1}{1-X_A}\right) < a + \frac{b}{Pe'} \qquad 0 \leq \frac{d_p}{R} \leq 0.6 \tag{2.30}$$

$$a = \frac{1 + a1\left(\frac{d_t}{2d_p}\right)}{a2n} \qquad a1=0.49 \;\; a2=12.6 \tag{2.31}$$

$$\frac{1}{b} = b1\left(\frac{d_t}{2d_p}\right)^2 + \frac{b2}{n}\left(\frac{d_t}{2d_p}\right)^{-b3} \qquad b1=0.064 \; b2=1.57 \;\; b3=0.075 \tag{2.32}$$

If this criterion is not fulfilled, serious maldistribution due to bypass of gas through voids near the reactor wall can be expected.

Radial heat transfer limitation

Assuming in an arbitrary way that the critical deviation between the temperature of the zone near the wall and the average temperature on an specific axial coordinate is 5%, Mears stablish the following criteria: (Mears, 1976)

Assuming in an arbitrary way that the deviation between two extremes of the film should be higher than 5%, it is possible to stablish the following criteria:

$$\Delta T = \frac{R_{v,A}^{obs}|\Delta H_r|(1-\varepsilon_b)(1-b){d_t}^2}{32\lambda_{er}} < \frac{0.05\, R{T_w}^2}{E_a} \qquad (2.33)$$

2.3.4 Pressure drops

According to Mears and Maestri (F. Maestri & Rota, 2005; Mears, 1976) in order to consider negligible the effect of the pressure drop**:**

$$\Delta P < 0.2\frac{P_{tot}}{n} \qquad (2.34)$$

2.4 Analytical Transport Phenomena Assessment

2.4.1 Methodology

To select a type of model to simulate the reforming reactor knowing which transfer phenomena limitation could not be neglected, it was performed a transfer phenomena assessment using the criteria explained in Section 2.3.

For the assessment, the pilot reactor geometry, the catalyst dimensions and the operative conditions projected for the experimental test were considered. The details about the catalyst remain confidential.

Table 2.1 Most relevant system parameter to the assessment

Parameter	unit	value
Reactor diameter (ID)	mm	4,75
Thermowell	mm	1,98
Reactor Length	mm	540
Reactor Length	mm	500
Catalyst	um	250-500
Inert material	um	210
Temperature	K	653
Pressure	Pa	1256
Volumetric Flow	$[m3/s]$	1,117E-06

The viscosity and the thermal conductivity of the gas mixture (hydrogen, methylcyclohexane and toluene) were calculated through the Wilke Method (Fairbanks & Wilke, 1950) which represents a simplification of the rigorous kinetic theory approaches based on Chapman and Enskog law (Reid, Prausnitz, & Poling, 2001) , tested for polar gas mixtures (Mathur, S., Saxena, 1966) and extensibility described in the literature by different authors (Bird, R., Stewart. W., Light, 1960; Reid et al., 2001).

The different binary molecular diffusivities were calculated following the Brokaw method for polar mixtures (Brokaw, 1969) based on the Stockmayer potential (see appendix). The methylcyclohexane molecular diffusivity in the mixture was calculated using the Stefan-Maxwell equation (Reid et al., 2001). For the effective diffusion of methylcyclohexane was considered to use both the molecular and the Knudsen diffusion according with the Caretto's formula. (Caretto, 1963; Krishna & Wesselingh, 1997).

$$D_{e,p} = \frac{\varepsilon_p/\tau_p}{\frac{1}{D_{A,m}} + \frac{1}{D_{A,K}}} \qquad (2.35)$$

The mass radial dispersion coefficient was calculated using the empirical correlations proposed by Delgado in 2005 and 2007 in which they study the dispersion in porous media and its correlation with the Smith and Reynolds numbers (De Carvalho & Delgado, 2005; Delgado, 2007). To the obtained value was applied the *Kulkarni et al.* correction for the radial variation of the radial Peclet number. (Kulkarni & Doraiswamy, 1980).

The fluid dynamic regime according to this correlation seems to be just in the limit between the pure diffusion regime and the mechanical dispersion regime.

$$\frac{1}{Pe_{m,r,p}} = \frac{\varepsilon_b}{\tau_b \, Re \, Sc}\left(1 + \frac{1}{2.7e{-}5 \, Sc \, \frac{12 \, \varepsilon_b}{\tau_b \, Re \, Sc}}\right) \qquad 1 < \frac{\mathrm{Re\ Sc}}{\varepsilon_b} < 1600 \tag{2.36}$$

$$Pe_{m,r,p} = \frac{u_o d_p}{D_{er}} \tag{2.37}$$

The mass axial dispersion coefficient was calculated using the model proposed by Tsotsas & Schlünder in 1988 in which they study the effect of axial dispersion in packed bed reactors and correlate it with several flow scales (Evangelos Tsotsas & Schlünder, 1988).

$$\frac{1}{Pe_{m,a,p}} = \frac{1}{\tau_b}\left(\frac{1}{PE_{ax}} + \frac{\varepsilon_b(1-\xi_c^2)}{Re \, Sc}\right) + \frac{1}{32} D_h^2 \left[PE_{rad} \, \xi_c^2 \, (1-\xi_c^2)^2 + \frac{Re \, Sc}{\varepsilon_b} \, 4 \, \xi_c^2 - 3 - 4Ln(\xi_c) - \xi_c^2 \right] \tag{2.38}$$

$$\frac{1}{PE_{ax}} = \frac{\varepsilon_b \xi_c^2}{Re \, Sc} + \left(\frac{1}{1.14(1 + \frac{\varepsilon_b \xi_c^2}{Re \, Sc}}\right) \tag{2.39}$$

$$\frac{1}{PE_{rad}} = \frac{\varepsilon_b \xi_c^2}{Re \, Sc} + \frac{1}{8} \tag{2.40}$$

$$\xi_c = 0.2 + 0.21 \exp(2.81(\log(Re) + 1) \tag{2.41}$$

$$D_h = \frac{2\varepsilon_b}{3(1-\varepsilon_b)} \tag{2.42}$$

$$Pe_{m,a,p} = \frac{u_o d_p}{D_{ea}} \tag{2.43}$$

The J-h and J-m transfer factor, introduced by Colburn (Colburn, 1933) and extended to mass transfer by McCune (McCune & Wilhelm, 1949) where obtained through the packed bed correlations developed by *Wakao et al.* (Yagi, Kunii, & Wakao, 1960) for the heat transfer case and Dwivedi (Dwlvedi & Upadhyay, 1977) for mass transfer. With these transfer factors the Nusselt, Sherwood and the interphase transfer coefficients were obtained.

$$\varepsilon_b\, j_m = \frac{0.765}{Re_p^{0.82}} + \frac{0.365}{Re_p^{0.386}} \tag{2.44}$$

$$\begin{cases} j_h = \dfrac{2}{Re_{\,p}\mathrm{Pr}^{1/3}} + \dfrac{1.1}{Re_p^{0.4}} & (2.45) \\ \\ Nu = 2 + 1.1\, Re_p^{0.6}\, \mathrm{Pr}^{1/3} & (2.46) \end{cases}$$

Since the 1D heat model is suitable for this case, the effective heat transfer coefficient was calculated using the correlation developed by *Tsotsas et al.* (E. Tsotsas & Schlünder, 1990).

$$\overline{\mathrm{Nu}_{er}} = \frac{h_e d_t}{\ddot{\lambda}_{er,0}} = C_f \sqrt{5.78^2 + \frac{4}{pi} GZ} \tag{2.47}$$

$$C_f = 1.6 + 0.13 \ln\left(\frac{5}{GZ}\right) \tag{2.48}$$

$$GZ = \frac{\lambda_f}{\ddot{\lambda}_{er,0}} \frac{Re\,\mathrm{Pr}\, d_t^2}{h_b\, d_p} \tag{2.49}$$

$$C_f = 1.6 + 0.13 \ln\left(\frac{5}{GZ}\right) \tag{2.50}$$

$$\frac{\ddot{\lambda}_{er,0}}{\lambda_f} = \varepsilon_b \left(1 + \beta \frac{d_p \alpha_{rv}}{\lambda_f}\right) + \frac{\beta(1-\varepsilon_b)}{\frac{1}{\frac{1}{\frac{1}{\phi}} + \frac{\alpha_{rv} d_p}{\lambda_f}} + \frac{\gamma}{\kappa}} \tag{2.51}$$

$$\alpha_{rv} = \frac{4\sigma}{1 + \frac{\varepsilon_b}{2(1-\varepsilon_b)} \frac{1-e}{e}}\, T^3 \tag{2.52}$$

$$\alpha_{rs} = 4\sigma\, \frac{e}{2-e} T^3 \tag{2.53}$$

The radial porosity profile was calculated taking into account the presence of the thermowell, which occupies an important portion of the inner reactor zone. The correlation developed by *Mueller et al.* was used (Mueller, 1999).

For the pressure drop, the classical Ergun equation was used (Ergun & Orning, 1949). In the figure 2.16, it can be observed that the void fraction is higher closer to both walls.

$$\varepsilon_r = \varepsilon_0 + (1 - \varepsilon_b)\, J_0(\alpha r^*) \exp(-\beta^* r) + J_0[\alpha^*(R^* - r^*)]\exp[\beta(R^* - r^*)] \tag{2.54}$$

$$\alpha = 6.64 - 6.1exp(-R^*)$$

$$\beta = -0.69 - 0.015(R^*)$$

$$\varepsilon_0 = 0.456 - 0.3exp(-R^*) \tag{2.55}$$

$$r^* = \frac{r}{dp} \tag{2.56}$$

$$R^* = \frac{d_{t,e}}{2dp} \tag{2.57}$$

2.4.2 **Results**

The figure 2.16 shows the theorical shape of the radial porosity profile inside the reactor. As expected, the porosity grows close to the wall. According to the particle diameter to reactor radio diameter and the porosity distribution, preferential channels along the reactor could exist

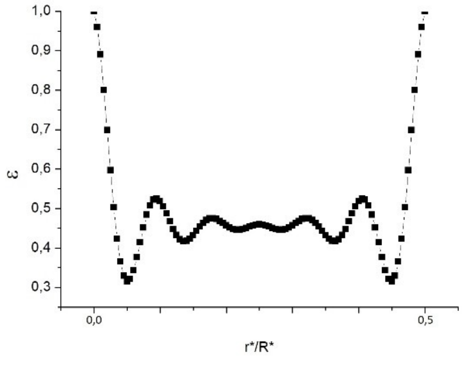

Figure 2.16 Calculated porosity radial profile

For greater values of the Reynolds number in this system, the Peclet number practically does not change until the pure mechanical dispersion (see figure 2.17). It is of course desirable to fix the test conditions to have the less possible dispersion on the system to simplify the system flow model.

The value of the radial mass Peclet number is about 2 and axial one is about 11(both for the particle), which indicates almost fully developed flow and practicably negligible axial and radial dispersion (Aris & Amundson, 1957; James J Carberry, 1958; McHenry & Wilhelm, 1957) which is still confirmed by the bode number which is about 785.

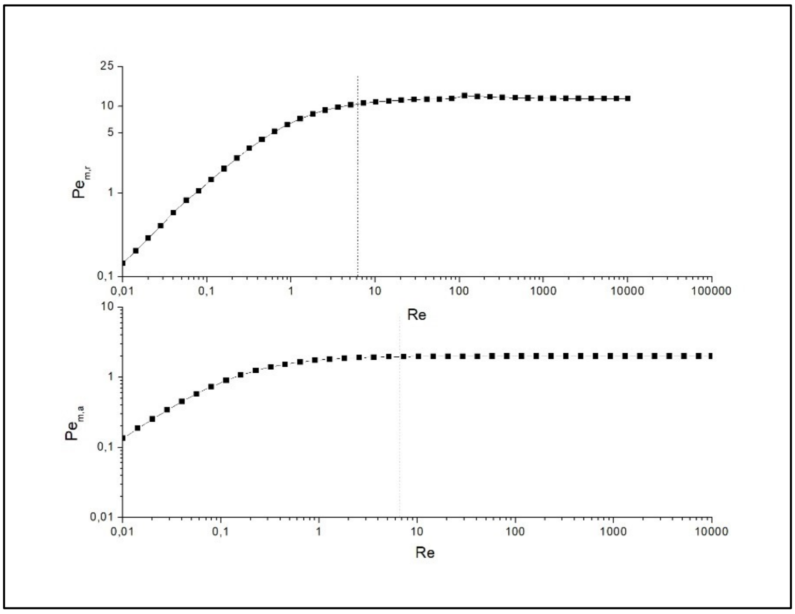

Figure 2.17 Radial and Axial Mass Pleclet's numbers results

Dispersion

The axial dispersion criterium is satisfied as the calculated value for the system is very superior to the minimum value. The axial dispersion can be neglected (Mears, 1971b). (See Table 2.2)

Table 2.2 : Axial dispersion criteria

Parameter	Units	Value
hbed /dp *	[adim]	1,18
hbed /dp	[adim]	401,54

The Berger radial dispersion criterium (R. J. Berger & Kapteijn, 2007)which considers the conversion is satisfied. However, the Mears criterium is not (Mears, 1971b) . This result is taken with precaution. The radial dispersion can be neglected with precautions. There exists the possibility of having channeling. (See Table 2.3)

Table 2.3: Radial dispersion criteria

Parameter	Units	Value
dR /dp*	[adim]	8,00
dR /dp	[adim]	5,52
Berger * *	[adim]	0,33
Berger	[adim]	0,25

The Mears's criterium (Mears, 1971b) is largely satisfied. The radial heat transfer limitation into the bed can be neglected. (See Table 2.4)

Table 2.4 : Radial heat transfer limitations criteria

Parameter	Units	Value
ΔT**	[K]	0,88
ΔT	[K]	1,07E-2

External Transfer limitation

The resistance due to external mass transfer is much less than 5% of the resistance due to chemical reaction since the Ca is very under its limit value (Mears, 1971b). (See Table 2.5)

Table 2.5: External mass transfer limitation criteria

Parameter	Units	Value
Carberry's number** (Ca)	[adim]	0,050
Carberry's number (Ca)	[adim]	5,343E-06
Efficiency		≈ 1

The Mears's criterium (Mears, 1971b)is satisfied. The heat transfer limitation through the pellet film can be neglected. (See Table)

Table 2.6 : External heat transfer limitation criteria

Parameter	Units	Value
| DT(film) |**	[K]	0,88
| DT(film) |	[K]	8,4E-04

Intraparticle transfer limitation

There is no evidence of internal mass transfer limitation. The Weisz-Prater modulus is under its limit value . (See Table2.7)

Parameter	Units	Value
Weisz-Prater modulus (ϕ)*	[adim]	0,08
Weisz-Prater modulus (ϕ)	[adim]	8,31E-05

Pressure Drop

The pressure drop is under the maximum recommended value for catalytic tests. (See Table 2.8)

Table 2.8: Recommended pressure drop

Parameter	Units	Value
ΔPcat**[Pa]		251286
ΔPcat [Pa]		1693

2.4.3 Conclusion

Since there is no evidence of transfer limitations of any kind, the plug flow model is selected in order to simulate the reactor and perform the study.

2.5 Methodology to study the thermal profiles effect on the conversion

2.5.1 Deviation Parameter

The deviation caused to system by the thermal profiles was quantified in terms of chemical conversion. The conversion that would be obtained in an ideal isothermal test was compared to the conversion obtained in the case of the existence of the thermal profiles.

2.5.2 Analyzing the shape

From experimental thermal profiles taken from the archived data from different pilot plants, the shape of the profiles was analyzed. The profiles shapes are tightly related to the type of control system and heating technology installed in the pilot plant. Generally, the heating system is composed of thermal shells that surround the reactor and that are heated by means of electrical resistances place within the shells.

There are temperature sensors along these shells. There are three type of sensor in there:

1- Sensors measuring the temperature of the electrical resistance.
2- Sensors measuring the temperature of the external reactor’s wall.
3- Sensors measuring the temperature of the external reactor’s wall used to perform the control action.

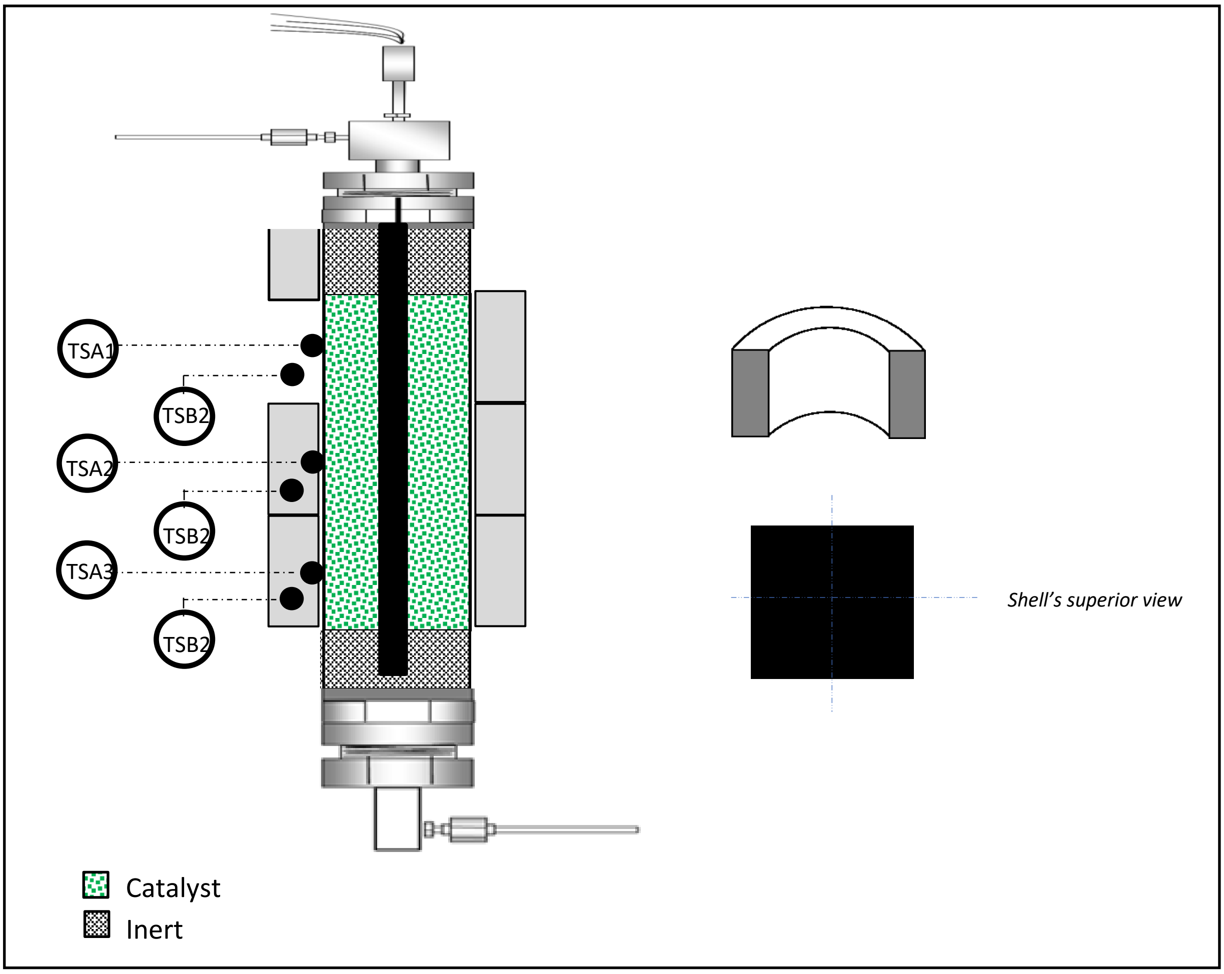

Figure 2.18 Reactor example scheme

According to to the number of shells, the control system can be programmed to control the temperature using the sensors in one or several particular shells.

On internal research documents, there are reports into which is underlined the presence of very soft thermal profiles in tests with empty reactors with a maximum overshoot of 2°C. Which clearly suggest that the prominence of the thermal profile is caused influence also by the control system element and possibly the non-homogenous composition of the shells materials.

If it is looked at the point into which the thermal profile crosses the set the taargeted temperature, can be seen that in that pretty close to that point there is a temperature sensor. With this observation in mind, the behavior of this profiles can be described as follows:

- At the entrance of the bed, the temperature inside decays importantly, because of which the control system increases the heating power.
- The power will be increased until the sensor's temperature match with the set targeted temperature.

- As a result of the power increment, the temperature in the next shell is clearly very superior to the targeted temperature, and the control system acts decreasing the power until the temperature in the point where the sensor is placed match with the operative temperature.

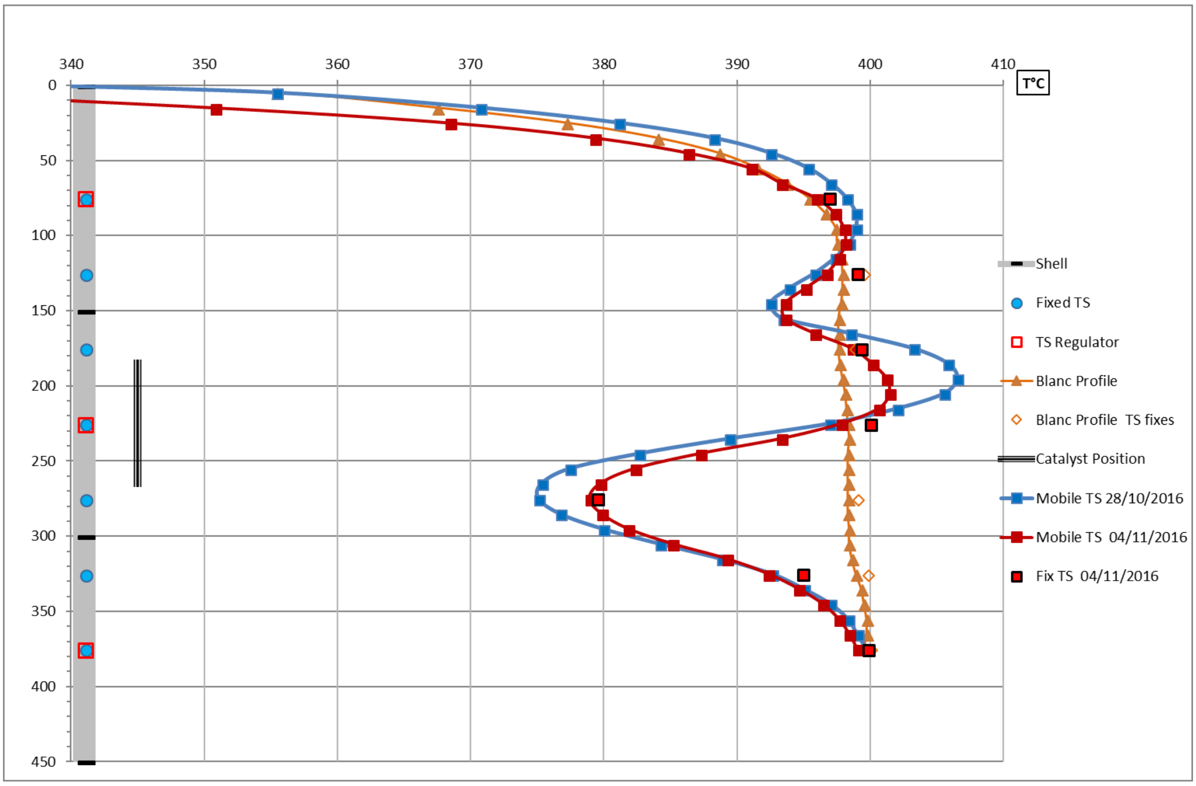

Figure 1.2 . Experimental Thermal Profiles

The undershoot magnitude decreases as the reaction advances. It is totally logical since the reaction heat decreases with the deployment in the reactive concentration. So, the profiles have a sinusoidal behavior with constant wavelength (distance between the sensors) and decreasing amplitude.

2.5.3 Profile modelling

Having enough qualitative information, it was decided to impose the axial thermal profile instead of predicting it.

The desirable characteristics to simulate the shape of this profiles in a realistic and advantageous way are:

- Wave behavior
- The shape of the wave must be easily and technically deformable.
- Normalized area

The mathematical functions that have already two of those three characteristics are the statistic distributions. The waved behavior can be produced by extending the function and the lower section of the waved can be obtained by multiplying by a negative operator the function.

$$f(x) = \frac{\Gamma(\alpha+\beta)}{\Gamma(\alpha)+\Gamma(\beta)} x^{\alpha-1}(1-x)^{\beta-1} \qquad \alpha \geq 0 \qquad \beta \geq 0 \tag{2.58}$$

After the test the different statistical distribution, the chosen one was the beta distribution. The beta distribution is applied to model the behavior of random variables limited to intervals of finite length. Changing the **α and β it is possible to modify in a tremendously easy way the shape.**

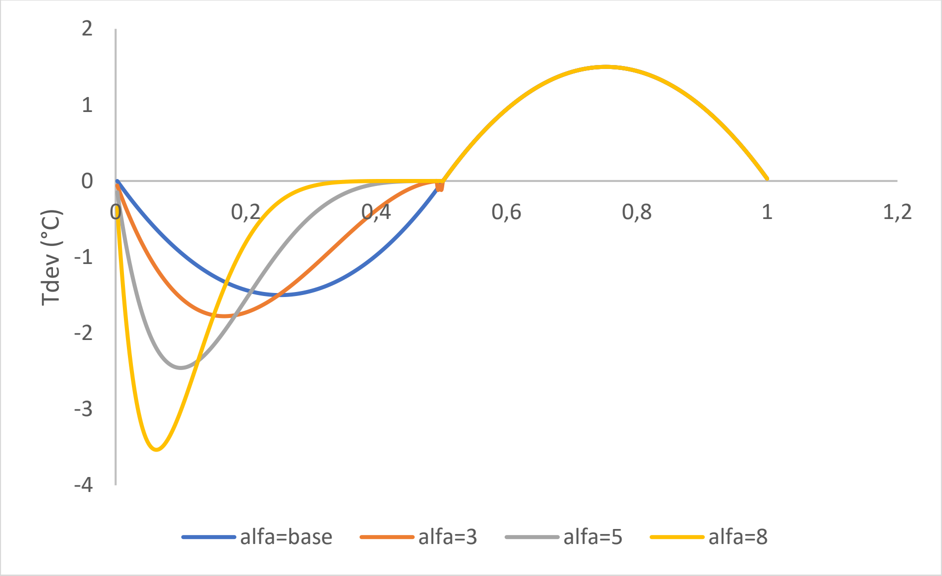

Figure 2.19. Profiles Shapes along the reactor for different alfa values

To make correspond every point of the simulated profile to a position along the reactor, the length of the reactor was normalized.

2.5.3 The concept area

The conversion deviation is affected by two intrinsic variables to the thermal profiles. One is the deviation temperature magnitude and the other one the extension of the reactor along that temperature persists. Usually, the conversion calculation is approached from the integral calculus. However, on the field, there is not yet the possibility to measure continuously all the temperature Even is the profile is known, sometimes, the kinetics of the reaction is not well known. Consequently, it is very hard to calculate exact deviation between the isothermal conversion and the real conversion for every case.

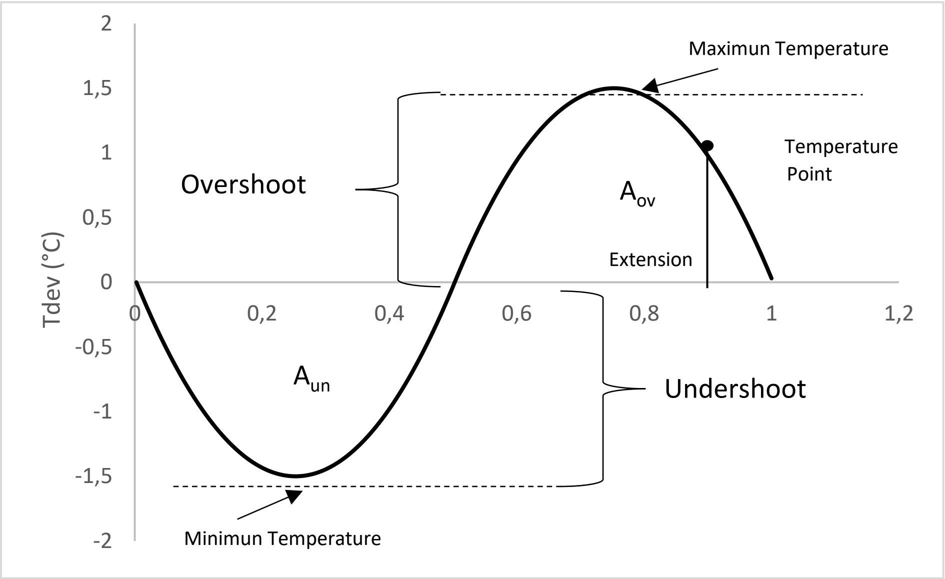

Figure 2.20. Profile model description

The magnitude of the area under the curve belonging to the overshoot and the undershoot considerate separately can express a magnitude that correlates the value of the temperature and position inside the reactor that corresponds to that temperature.

To develop a methodology to estimate the conversion deviation based on the profiles area can be very useful.

For this work, an unity of Aov or Aun is defined as a peak with 0.5 unities of area and a maximum/minimum of 1.5 or -1.5 degrees (according to the case)

2.5.4 Computational simulation

A computational simulation will be created to test different scenarios. The elaboration of the computational simulation allows to test different scenarios and to analyze how the system reacts to modifications on the operation paraemters. Different model for the adiabatic reactor design and determination of kinetics parameters have been done before for this reaction (Touzani, Klvana, & BÉLanger, 1987; Usman, Cresswell, & Garforth, 2014), however none of them have the same area concept designed for this work.

The isothermal conversion and the conversion obtained with the thermal profiles will be registered in order to calculate their relative and the absolute deviation. The relative deviation will be considerated without the application of the module since a negative deviation has a physical sense that can deliver important information.

The effect of the following parameters on the deviation will be studied:

Profile Shape
Profile extension and maximum temperature deviation within the profile
Temperature
Pressure
Weightily Hour Space Velocity (WHSV)

Hydrogen to Hydrocarbon Ratio (HHR)

Table 2.9: Operation Variables

Variable	Units	Fixed Values	Ranges
T	°C	385	370-420
P	bar	10	3-25
WHSV	h-1	10	10-30
HHR	mol/mol	3	2-25

2.5.5 Compilator

Through the wide universe of programming software, Matlab® was selected. It is an easy language handled compilator with a lot of pre-defined functions that is also commonly used; which left available an important database for users.

Matlab® also contains graphical and statistics suites that facilitate the processing and analysis of the results.

2.5.6 Modeling Assumptions

Based on the conclusions of the section 2.4:

- The absence of axial and radial dispersions.
- There are no preferential channels.
- At the entrance of the catalytic bed, all the flow is in the gas phase and there are no entrance effects.
- There is not coke formation.
- The methylcyclohexane is considered pure.
- The hydrogen is considered as pure.

2.5.7 Reforming Reactions

The chemical reaction programmed will considerate:

- The kinetic equation.
- The equilibrium constant for every different case.
- The change of volume

2.5.8 Programming code

The basic programmed code executes the following actions:

- Read the entries
- Normalize the entries
- Generates the profiles
- Calculates the fluid properties
- Calculates the reaction properties
- Calculates the equilibrium constant
- Calculates the isothermal conversion
- Calculates the profiles conversion
- Generates the exit

The more specific functions explained after are more complex version of this code but always with this as the nucleus.

2.5.9 Sensibility Analysis

The impactof physical or chemical systems depends on the values of the parameters that control these systems. The analysis of the system response varying these parameters is called parametric sensitivity. The use of the parametric sensitivity applied to chemical reactors was introduced by Bilous and Amundson (Bilous & Amundson, 1956).

In the context of this study, the variable of interest is the deviation caused by the thermal profiles on the conversion. The process consists in quantifying the variation of the deviation of the reactor following variying the process parameters (Temperature, Pressure, WHSV, HHR, Activation Energy, Profiles Shapes….).

In order to able also to compare the sensibility to the different parameters varied, the concept of the normalized sensitivity is approached.

$$s(\delta, \phi_j) = \frac{\phi_j}{\delta}\frac{d\delta}{d\phi_j} \tag{2.59}$$

The study is done along the full range of possible conversions to have a better look of the situation.

2.5.10 Maximum Tolerated Deviation Function

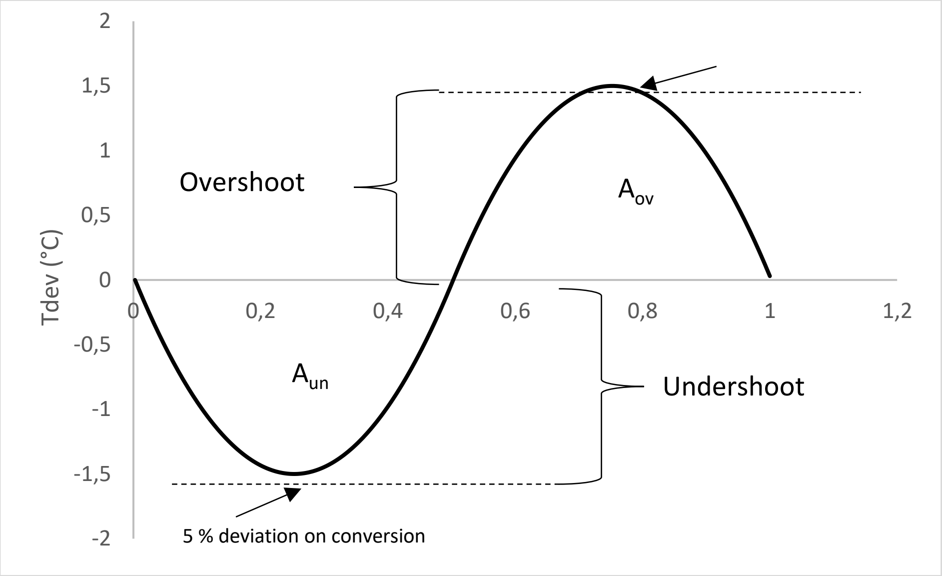

Figure 2.21. Profile model description for five percent deviation

In this computational function, a study about how big and extensive the temperature deviation in order should be to overcome a five percent deviation in terms of conversion. Cases with different temperatures, weight hour space velocity, Pressures, HHR and shapes of the profiles were evaluated.

2.5.11 Zero Deviation Case

It is normal to think that must exist a quantity in overshoot area (A_{ov}) that can compensate the deviation caused by the undershoot in terms of area (A_{un}).

In this computational function, the compensation relation between A_{ov} and A_{un}, is made.

2.5.12 Mathematical Model

Once the analysis of the results coming from the different created functions was performed and the kind of response between the different parameters was identified, a set of 12^6 point was generated covering a broad band of conditions with ranges.

Taking in to account the area concept that was previously developed, different multiple regression was performed an evaluated. The best one was defined as the response model.

To make the statistical analysis a Minitab 18 ® was used.

2.6 Results

2.6.1 Sensibility analysis

The sensibility was done considering a system with a negative undershoot with a 1/3 in overshoot area to reproduce the normal positive overshoot associated with a control system for this case.

During the process, an important quantity of information was generated. Here are just presented some useful examples. The complete set of graphics can be found in the appendix of this work.

A careful analysis was done to impose a set of conditions as far as possible from the equilibrium limits, which can be expanded or constrained (or both) along the reactor due to the presence of the thermal profile.

a. Profiles effect

The effect of an overshoot is exponentially bigger than the undershoot effect due to the relation between the temperature and the reaction rate.

In the figure 2.22, is shown a 3D graphic that shows how the deviation varies according to to different overshoots and undershoots areas for a set of conditions. A more pronounced slope is the product of the intersection between the surface and a generic plane having a direction perpendicular to the Aov axis. Also, as Aun decreases, the slope increases, which shows that in those conditions, the deviation grows faster with the change in Aov.

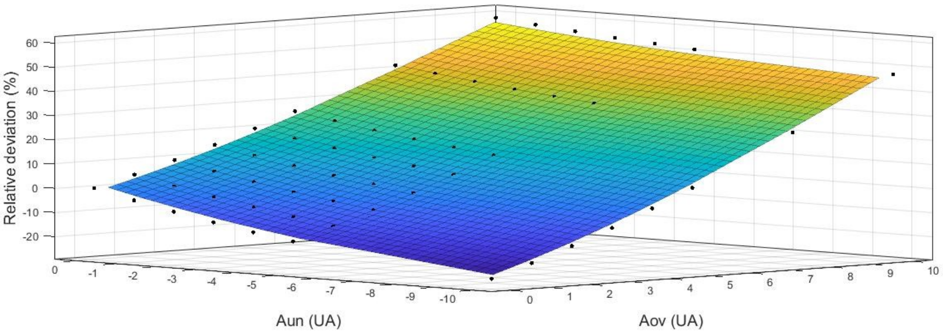

Figure 2.22 Surface plot of the deviation as response for undershoot and overshoot areas

This states clearly that there is not exist a fix rapport between the two to have a zero-deviation o any other fixed deviation value.

The figure 2.22 shows a lateral view of the generated surface, which presents a degree of contortion that corresponds clearly with the change in the reaction rate when the Arrhenius term increases (compare with Fig 2.23), due to the increment in the activation energy.

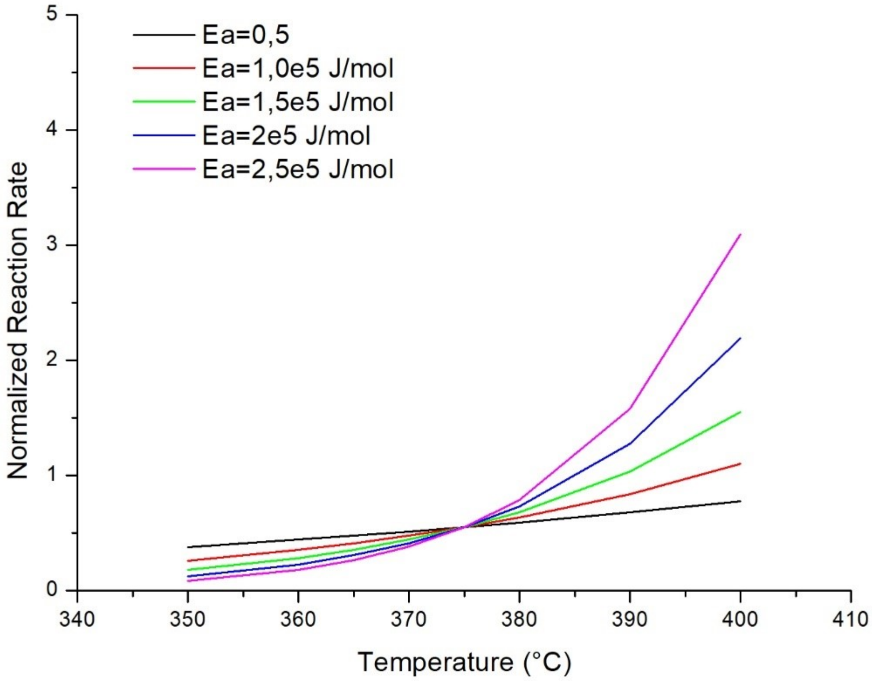

Figure 2.23 Normalized reaction rate as function of the temperature for different activation energy values

A normalized sensibility analysis was done to study the deviation (from now on, the noun deviation will be used exclusively to talk about the relative deviation of the conversion caused by the profiles respect to the isothermal conversion) caused by different undershoot levels as the overshoot varies for a fixed isothermal conversion value of X=0.5.

In this analysis, it is possible to explode the sign of the sensibility and the relative deviation. A negative deviation means that the thermal profile causes a conversion under the isothermal conversion and a positive one that the conversion caused by the profile is over the isothermal conversion.

The figure 2.24 starts from 1 since it is a normalized sensitivity. There is a fast section into which the effect of the undershoot it is still relevant compared with the overshoot effect. Through this fast section, the effect of the overshoot grows until it became bigger that the undershoot contribution to deviation and the sensitivity changes sign. As the overshoots continue to grow, eventually the effect of the undershoot becomes negligible and the behavior of the curve is exponential and intrinsic of the overshoot.

As $\mathbf{A_{un}}$ is bigger, it takes more $\mathbf{A_{ov}}$ to compensate the effect of the undershoot, which can be appreciated looking at the shifting of the curve to the right as the undershoot level increases.

The presence of a deeply marked undershoot can put in play the effect of the equilibrium, causing important deviations.

The presence of thermal profiles can affect importantly the conversion at the outlet of the reactor when the reaction has a high activation energy. Because of this, attention must be paid to this factor when the heat of reaction is also high.

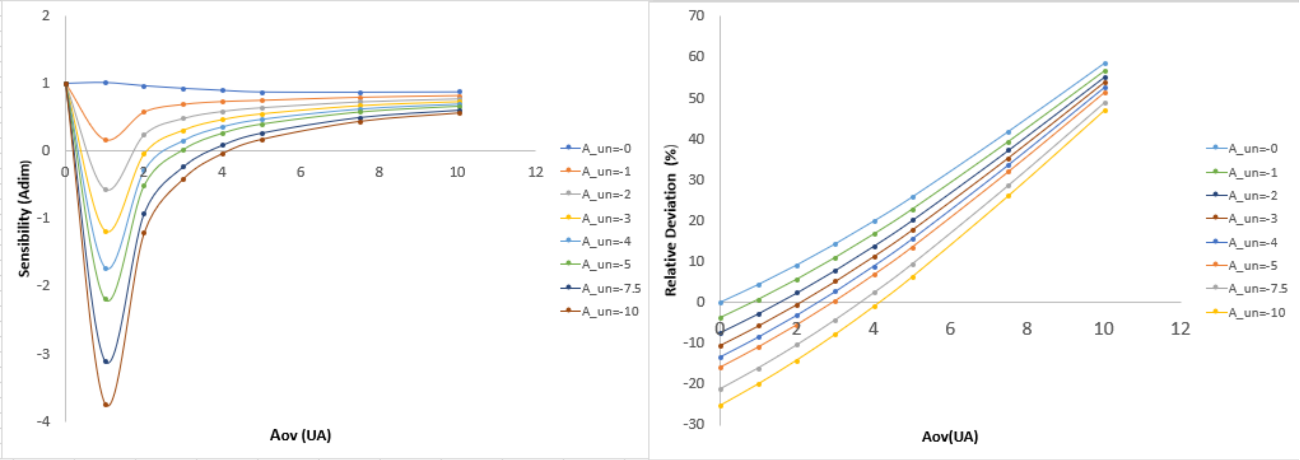

Figure 2.24 Sensibility of the deviation as the overshoots increases for different Undershoot levels

b. General sensibility analysis

The sensibility of the deviation increases mainly with the operative temperature, the pressure, and the activation energy. Meanwhile, the space velocity and the H/HC ratio play a secondary role as the deviation is less sensitive to this parameter which does not mean it is unaffected by those.

All the operation parameters studied affect the deviation, mainly the temperature and the pressure.

The pressure effect is important due to the reaction is done in gas phase, so the pressure is tied to the concentration.

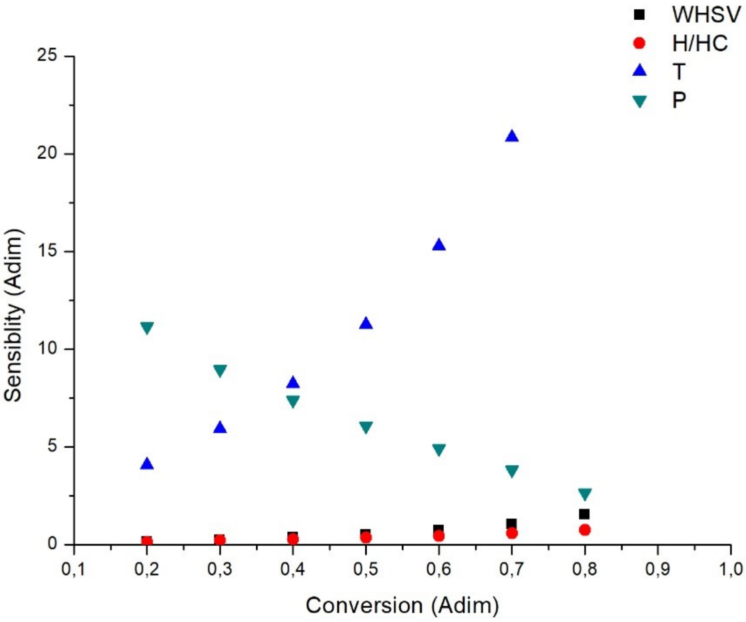

Figure 2.25 Sensibility of the deviation to the different parameters

The activation energy, as was always stated, define the sensitivity level of the reaction rate to the temperature, which directly affects the deviation associated with the temperature profiles.

The evaluation of the sensibility along the complete range of conversions allows to see also its implication on the deviation.

The conversion is related to studied parameters as it is well known in the literature already. Just for clearance, as the activation energy, the pressure, the H/HC ratio or the spatial time increases, the conversion also does it. On the other hand, if the temperature increases, the conversion also does it.

Different simulations were done changing a parameter and measuring the deviation for the different levels of a third parameter in order to the evaluate also the relation between those two independent parameters. Let's call the variable that changes of level, primary variable "PV" and calls secondary variable "SV" to the variable that changes in order to reach the desired conversion.

For all the possible set of variables considered A larger relative deviation will be obtained at the lowest conversion. It is possible to attribute it to two reasons:

1. Numerical: As the isothermal conversion value is smaller, little variations on the targeted value cause important relative errors.

2. Absolute deviation: The absolute deviation is bigger at low and high conversions, generating a minimum for medium conversions. A high absolute deviation at high conversion is due to the equilibrium effect.

At high conversions, the relative error decreases even if the absolute deviation increases because the magnitude is bigger.

If a lower conversion is set for the test, the thermal profile will have a bigger impact on the error.

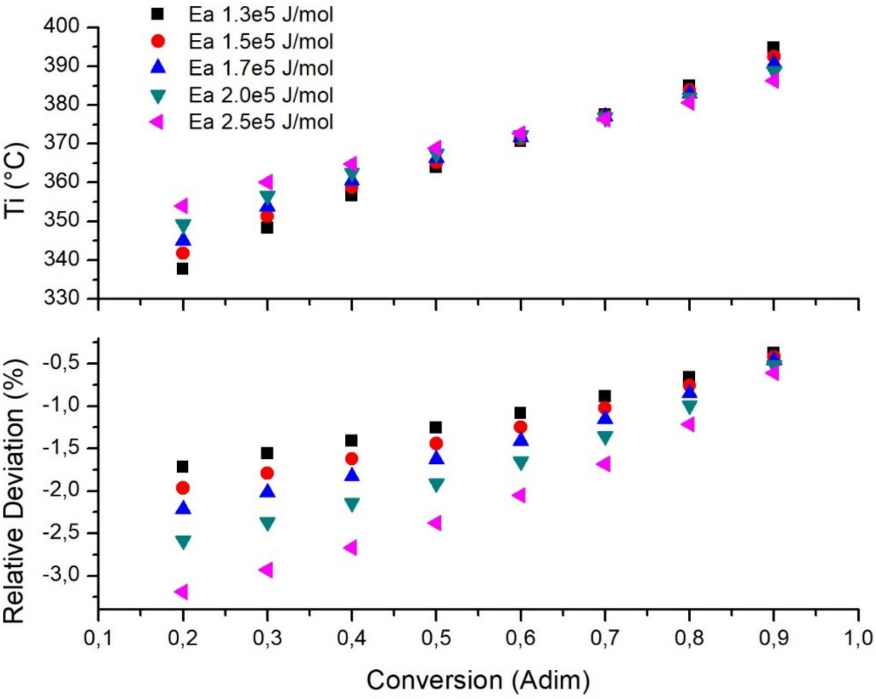

*Figure 2.26 (*a)Conversion for different temperature values and different activation energy levels.
(b) Relative deviation values for the condition evaluated in *(a)*

For different levels of activation energy PV , as this variable increases, the deviation always (for all the considered variables) increases with a behavior that recalls an inverse exponential.

Instead of, when the temperature and the pressure are considered as PV, the deviation decrease as those increase both exponentially. For the temperature, it can be easily explained considering the range amplitude of the thermal profile, which offers two contributions.

- As the temperature of the test is higher, a undershoot could influence less the deviation. The velocity of the reaction in the minimum point of the set off is every time less comparable in magnitude to the reaction rate in the points closer to the operative temperature. A simple analogy can be done in order to understand the phenomena: let’s imagine ten particles carrying a low-level quantity of energy moving in one dimension, this particle will collision elastically with an object at the same time. As all of them are carrying a low quantity of energy, every particle will affect importantly the final energy level of the object (the sum of every contribution). Let’s now think that the particles are carrying a distribution of energy similar to the negative set off of our thermal profile that increase exponentially as the initial position coordinate increases. The effect of the particle with the lowest level of energy will be every time less important as the initial position coordinate increases. This phenomenon could be approximated to have a negative set off every time less pronounced as the temperature of test increases.
- The second contribution is related to the overshoot, which (following the same logic of the first contribution) will compensate every time more the negative deviation caused by the undershoot. Of course, at the certain point, the contribution to the

deviation offered by the positive set off will be greater, causing a positive deviation (crossing the zero-deviation point).

For the pressure case, the reason for this behavior is the equilibrium. As the pressure increases, the system has conversions that are closer to the equilibrium; under these conditions, an overshoot can push over the equilibrium limit causing even positive deviation.

When the space velocity was fixed as PV, it does not affect the deviation when the H/HC ratio and the temperature variates along the conversion range.

From the Figure 2.24 , a very important conclusion can be done, more attention must be paid to an overshoot than an undershoots in terms of relative deviation.

2.6.2 Zero Deviation function

As was stated before, a fixed ratio of Aov/Aun does not generates a unique value of deviation. Through the zero-deviation function, it was possible compared the requested area under different conditions to annulate the deviation.

Can be concluded, reasoning with the results of the two previous sections, that the Aov/Aund compensation ratio will be always between 0 and 1. Besides, typically, this value will be between 0.4 and 0.8. Using this results, a rule of thumb can be established.

Agreeing with the previous analysis, changes in the operative variables can vary the necessary ratio to compensate the deviation. As the conversion decreases, the ratio also increases for any case.

As the activation energy increases (PV), the overshoot area to take the deviation to zero will always increase. The same scenario was founded for the H/HC ratio, which is probably related to equilibrium.

If a system with and fixed Aov and Aun with a negative deviation is studied, as the targeted temperature increases, the negative deviation decreases approaching to zero. But, if it is desired increase Aov until reach a zero-deviation, as the targeted temperature increases, the Aov required for the compensation will be higher. Once the zero-deviation is reached, as Aov increases, the deviation will grow faster as the operative temperature is bigger.

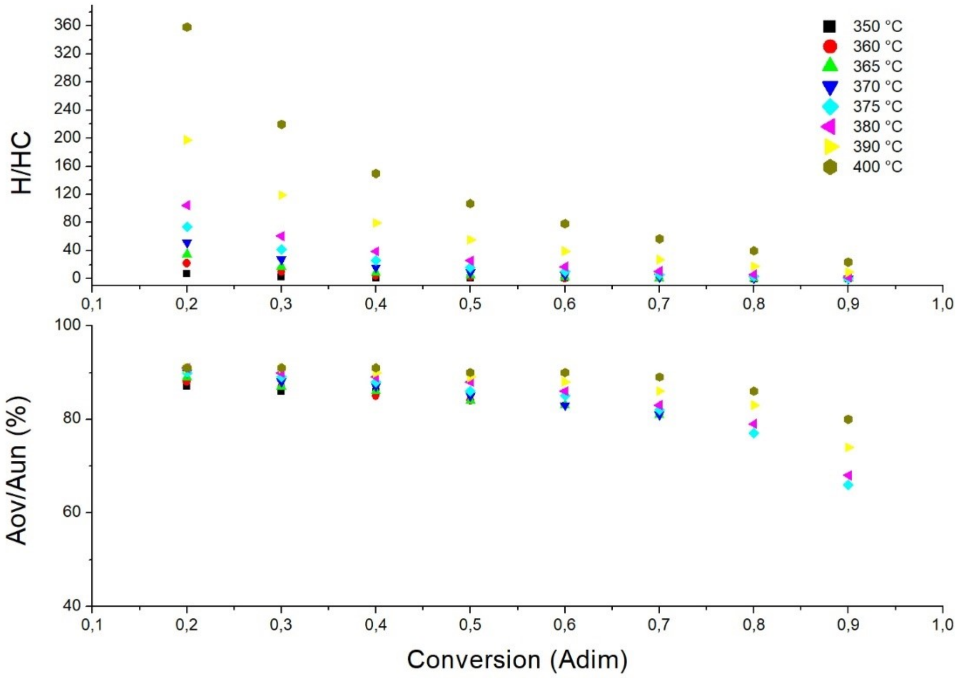

Figure 2.27 a) Conversion for different H/HC values and different temperature levels.
b) Overshoot/Undershoot area ratio that lead to zero deviation for the same condition evaluated in a)

For the pressure fixed as PV, as the pressure level is higher, the required fraction for the compensation will be lower. This situation has an evident limit, the equilibrium. As the pressure increases, the system has conversions that are closer to the equilibrium. In this scenario, an overshoot can push over the equilibrium limit causing a positive deviation.

If the spatial time is fixed as PV, the fraction will decrease as the spatial time is lower, but its effect its direct effect on the fraction is very much smaller (as well the H/HC effect) compared with the temperature and pressures effects. The results are coherent with the initial sensitivity analysis.

2.6.3 Five percent deviation function

Knowing how the changes in the profiles, operative variables and some reactions intrinsic properties affect the deviation, the problem of a maximum allowed deviation can be boarded. The limit of five percent as a critical deviation was fixed arbitrarily.

According to the conversion value, the maximum Aun allowed (the value of Aun a takes the system to have a deviation of -5%) will vary. It decreases as the conversion value decreases also.

However, it is important to consider that the rate of the deviation in the negative sense caused by the undershoot is lower than the one cause in the positive sense by the undershoot. So, it is easier, to have a positive five percent deviation than a negative one.

This case can be observed even when Aov/Aund ratios lower than one for a medium temperature level (with respect to the equilibrium), high pressure and conversions over 0.5.

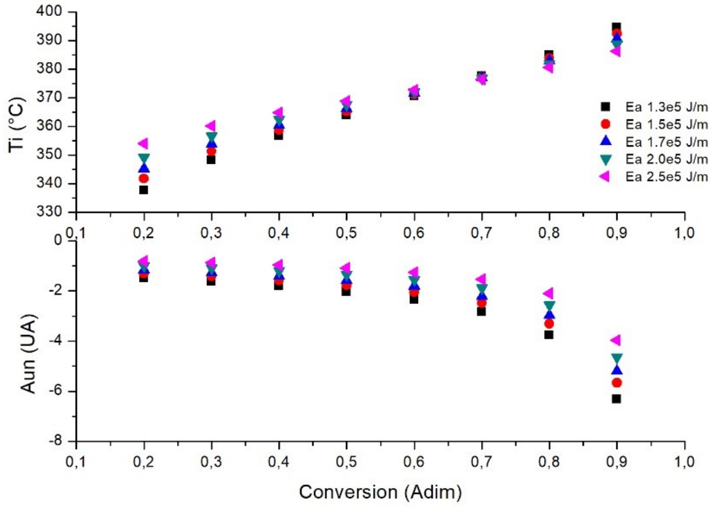

Figure 2.28 a) Conversion for different temperature values and different activation energy levels
b) Overshoot/Undershoot area ratio that lead to zero deviation for the same condition evaluated in a)

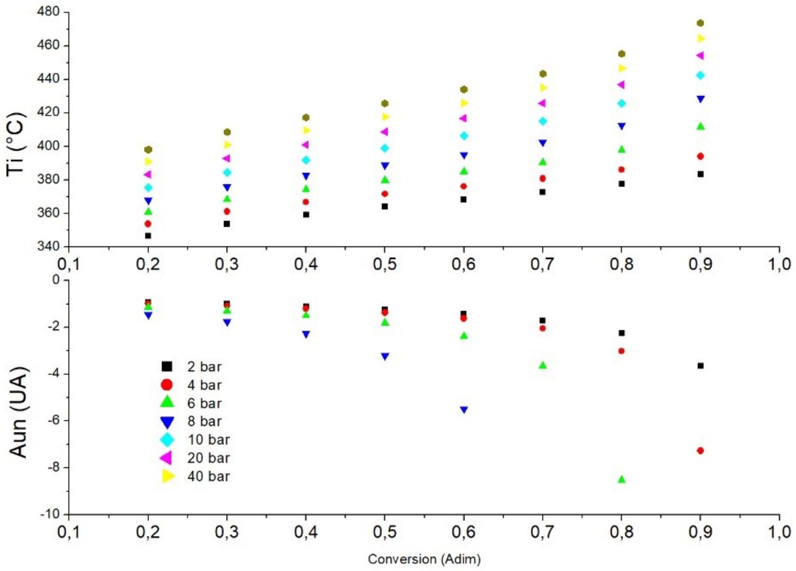

Figure 2.29 a) Conversion for different temperature values and different pressure levels
b) Overshoot/Undershoot area ratio that lead to zero deviation for the same condition evaluated in a)

2.6.4 Mathematical Model

The mathematical model was developed based on the area concept. The use of the areas as an input will allow making a fast estimation on the field.

$$\delta = a + b * \alpha + c * \beta + Ln\left(\frac{\frac{H}{HC}^{D} * whsv^{e} * P^{f} * Ea^{g}}{RT}\right) \tag{2.59}$$

Where:

δ Relative Deviation [%]

α Total Undershoot Area

β Total Overshoot Area

Table 2.9: Model statistical parameters

S	R-squa	R-square (Adjusted)	R-cuad (Predicted)
1.87	83.55%	83.53%	83.49%

The FIV value for all the parameter coefficients is 1 and a zero p-value, which means that there is statistical significance.

The great dispersion was observed for Aov and Aun over 10 basic units, which means for peaks over 15 degrees Celsius of deviation.

2.6.5 Contour Plots

Using the model is easy to generate contour plots that indicate the recommended operation zones, based in all the different parameters.

The worse conditions to operate are:

- High pressures: X/Xequi under 0.8.
- Low temperature: X/Xequi under 0.8.
- Aov/Aund > 0.9
- Aov/Aund <0.1
- Low coversions (X<0.4).

The recommended proportion of Aov/Aund is 0.5.

The figures 2.30-2.33 illustrates for a determined set of conditions, the operation zones in order to get a deviation under certain limit. This graph is extremely useful, since it allows to estimate the area that the thermal profile must have in order to obtain a certain deviation.

This curve gives two advantages:

- Estimate quantitatively if the thermal profile of the test will generate a deviation within the acceptable tolerance.
- Design the experiment in a more accurate way.
- Save the resources that would necessary in order to repeat the test until qualitative acceptable condition would be obtained.

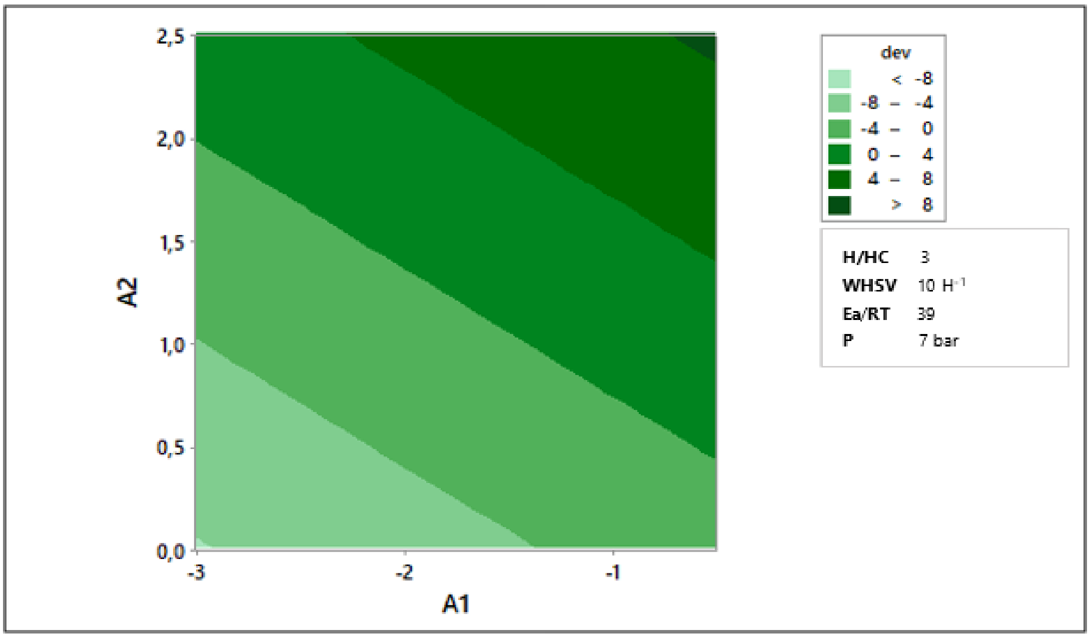

Figure 2.30. Contour Curve to identify a convenient operation points as a function of the areas

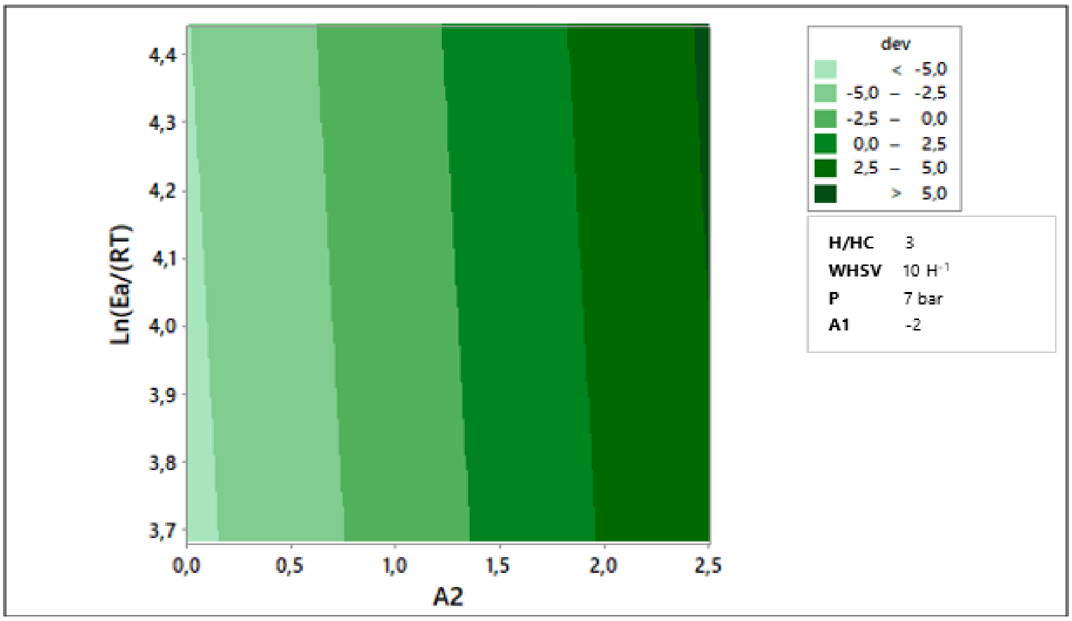

Figure 2.31 Contour Curve to identify convenient operation points as a function of the overshoot, the temperature and the activation energy.

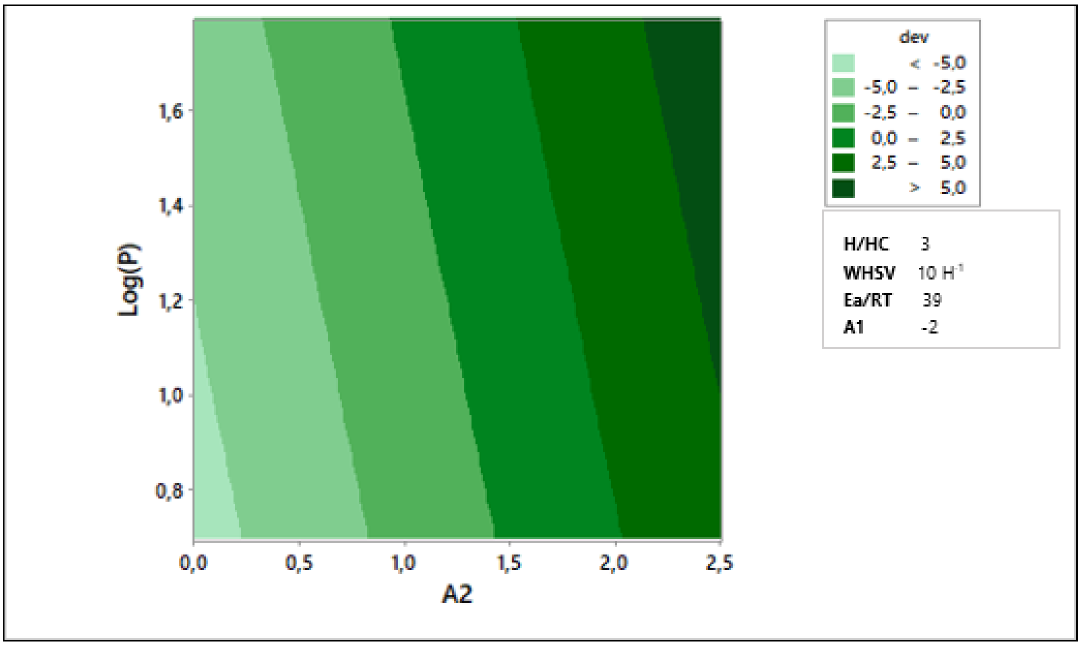

Figure 2.32 Contour Curve to identify convenient operations points as a function of the overshoot and the pressure

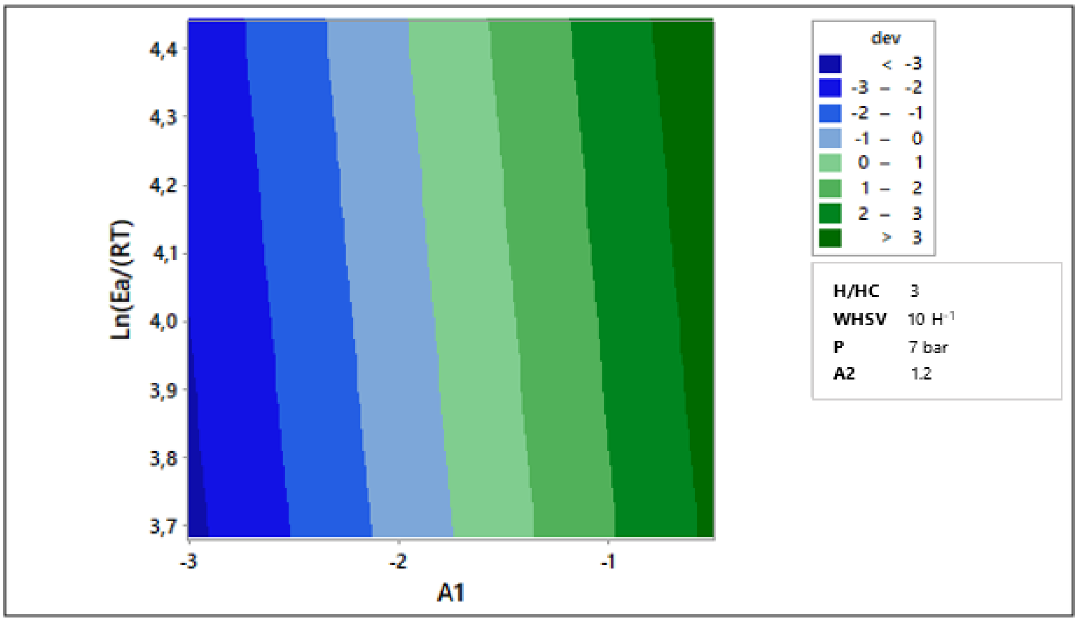

Figure 2.33 Contour Curve to identify a convenient operation points as a function of the undershoot area, the temperature and the activation energy.

A complete set of this operation diagram is available in the appendix section.

3. Experimental Verification

3.1 Objectives

1- Predefined thermal profiles are intended to be forced in a catalytic tubular reactor in order to verify the conclusions of the first section of this work.
2- The results will be confronted with the simulation and the mathematical model in order to verify also the accuracy of the both.

3.2 Start-Up of the Pilot Unit

To verify the previous analyses about the sensibility of the system, several tests was conducted in a pilot plant unit. At the same time, the veracity and usefulness of the model were tested.

A small pilot plant mechanically prepared and equipped for gas phase reactions was used for the test. This unit was revamped within the frame of this work to carry out reforming reactions.

3.2.1 Pilot Unit Description

The PID due to the important quantity of technical information remains confidential. A very simplified scheme of the unit is shown in the figure 3.1.

This pilot unit four different sections can be identified:

- Supply
- Reaction
- Analysis
- Separation

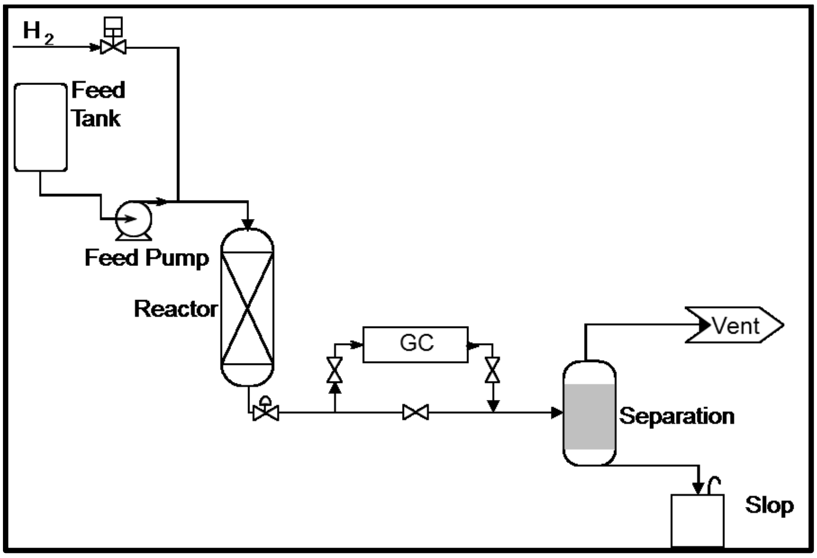

Figure 3.1 U855 Simplified Pilot Unit Scheme

In the first section, the liquid charged is stoked in a pressurize gas-sealed inox-steel vessel from where it is pumped to the reaction system by an HPLC pump. The hydrogen feed came from the utility system of the hall.

The reaction section is composed by a tubular reactor covered by a heating system conformed by eight independent and demountable shells disposed along the length the of the reactor, covering 80% of its external surface, each one equipped with a thermocouple. The whole reaction system is isolated through an isolating box. The heating power exerted by the shells is controlled through and SCADA control system and monitored remotely.

The reactor has an effective volume of 7,1 cm3. It is longitudinally traversed by a small thermowell. The gasification of the reaction mix is done at the initial section of the reactor, after of which the reactive mix enters in the catalyst section where the reactions occur.

The gas mix at the outlet of the reactor if conducted through an isolated-heated line directly to the gas chromatograph, which is equipped with an FID detector. After the analysis, the gas mix enters to a liquid-gas separator where the non-condensable fraction is removed and the condensable fraction can be recovered for the mass balance.

The system counts with several levels of security and it is totally automatized. The whole process and system variables can be monitored and changed remotely from the control room. The unit operated 24/7 with nocturn security operators.

The pressure in the unit is regulated using a back-pressure regulating valve placed before the gas analysis section.

3.2.2 System data acquisition

The acquisition of the information was made through a SCADA system and the data was handled using HISTORIAN ® .

With HISTORIAN ® it is possible to read the data acquired by the SCADA system in real time accessing to the value of the different sensors, historic data base and modify the sampling time.

3.2.3 Revamping

Several modifications were done to the unit in order to adapt it for the test. The main modifications were:

- Design an installation of a new reactor.
- Installation of a new liquid storage system.
- News pipelines and minor instrumentation functioning test.

3.2.4 Desulphurization

The reforming catalyst is severely affected by sulfur, which use to be reactive in the kind of test that used to be done in this particular unit. To guarantee the lowest possible sulfur content into the pilot, it was performed a desulphurization operation of the unit using cyclohexane as solvent until guarantee a level of Sulphur under 5 ppm in the outcoming solvent. The decreasing concentration in Sulphur is shown in figure 3.2

Table 3.1: Desulphurization conditions

P (bar)	15
T(°C)	250
Liquid Flow* (ml/min)	5
Gas Flow**(L/H)	15
Reactor Load	None
***Cyclohexane **Hydrogen**	

Cyclohexane was pumped through the system at 15 bar and 250 °C (conditions to maintain the cyclohexane in the liquid phase). Downstream in the unit, liquid samples were periodically taken. the sulfur content on the liquid samples was measured through a fluorescence spectroscopy

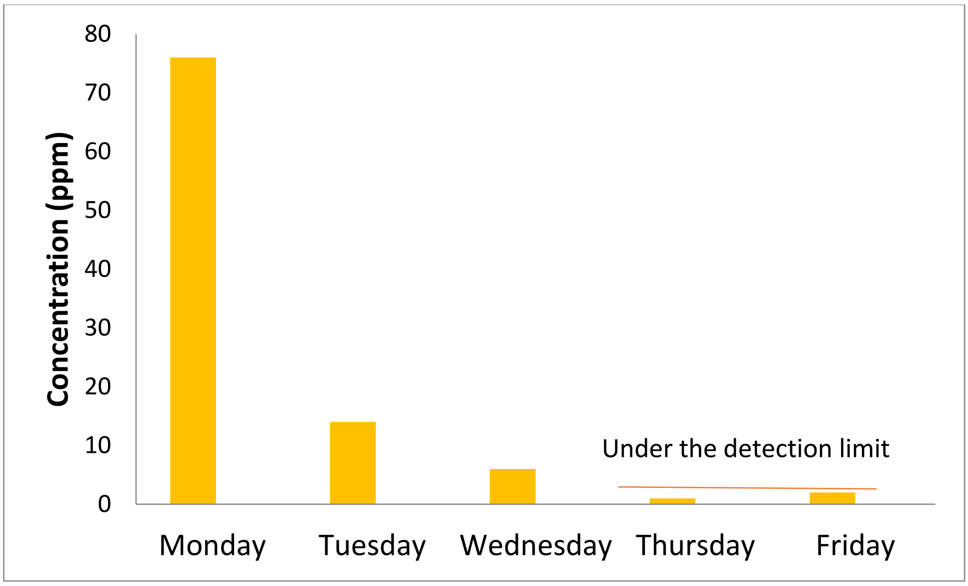

Figure 3.2 Sulphur content in the solvent at the outlet of the reactor in time.

3.2.3 Calibration of the heating system

To improve the temperature control inside the reactor, all the shells were calibrated at different temperatures under no reactive conditions.

To measure the temperature along the reactor was used a manual mobile thermocouple.

The calibration of the heating system consists basically in to calibrate the thermocouple that measures the temperature inside each shell. This measure provides also valuable information about the precision, limitations, and stability related to the temperature measured along the thermowell.

The conditions and temperatures used for the calibration are those shown in the Table 3.2

Table 3.2: Calibration Conditions

P (bar)	11
T(°C)	400 410 420 430 450
Liquid Flow*(ml/min)	1
Gas Flow**(L/H)	15
Reactor Load	Sic #210µm

*** Methylcyclohexane ** hydrogen**

For every set of conditions, the measure was done by triplicate.

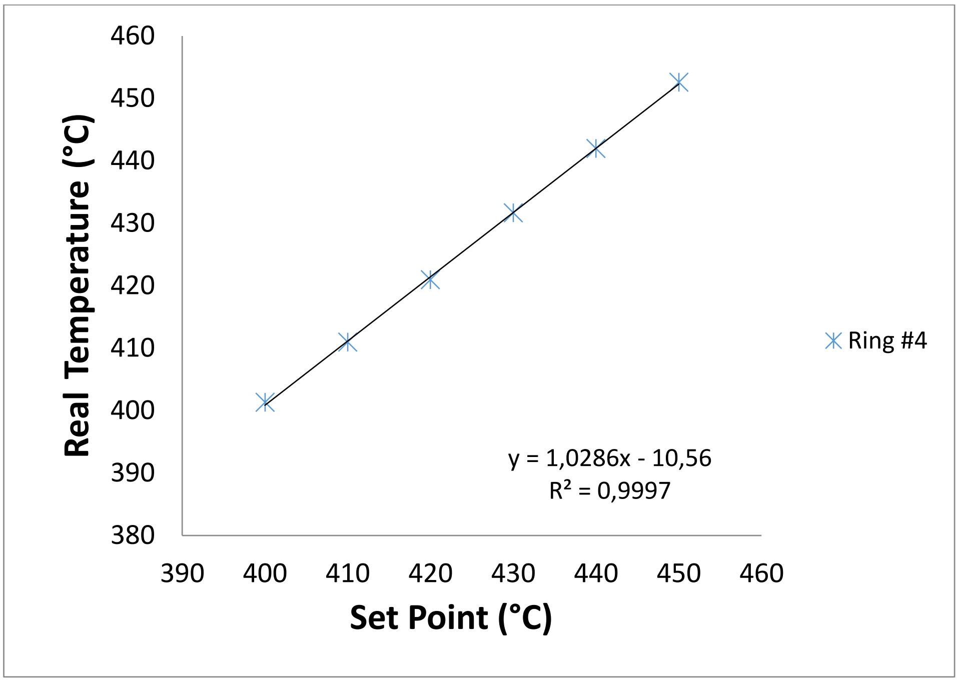

Figure 3. 3 Example of calibration curve: Calibration for the fourth heating shell

3.2.4 Height of **vaporization**

It was decided to vaporize the liquid charge inside the reactor before the catalytic zone. To guarantee that all the charge was vaporized in the defined zone, several tests at different liquids flow rates and pressures were done.

Several operation conditions were fixed for the test, having into account the WHSV considered for the test (Table 3.3).

Table 3.3. Height of Vaporization Test Conditions

P (bar)	10 11 12
T(°C)	430-450
Liquid Flow* (ml/min)	0,35/0,5 /0,75 /1
Gas Flow**(L/H)	15
Reactor Load	Sic #210µm

***Cyclohexane **Hydrogen**

The temperature profile along the reactor was measured with the liquid reactive and hydrogen as feed. It was compared with the profile measured just the presence of gas. No significant changes were observed in the profiles measured, as can be seen in the Figure 3.4. Which means that the liquid vaporizes at the very beginning of the gasification zone.

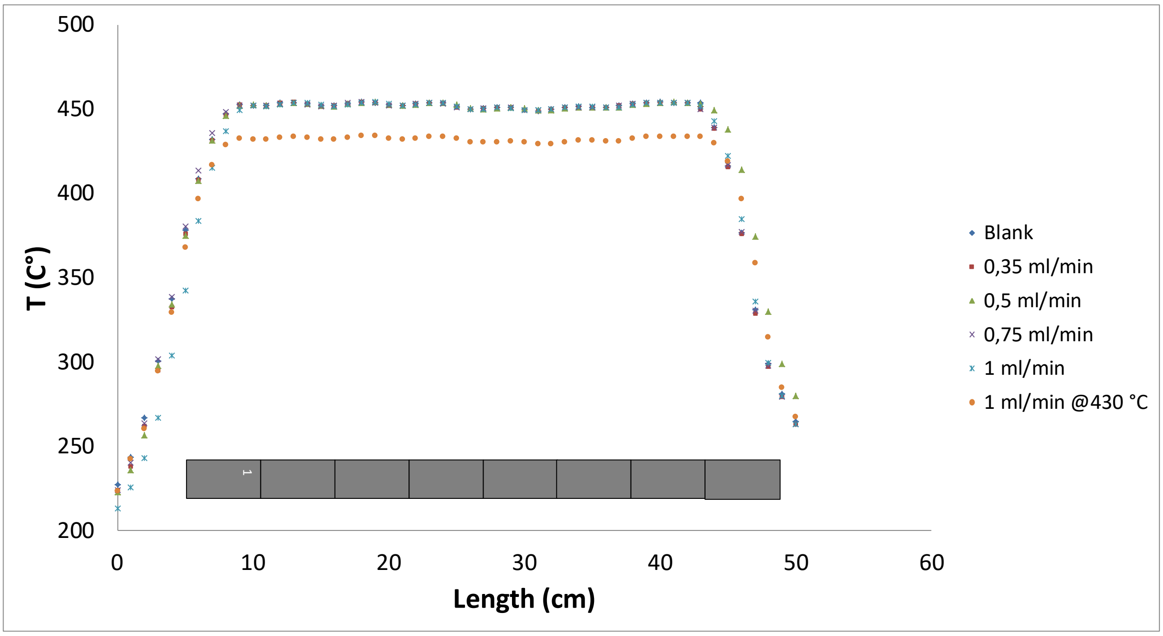

Figure 3.4 Temperature profile measured during the height of vaporization test.

This is scenario is totally feasible due to the flow rate pumped into the reactor is very small so that the heat used for the vaporization is very low and do not produces observables changes in the thermal profiles. Which means that liquid charge is vaporized in the very beginning of the reactor.

3.2.5 Analysis of the thermal response

For highly endothermic reaction, the rate of energy consumed can be overcome the rate of energy given by the heating system. Also, exist the case into which the heating system delivers such an enormous quantity of energy to a particular zone within the reactor that overheats the reactor downstream.

Several thermal tests were performed to analyze:

1. The temperature stabilization time along the reactor.
2. How accurately the reactor adopts the temperature imposed by with the control system without reaction.
3. How the system behaves when a perturbation like that one caused for an endothermic reaction is present in the system (physicals limits).
4. The stability of the temperature along the reactor.

To be totally aware of how the reaction section interacts with the control system has fundamental importance since it is intended to impose the thermal profile inside the reactor.

With this results, the control strategy to adopt during the test will be defined.

This kind of test allows deducing also the optimal zone to place the catalyst, which will be the zone with the greatest thermal stability.

The tests were performed for 2.5 ml/min of liquid, 10 bar, 7 H_2/HC in downflow with 210μm SiC packing. There are 8 heating shells so there are 8 different heating zones, the shell 1 is the top shell and the 8 is the last one (see figure 3.8).

Two different kinds of test were done:

a-) Shutting off couples of shells and measuring the whole profile inside the reactor.

This test consists in shutting off couples of shells in order to know the magnitude of the temperature perturbation in upstream and downstream and identify eventual limitations to the reach the target temperature.

The shells 1 and 8 were excluded from the test; the first one, because with that shell the vaporization needs to be granted and the shell 8 in order to sum stability to the system, it is not expected to induce or to have an extra consume of power in that volume.

In the figure 3.5, the temperature profile in stationary conditions is shown for every test. Always that two shells are shutting-off, the zone corresponding to the shell that is above is affected. In the R2-R3 test, the zone corresponding to the R1 does not reach the target temperature; In the R3-R4 test, the zone corresponding to the R2 does not reach the target temperature and so on. This exposed eventual limitation in specific zones to reach the target temperatures in cases in which the energy consumption is above a certain value.

Then, can be said that R1 and R2 zones should be submitted to high power consume in order to always grant the total vaporization of the liquid charge and to have the possibility to increase the temperature at the beginning of the catalytic zone.

The zone heated by the shell that is under the turned-off shells, does not present any considerable change in temperature. Which is why, increasing the temperature in this area allows to increase or decrease the temperature in the zone corresponding to the shell above. This will be very useful for the test that will be carry out.

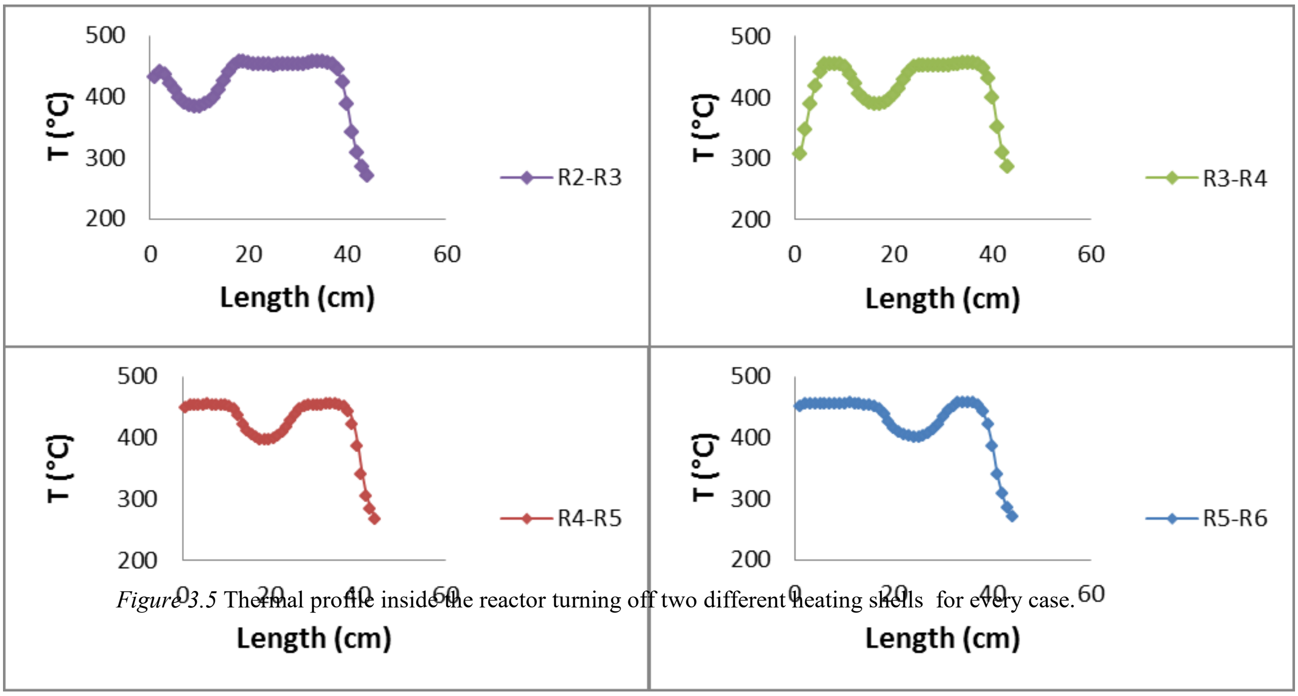

Figure 3.5 Thermal profile inside the reactor turning off two different heating shells for every case.

b-) Temperature stability inside the reactor at different temperatures.

The temperature value reached in a particular point along the reactor changes dynamically with time, even if the variation is maintained within a certain range, it has an associated deviation. The objective of this test was to measure the stability of temperature along the reactor in time. The results can be observed in the figure 3.6.

The stability of the shell 8 was not included because along this shell there is an important temperature change as will be seen in the figure 3.6.

The conditions used for the test were the same used for the calibration of the system (table 3.3)

As can be noted, the dispersion of the temperature values along the reactor in time is quite low. The deviation follows the same pattern for different values of temperature. The shell that works better without calibration is the shell 5 and the worse are the last two.

It is possible to say that:

- An extra demand of power in one of the eight zones over a certain value can affect seriously the temperature of the zone immediately above.
- A perturbation in the reactor temperature can impose a thermal limitation that is not detected for the thermocouples fixed at every shell but can be measure with the mobile thermocouple.
- In the case of local temperature limitations (one of the eight zones), could be advisable to increase the power of the shell that is before and after of the corresponding zone.

- The dispersion of the temperature values measured into the reactor for different times in stationary state can be considered as low.

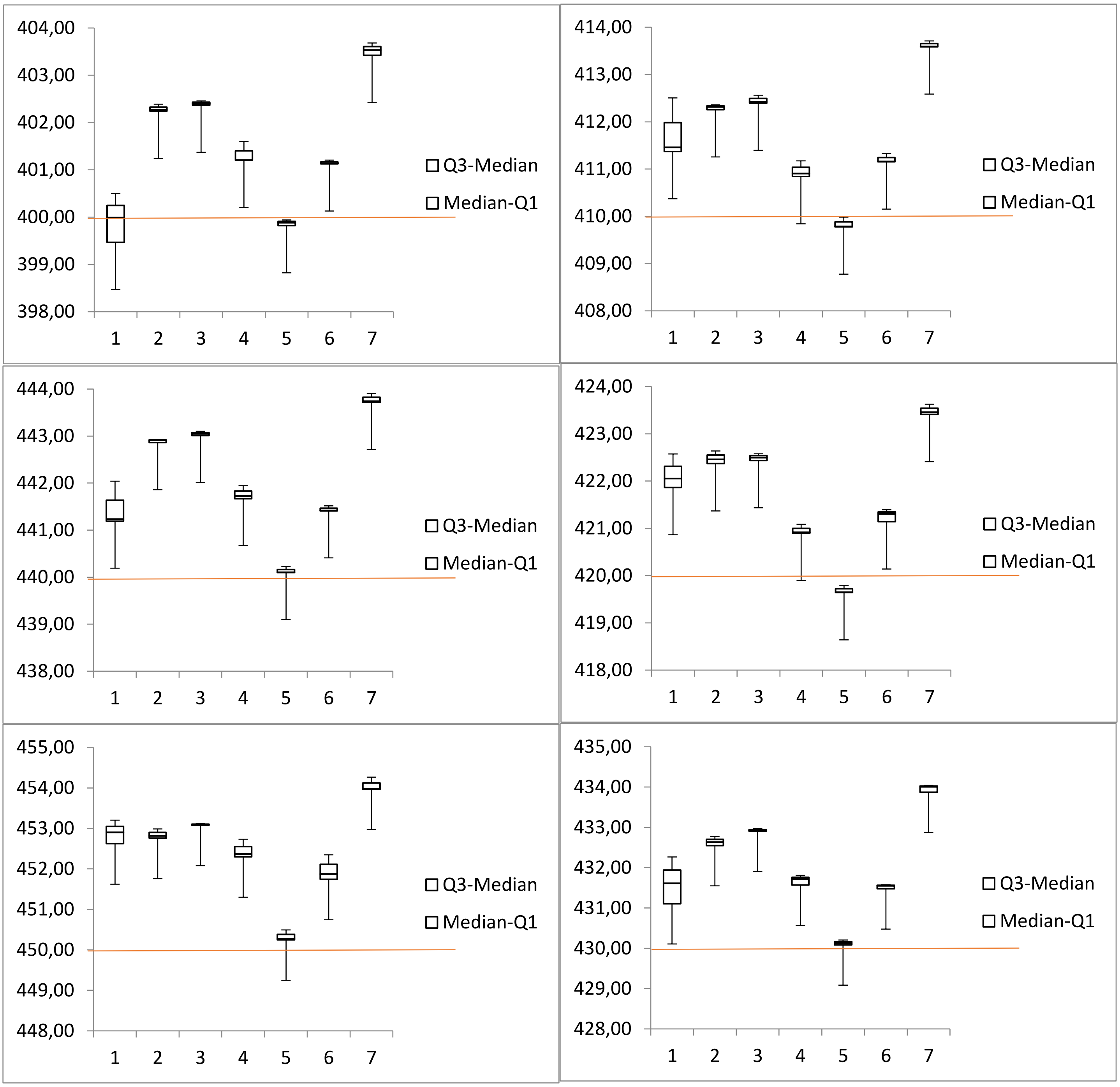

Figure 3.6. Plot boxes for the temperature distribution along the zones of the reactor

Optimal zone for the catalyst

Shells 1 and 8 are excluded from the possible zones to place the catalyst; the first one, because with that shell the vaporization needs to be granted and the shell 8 in order to sum stability to the system.

According to with the thermal behavior analysis, if the targeted temperature in a certain zone of the catalyst cannot be reached, will be useful to increase the power of the shell above and under that zone in order to reach the desired target.

Also, having into account the philosophy of the experimentation (that will be explained later) it is convenient to have a symmetrical distribution of the catalyst between heating zones/shells.

It can be seen from figure 3.7 that the most favorable zone that also has high-temperature stability (measured as the standard deviation of the temperature in time) is zone covered by the shell 4 and shell 5.

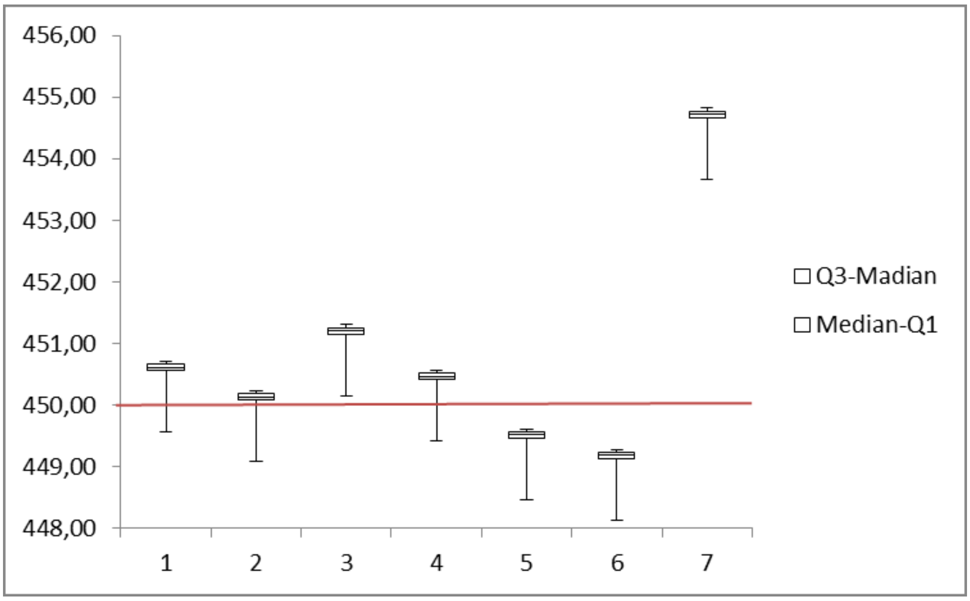

Figure 3.7 .Plot box for the temperature distribution along the zones of the reactor at 450 °C

3.2.6 Catalyst Preparation

A platinum-based catalyst was used for the test. The composition and the textural characteristic of the solid remain confidential.

First, the catalyst was crashed and sieved. To grant the total reduction of the active sites, the catalyst was reduced in two stages.

1. Ex-situ activation, after of which the catalyst was stocked and sealed in vials with an argon atmosphere.
2. In-situ activation for 48 hours.

The details of the activation protocol remain confidential.

3.2.7 Reactive Mix

Ultra-pure sigma Aldrich methylcyclohexane was used for the test. All the liquids charges were dehydrated using a molecular sieve, in order to avoid the deactivation of the catalyst.

Air-Liquid ‘s Ultra-high purity hydrogen was used for the gas phase.

3.2.8 Chromatograph Calibration

A gas-phase Agilent® chromatograph equipped with an FID detector an a PONA chromatographic column was calibrated in-situ a used to quantify the formed toluene and to study the distribution of products.

After the calibration, it was the verified that the selectivity to toluene was over 99,9%.

3.2.9 Reactor Scheme

The figure 3.8 represents a schematic diagram with the exact metric positions of the sensors, the projected position for the catalyst (according to with the thermal stability analysis) and the main elements inside the reactor. Can be observed in the figure 3.8 that before and after the catalyst is placed granulated Sic to improve the heat transfer between the reactive mix and the reactor; also, to reduce the entry effects.

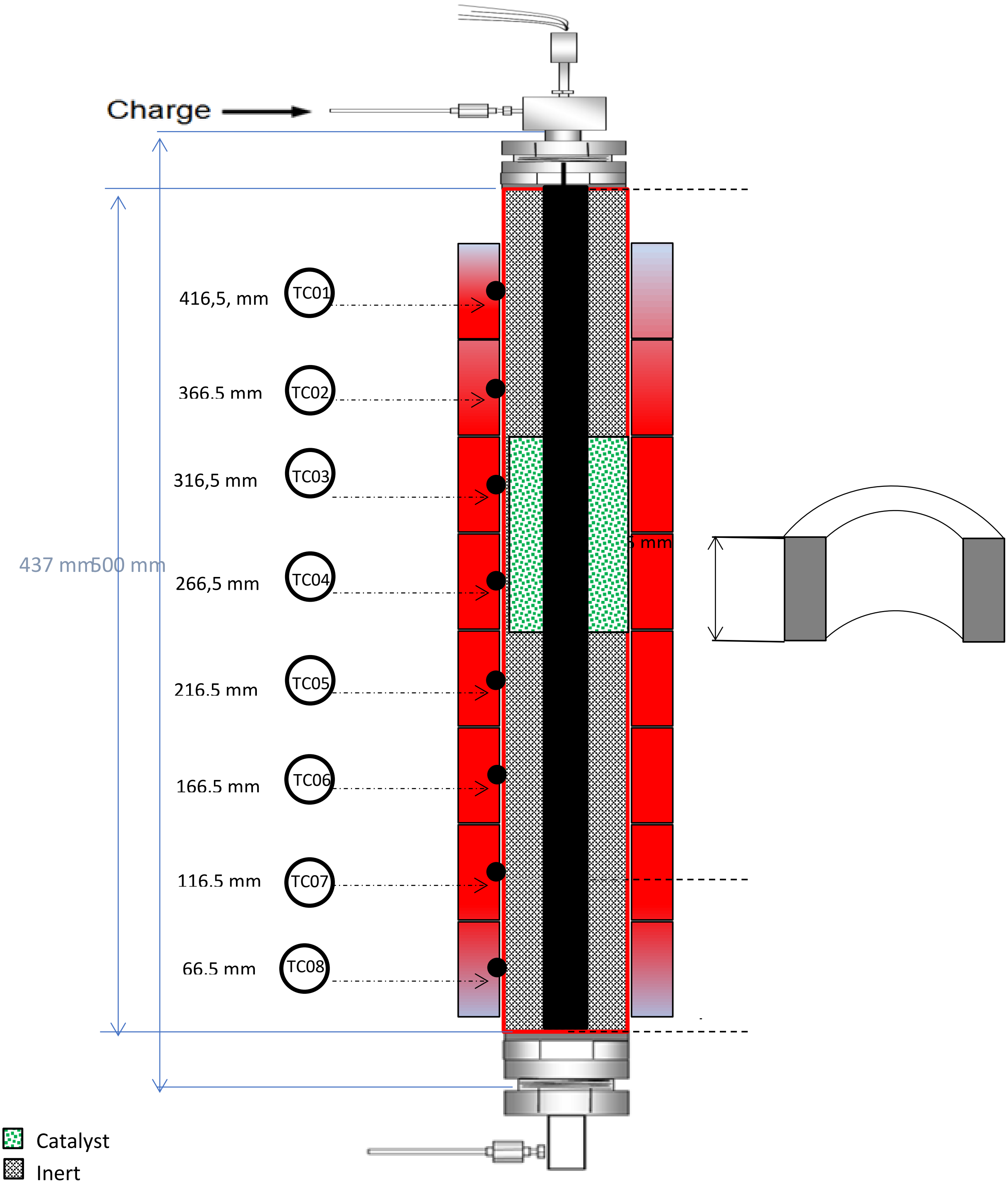

Figure 3.8. Detailed position of the catalyst and the sensors.

3.2.10 Experimental conditions

In the table 3.4, the profile type is related to the shape a the fixed area in every experiment. The first number is related to the shape and the second number to the relative's areas. A real profile of every kind and the scope of the shape is explained in further detail in the results section.

The experimental conditions fixed for the test for 1g of catalyst are written in table 3.4.

Table 3.4: Experiment Design

Isothermal Temperature (°C)	P (bar)	WHSV (H^{-1})	H_2/HC	Profile Type
380	10	10	3	1+1
380	10	10	3	1+2
380	10	10	3	1+3
380	10	10	3	2+1
380	10	10	3	2+2
380	10	10	3	2+3
380	10	10	3	3+1
380	10	10	3	3+2
380	10	10	3	3+3
380	12	10	3	1+1
380	12	10	3	1+2
380	12	10	3	1+3
380	12	10	3	2+1
380	12	10	3	2+2
380	12	10	3	2+3
380	12	10	3	3+1
380	12	10	3	3+2
380	12	10	3	3+3
390	10	10	3	1+1
390	10	10	3	1+2
390	10	10	3	1+3
390	10	10	3	2+1
390	10	10	3	2+2
390	10	10	3	2+3
390	10	10	3	3+1
390	10	10	3	3+2
390	10	10	3	3+3
390	12	10	3	1+1
390	12	10	3	1+2
390	12	10	3	1+3
390	12	10	3	2+1
390	12	10	3	2+2
390	12	10	3	2+3
390	12	10	3	3+1
390	12	10	3	3+2
390	12	10	3	3+3
400	10	10	3	1+1

400	10	10	3	1+2
400	10	10	3	1+3
400	10	10	3	2+1
400	10	10	3	2+2
400	10	10	3	2+3
400	10	10	3	3+1
400	10	10	3	3+2
400	10	10	3	3+3
400	12	10	3	1+1
400	12	10	3	1+2
400	12	10	3	1+3
400	12	10	3	2+1
400	12	10	3	2+2
400	12	10	3	2+3
400	12	10	3	3+1
400	12	10	3	3+2
400	12	10	3	3+3

For every set of conditions:

1. The isothermal conversion was determined fixing profiles as flat and as small as possible.
2. Different shapes of profiles were tested.
3. A low conversion was targeted in order to test the conversion zone with highest levels of deviation.

3.3 Results

As was mentioned in the statement of the problem, due to the high heat of reaction it is very difficult to control the temperature along the reactor. Finally, the control system and the considerations about the thermal behavior of the mechanical system are tested. Four type of general profile shapes are imposed.

1. In figure 3.9 it is accomplished the closest profile to the isothermal conditions reached for a test at 380 °C. The maximum temperature deviation along the profile does not overcome +/- 2 °C. The experimental conversion obtained when this thermal profile was imposed is considered as the experimental isothermal conversion for the employed set of operative's conditions. The same methodology is applied to the other set.

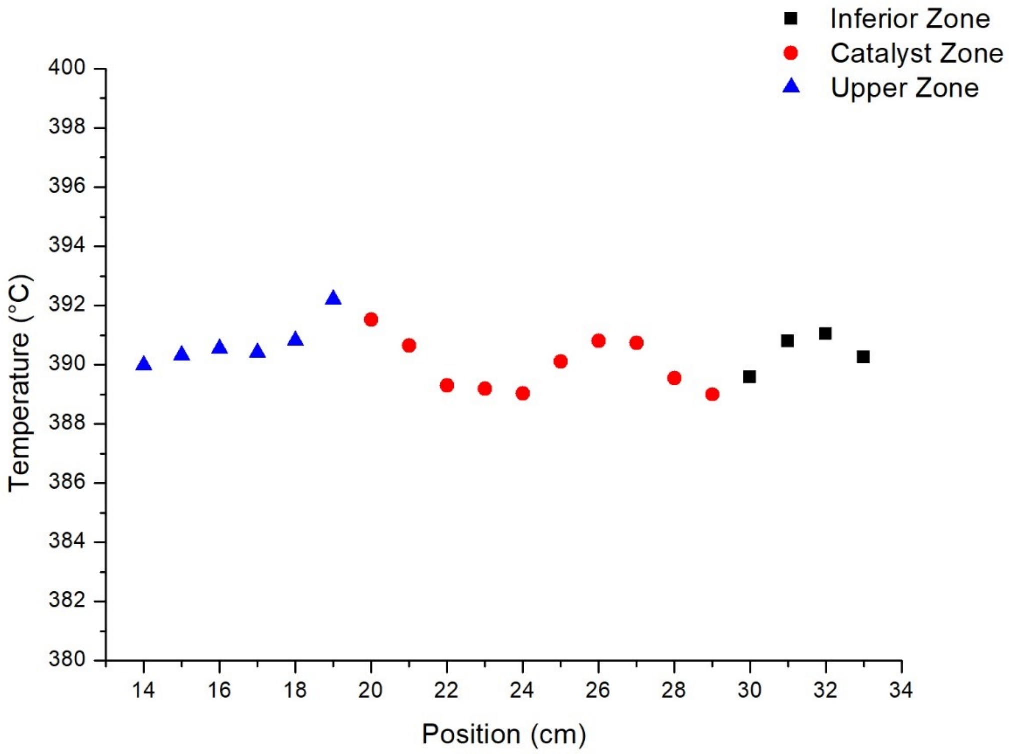

Figure 3.9. Thermal Profile for 390 °C as operation temperature. Reference Test Number #141253

In figure 3.9 it is also possible to differentiate between the temperature in the catalyst zone (heated by the shell 3 and the shell 4) and the temperature in the upper and the inferior zone.

The second type of profile geometry is shown in figure 3.10. In this case, just the effect of the undershoot is studied, obtaining different experimental Aun values.

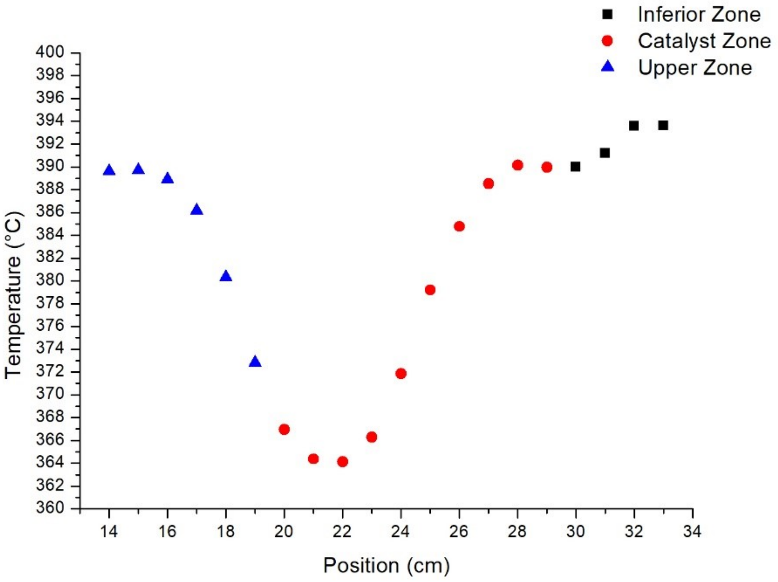

Figure 3.10. Thermal Profile for 390 °C as operating temperature. Reference Test Number #151033

The third type is done in order to test the effect on the deviation of the overshoot and the undershoot at the same time as shown in figure 3.11.

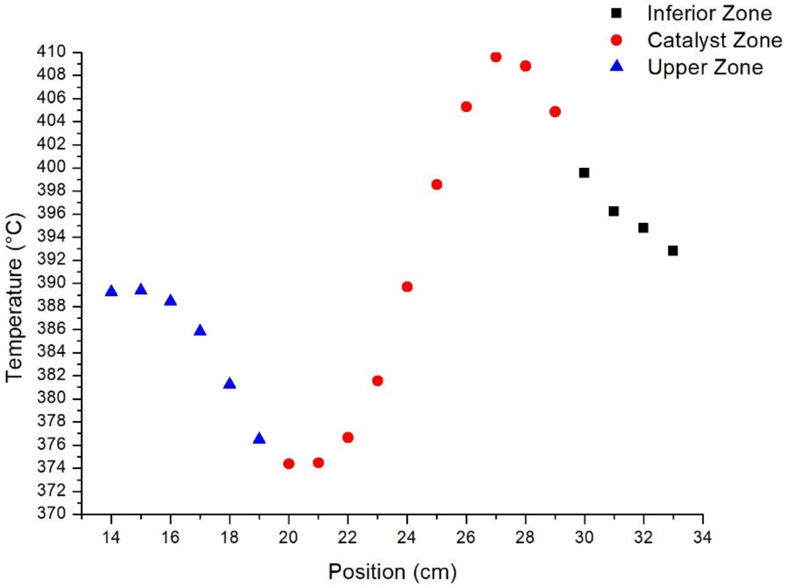

Figure 3.11. Thermal Profile for 390 °C as operation temperature. Reference Test Number #151552

The last type is done to test verify is the model can predict also the deviation caused by irregular profiles with several peaks.

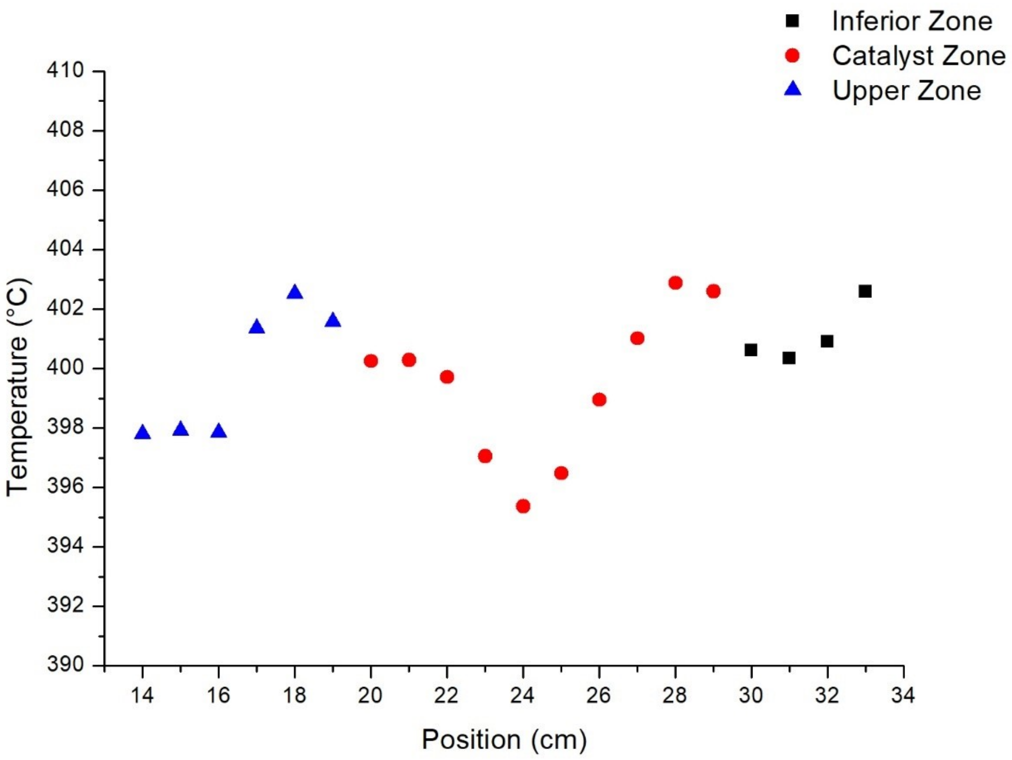

Figure 3.12. Thermal Profile for 400°C as operation temperature. Reference Test Number #210930

On the table 3.5, a brief of the key results is gathered. Several conclusion can be pointed to looking at this table. (The term relative error is used to talk about the error in the prediction of the experimental value).

Considering the simulation analysis done in the first part of this work:

- As the temperature of the test increases, the relative deviation also decreases.
- As the temperature of the test increases, the temperature required for compensating the undershoot effect increases.
- As the effect of the undershoot starts to be negligible in comparison with the overshoot effect, the relative deviation starts to grow faster in the positive sense.
- An Aov/Aun ratio larger than 0.9 must be avoided.
- As the pressure increases, the relative deviation decreases.

3.4 Comparation between the simulation, the model and the experiments

Comparing the deviation predicted by the model and the simulation with the experimental results:

- The simulation results are accurate in terms of conversion, which is lower than 5% relative error.
- The deviation predicted by the simulation has around 15% relative error in average.
- The deviation predicted by the model has a 5% of relative error in average for areas lower than 3 UA.
- For high values of Aun (under -10) the model over estimates the impact of the undershoot.
- For high values of Aov (under 10) the model underestimates the impact of the overshoot.

The model works well also for non-symmetric profiles

Table 3.5: Experimental results

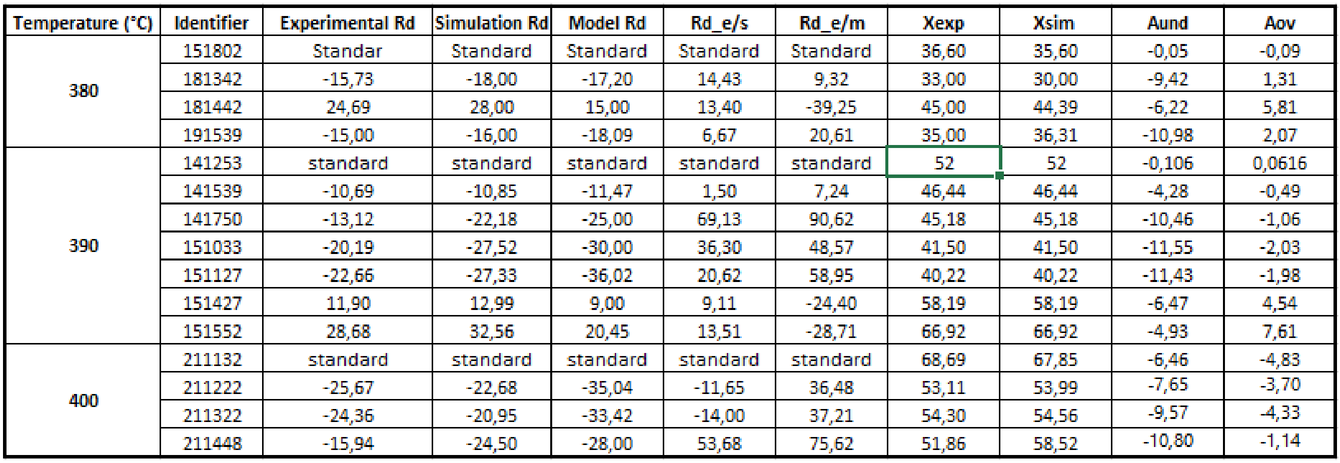

Temperature (°C)	Identifier	Experimental Rd	Simulation Rd	Model Rd	Rd_e/s	Rd_e/m	Xexp	Xsim	Aund	Aov
380	151802	Standar	Standard	Standard	Standard	Standard	36,60	35,60	-0,05	-0,09
	181342	-15,73	-18,00	-17,20	14,43	9,32	33,00	30,00	-9,42	1,31
	181442	24,69	28,00	15,00	13,40	-39,25	45,00	44,39	-6,22	5,81
	191539	-15,00	-16,00	-18,09	6,67	20,61	35,00	36,31	-10,98	2,07
390	141253	standard	standard	standard	standard	standard	52	52	-0,106	0,0616
	141539	-10,69	-10,85	-11,47	1,50	7,24	46,44	46,44	-4,28	-0,49
	141750	-13,12	-22,18	-25,00	69,13	90,62	45,18	45,18	-10,46	-1,06
	151033	-20,19	-27,52	-30,00	36,30	48,57	41,50	41,50	-11,55	-2,03
	151127	-22,66	-27,33	-36,02	20,62	58,95	40,22	40,22	-11,43	-1,98
	151427	11,90	12,99	9,00	9,11	-24,40	58,19	58,19	-6,47	4,54
	151552	28,68	32,56	20,45	13,51	-28,71	66,92	66,92	-4,93	7,61
400	211132	standard	standard	standard	standard	standard	68,69	67,85	-6,46	-4,83
	211222	-25,67	-22,68	-35,04	-11,65	36,48	53,11	53,99	-7,65	-3,70
	211322	-24,36	-20,95	-33,42	-14,00	37,21	54,30	54,56	-9,57	-4,33
	211448	-15,94	-24,50	-28,00	53,68	75,62	51,86	58,52	-10,80	-1,14

4. Development of a computational portable tool

The objective of developing a model of the kind produced was to allow the engineers and technicians to perform fast quantitative estimations to design a catalytic test or to verify if the done test can be considered as isothermal.

To make easier this task a computational tool was developed using a commercial compilator to program the model and an HMI to obtain easy and fast the desired results. The tool was called ***Thermal Oriented Reaction Simulator*** **-TORS V 1.0**

Figure 3.13. Screenshot of TORS V1.0 presentation

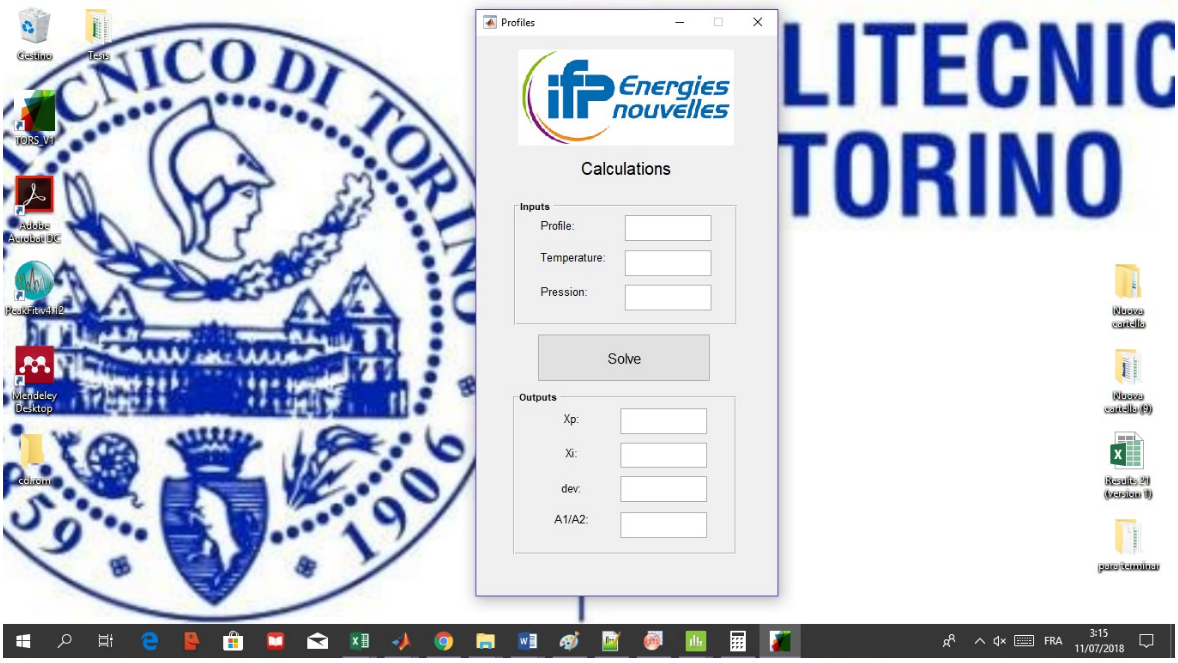

Figure 3.14. Screenshot of TORS V1.0 HMI

5. Conclusions

The presence of thermal profiles can affect importantly the conversion at the outlet of the reactor when the reaction has a high activation energy. Because of this, attention must be paid to this factor when the heat of reaction is also high.

The effect of an overshoot is exponentially bigger than the undershoot effect due to the relation between the temperature and the reaction rate. This states clearly that there is not exist a fix rapport between the two to have a zero-deviation o any other fixed deviation value.

The presence of a deeply marked undershoot can put in play the effect of the equilibrium, causing serious deviations, reason by which it is advisable to consider the reaction equilibrium type.

All the operation variables studied affect the deviation, mainly the temperature and the pressure.

A larger relative deviation will be obtained at the lowest conversion. It is possible to attribute it to two reasons:

4. Numerical: As the isothermal conversion value is smaller, little variations on the targeted value cause important relative errors.

5. Absolute deviation: The absolute deviation is bigger at low and high conversions, generating a minimum for medium conversions. A high absolute deviation at high conversion is due to the equilibrium effect.

For different levels of activation energy (PV), as this variable increases, the deviation always (for all the considered variables) increases. Instead of, when the temperature and the pressure are considered as PV, as both increase, the deviation decrease.

The overshoot existence in the profile must be considered much more carefully than the undershoot existence into the temperature. The overshoot effect on the deviation is greater in magnitude than the undershoot effect.

The Aov/Aun compensation ratio will be always between 0 and 1. Besides, typically, this value will be between 0.4 and 0.8

As the activation energy increases (PV), the overshoot area to take the deviation to zero will always increase. The same scenario was founded for the H/HC ratio.

If a system with and fixed Aov and Aun with a negative deviation is studied, as the operative temperature increases, the negative deviation decreases approaching to zero. But, if it is desired increase Aov until reach a zero-deviation, as the temperature increases, the Aov required for the compensation will be higher. Once the zero-deviation is reached, as Aov increases, the deviation will grow faster as the operative temperature is bigger.

For the pressure fixed as PV, as the pressure level is higher, the required fraction for the compensation will be lower. This situation has an evident limit, the equilibrium. As the pressure increases, the system has conversions that are closer to the equilibrium. In this scenario, an overshoot can push over the equilibrium limit causing a positive deviation.

The WABT does not necessarily represent a good approximation to the isothermal temperature of the test. It could be useful in terms of dilution of the catalyst but not to quantify the impact of the temperature profile on the conversion of chemical reactions with high reaction heat. The reason is that the WABT formula does not weight the impact of the temperature deviation according to the magnitude of the temperature, but just in terms of mass of catalyst in a section.

The worse conditions to operate are:

- High pressures: X/Xequi under 0.8.
- Low temperature: X/Xequi under 0.8.
- Aov/Aund > 0.9
- Aov/Aund <0.1
- Low coversions (X<0.4).

The recommended proportion of Aov/Aund is 0.5.

With the experimental tests, it was possible to confirm that

1. For the verification of the simulation analysis done in the first part of this work.

- As the temperature of the test increases, the relative deviation also decreases.
- As the temperature of the test increases, the temperature required for compensating the undershoot effect increases.
- As the effect of the undershoot starts to be negligible in comparison with the overshoot effect, the relative deviation starts to grow faster in the positive sense.
- An Aov/Aun ratio larger than 0.9 must be avoided.
- As the pressure increases, the relative deviation decreases.

2. Comparing the deviation predicted by the model and the simulation with the experimental results.

- The simulation results are accurate in terms of conversion, which is lower than 5% relative error.
- The deviation predicted by the simulation has around 15% relative error in average.
- The deviation predicted by the model has a 5% of relative error in average for areas lower than 3 UA.
- For high values of Aun (under -10) the model over estimates the impact of the undershoot.
- For high values of Aov (under 10) the model underestimates the impact of the overshoot.

3. The model works well also for non-symmetric profiles

6. For future work

- A model to have into account the dilution in the catalytic bed should be done.

- A modification for the WABT equation can be proposed to take into account also the influence caused by every different value of temperature along the profile on the final conversion (as it was mentioned, the effect of the different values of temperature is not the same. A simple average should not be taken as right).

- Simulations and experimental work should be done to understand how many is the minimal number of measures that must be done to have a better approximation of the average temperature along a catalytic bed.

- A model under the same considerations can be done for more complex charges and reactions.

- More experiments should be performed in order to understand better the behavior of the deviation at high and low conversions.

Bibliography

Aris, R., & Amundson, N. R. (1957). Some remarks on longitudinal mixing or diffusion in fixed beds. *AIChE Journal*, *3*(2), 280–282. https://doi.org/10.1002/aic.690030226

BC Gates, JR Katzer, G. S. (1979). Chemistry of Catalytic Process.

Beek, J. (1962). Design of Packed Catalytic Reactors. *Advances in Chemical Engineering*, *3*(C), 203–271. https://doi.org/10.1016/S0065-2377(08)60060-5

Berger, R. J., & Kapteijn, F. (2007). Coated-wall reactor modeling-criteria for neglecting radial concentration gradients. 2. Reactor tubes filled with inert particles. *Industrial and Engineering Chemistry Research*, *46*(12), 3871–3876. https://doi.org/10.1021/ie061232v

Berger, R., & Kapteijn, F. (2007). Coated-wall reactor modeling Criteria for neglecting radial concentration gradients. 1. Empty reactor tubes. *Industrial & Engineering Chemistry …*, 3863–3870. https://doi.org/10.1021/ie0612313

Bilous, O., & Amundson, N. R. (1956). Chemical reactor stability and sensitivity: II. Effect of parameters on sensitivity of empty tubular reactors. *AIChE Journal*, *2*(1), 117–126. https://doi.org/10.1002/aic.690020124

Bird, R., Stewart. W., Light, F. (1960). *Transport Phenomena*. *Transport Phenomena*. New York: John Wiley & Sons. https://doi.org/10.1002/aic.690070245

Borkink, J. G. H., & K.R., W. (1994). Significance of the radial porosity profile for the description of heat transport in wall-cooled packed beds. *Chemical Engineering Science*, *49*(6), 863–876. https://doi.org/10.1016/0009-2509(94)80023-5

BP. (2017). *BP Energy Outlook Energy 2017*. *BP Statistical Review of World Energy*. https://doi.org/10.1017/CBO9781107415324.004

Brokaw, R. S. (1969). Predicting transport properties of dilute gases. *Industrial and Engineering Chemistry Process Design and Development*, *8*(2), 240–253. https://doi.org/10.1021/i260030a015

Carberry, J. J. (1958). First Order Rate Processes and Axial, 207–209.

Carberry, J. J. (1961). The catalytic effectiveness factor under nonisothermal conditions. *AIChE Journal*, *7*(2), 350–351. https://doi.org/10.1002/aic.690070239

Carberry, J. J., & Bretton, R. H. (1958). Axial dispersion of mass in flow through fixed beds. *AIChE Journal*, *4*(3), 367–375. https://doi.org/10.1002/aic.690040327

Carberry, J. J., & Wendel, M. M. (n.d.). Computer Cases Catalytic Reactor : The Adiabatic and Quasi-adiabatic Cases. *AIChE Journal*, *9*(1), 129–133.

Caretto, L. . (1963). *No Title*. Univ. California.

Castañeda-López, L. C., Alonso-Martínez, F., Ancheyta-Juárez, J., Maity, S. K., Rivera-Segundo, E., & Matus-Guerra, M. N. (2001). Comparison of the performance of upflow and downflow small-reactors in hydrodesulfurization reactions. *Energy and Fuels*, *15*(5), 1139–1144. https://doi.org/10.1021/ef010006p

Colburn, A. P. (1933). Mean temperature difference and heat transfer coefficient in liquid heat exchangers. *Industrial & Engineering Chemistry*.

De Carvalho, J. R. F. G., & Delgado, J. M. P. Q. (2005). Overall map and correlation of dispersion data for flow through granular packed beds. *Chemical Engineering Science*, *60*(2), 365–375. https://doi.org/10.1016/j.ces.2004.07.121

de Wasch, A. P., & Froment, G. F. (1972). Heat transfer in packed beds. *Chemical Engineering Science*, *27*(3), 567–576. https://doi.org/10.1016/0009-2509(72)87012-X

Delgado, J. M. P. Q. (2007). Longitudinal and transverse dispersion in porous media. *Chemical Engineering Research and Design*, *85*(9 A), 1245–1252. https://doi.org/10.1205/cherd07017

Duarte, S. I. P., Ferretti, O. A., & Lemcoff, N. O. (1984). A heterogeneous one-dimensional model for non-adiabatic fixed bed catalytic reactors. *Chemical Engineering Science*, *39*(6), 1025–1031. https://doi.org/10.1016/0009-2509(84)87011-6

Dwlvedi, P. N., & Upadhyay, S. N. (1977). Particle-Fluid Mass Transfer in Fixed and Fluidized Beds. *Industrial and Engineering Chemistry Process Design and Development*, *16*(2), 157–165. https://doi.org/10.1021/i260062a001

Elia, M. (2013). *Etude de la stabilité thermique dans les réacteurs chimiques*.

EM Blue, GD Gould, CJ Egan, T. H. (1975). Production of Aromatic Hydrocarbons by Low-Pressure Rheniforming,.

Ergun, S., & Orning, A. A. (1949). Fluid Flow through Randomly Packed Columns and Fluidized Beds. *Industrial & Engineering Chemistry*, *41*(6), 1179–1184. https://doi.org/10.1021/ie50474a011

Fairbanks, D. F., & Wilke, C. R. (1950). Diffusion Coefficients in Multicomponent Gas Mixtures. *Industrial & Engineering Chemistry*, *42*(3), 471–475. https://doi.org/10.1021/ie50483a022

Gilbert F Froment, Juray De Wilde, K. B. B. (2011). *Chemical reactor analysis and design*. Wiley.

H Henningen, M. B.-N. (1970). No Title. *British Chem Eng.*, *15*, 1433.

HG Krane, BA Groth, LB Schulman, H. S. (1959). Congress-, Fifth World Petroleum III, Section.

Hickman, D. A., Degenstein, J. C., & Ribeiro, F. H. (2016). Fundamental principles of laboratory fixed bed reactor design. *Current Opinion in Chemical Engineering*, *13*, 1–9. https://doi.org/10.1016/j.coche.2016.07.002

Hsu, C. S. (2017). *Handbook of Petroleum Technology*. pringer International Publishing.

J., V. (1997). *Kinetische studie van de katalytische reforming van nafta over een Pt-Sn/Al_2O_3 katalysator*.

JH Jenkins, T. S. (1980). No Title. *Hydrocarbon Processing*, *59*, 163.

JP Frank. (1994). Workshop-Catalysis in the Downstream Operations.

Juarez, J. A., & Aguilar-Rodriguez, E. (1994). No Title. *Oil Gas J*, *92,93*.

KR Murthy, N Sharma, N. G. (1995). *Catalytic Naphtha Reforming*.

Krishna, R., & Wesselingh, J. A. (1997). The Maxwell-Stefan approach to mass transfer. *Chemical Engineering Science*, *52*(6), 861–911. https://doi.org/10.1016/S0009-2509(96)00458-7

Kulkarni, B. D., & Doraiswamy, L. K. (1980). Catalysis Reviews : Science and Engineering. Estimation of Effective Transport Properties in Packed Bed Reactors, (22(3)), 431–483.

Levenspiel, O., & Chemical. (2009).) 1 / 3 ;, *93*(8), 11326–11328. https://doi.org/dx.doi.org/10.1021/jp509731y

Little, D. (1985). *Catalytic Reforming*. Tulsa, Oklahoma: PennWell Publ. Co.

Maestri, F., & Rota, R. (2005). Thermally safe operation of liquid-liquid semibatch reactors Part II: Single diffusion controlled reactions with arbitrary reaction order. *Chemical Engineering Science*, *60*(20), 5590–5602. https://doi.org/10.1016/j.ces.2005.04.070

Maestri, M., Tronconi, E., Berger, R. J., Kapteijn, F., & Moulijn, J. A. (n.d.). *Overview of requirements for measurement of intrinsic kinetics in and overview of correlations for characteristics of the G-S and L-S fixed-bed reactor*.

Mathur, S., Saxena, S. C. (1966). Viscosity of polar gas mixtures: Wilke's method. *Appl. Sci. Res. Section A*, *15*, 404–410.

McCune, L., & Wilhelm, R. (1949). Mass and Momentum Transfer in Solid-Liquid System. *Industrial & Engineering Chemistry*, *41*(6), 1124–1134. Retrieved from http://pubs.acs.org/doi/abs/10.1021/ie50474a006

McGuire, M., & Lapidus, L. (1965). On the stability of a detailed packed bed reactor. *AIChE Journal*, *11*(1), 85–95. https://doi.org/10.1002/aic.690110120

McHenry, K. W., & Wilhelm, R. H. (1957). Axial mixing of binary gas mixtures flowing in a random bed of spheres. *AIChE Journal*, *3*(1), 83–91. https://doi.org/10.1002/aic.690030115

Mears, D. E. (1971a). Tests for Transport Limitations in Experimental Catalytic Reactors. *Industrial and Engineering Chemistry Process Design and Development*, *10*(4), 541–547. https://doi.org/10.1021/i260040a020

Mears, D. E. (1971b). The role of axial dispersion in trickle-flow laboratory reactors. *Chemical Engineering Science*, *26*(9), 1361–1366. https://doi.org/10.1016/0009-2509(71)80056-8

Mears, D. E. (1976). On Criteria for Axial Dispersion in Nonisothermal Packed-Bed Catalytic Reactors. *Industrial and Engineering Chemistry Fundamentals*, *15*(1), 20–23. https://doi.org/10.1021/i160057a004

Mueller, G. E. (1999). Radial void fraction correlation for annular packed beds. *AIChE Journal*, *45*(11), 2458–2460. https://doi.org/10.1002/aic.690451119

Oliveira, D. (2016). *Influence of Operating Conditions on the precision of the kinetic* *parameters for different kinetic laws*.

Raseev, S. (2003). *Thermal and Catalytic Processes in Petroleum Refining*. (C. Press, Ed.).

Reid, R., Prausnitz, J., & Poling, B. (2001). *The Properties of Gases and Liquids*.

Speight, J. G. (2014). *The Chemistry and Technology of Petroleum*. CRC Press.

Tajbl D.G., Simons J.B., C. J. J. (1966). Heterogeneous catalysis in a continuous stirred tank reactor. *I&EC*.

Thiele, E. W. (1939). Relation between Catalytic Activity and Size of Particle. *Industrial and Engineering Chemistry*, *31*(7), 916–920. https://doi.org/10.1021/ie50355a027

Touzani, A., Klvana, D., & BÉLanger, G. (1987). A mathematical model for the dehydrogenation of methylcyclohexane in a packed bed reactor. *The Canadian Journal of Chemical Engineering*, *65*(1), 56–63. https://doi.org/10.1002/cjce.5450650110

Tsotsas, E., & Schlünder, E. U. (1988). On axial dispersion in packed beds with fluid flow. *Chemical Engineering and Processing: Process Intensification*, *24*(1), 15–31. https://doi.org/10.1016/0255-2701(88)87002-8

Tsotsas, E., & Schlünder, E. U. (1990). Heat transfer in packed beds with fluid flow: remarks on the meaning and the calculation of a heat transfer coefficient at the wall. *Chemical Engineering Science*, *45*(4), 819–837. https://doi.org/10.1016/0009-2509(90)85005-X

Usman, M. R., Cresswell, D. L., & Garforth, A. A. (2014). Mathematical Modeling of a Laboratory Methylcyclohexane Dehydrogenation Reactor and Estimation of Radial Thermal Conductivities and Wall Heat Transfer Coefficients. *Chemical Engineering Communications*, *201*(9), 1240–1258. https://doi.org/10.1080/00986445.2013.804816

Varma, A., & Amundson, N. R. (1973). The non-adiabatic tubular reactor: Stability considerations. *The Canadian Journal of Chemical Engineering*, *51*(4), 459–467. https://doi.org/10.1002/cjce.5450510411

Vo¨ lter, G Lietz, M. U. (1981). No Title. *J Catalysis*, *68*, 42.

Wakao, N., Kaguei, S., & Funazkri, T. (1979). Effect of fluid dispersion coefficients on particle-to-fluid heat transfer coefficients in packed beds. Correlation of nusselt numbers. *Chemical Engineering Science*, *34*(3), 325–336. https://doi.org/10.1016/0009-2509(79)85064-2

Weisz, P. B. (1955). Effect of intra-particle diffusion on the kinetics of catalytic dehydrogenation of cyclohexane. *Journal of Physical Chemistry*, *59*(9), 823–826. https://doi.org/10.1021/j150531a006

Westerink, E. J., Koster, N., Reaction, C., & Laboratories, E. (1990). Design of Tubular Reactors for, *45*(12), 3443–3455.

Yagi, S., Kunii, D., & Wakao, N. (1960). Studies on axial effective thermal conductivities in packed beds. *AIChE Journal*, *6*(4), 543–546. https://doi.org/10.1002/aic.690060407

Yagi, S., & Wakao, N. (1959). Heat and Mass Transfer from Wall to Fluid in Packed Beds. *AIChE Journal*, *5*(1), 79–85. https://doi.org/10.1002/aic.690050118

Appendix

Appendix I: Transport Properties and Dimensionless Numbers Calculated for the fluid- dynamic assessments

Table A.1: Experimental results Transfer coefficients at the average operative conditions

Coefficient	Units	Value
K_G	$[m3/m2.s]$	0,0272
h_w	$[W/m2.K]$	1994,52
h_e	$[W/m2.K]$	579,32

Table A.2: Dimensionless numbers at the average operative conditions

Dimensionless numbers	
Pep	1,96
$Pe_{m,r,p}$	11,16
$Pe_{m,a,p}$	1,96
$Pe_{m,a,r}$	785
Pe	6760
Pe'	3,80
Re	6,23
Nu	2,40
Sh	5,50
Pr	0,32
Sc	3,66
jh	0,56
jm	0,85

Table A.3: Properties at the average operative conditions

Property	Units	Value
$D_{MCH,m}$	$[m2/s]$	8,3516E-07
$D_{MCH,k}$	[m2/s]	2,2411E-06
$D_{\text{MCH e,p}}$	$[m2/s]$	7,3011E-08
D_{ea}	$[m2/s]$	9,7154E-06
D_{er}	$[m2/s]$	1,7075E-06
$\square_{\text{mixture}}$	$[kg/m.s]$	1,8441E-05
$\square_{\text{mixture}}$	$[J/s.m.K]$	2,0778E-01

Appendix II: Sensibility Function Results

- Activation Energy PV

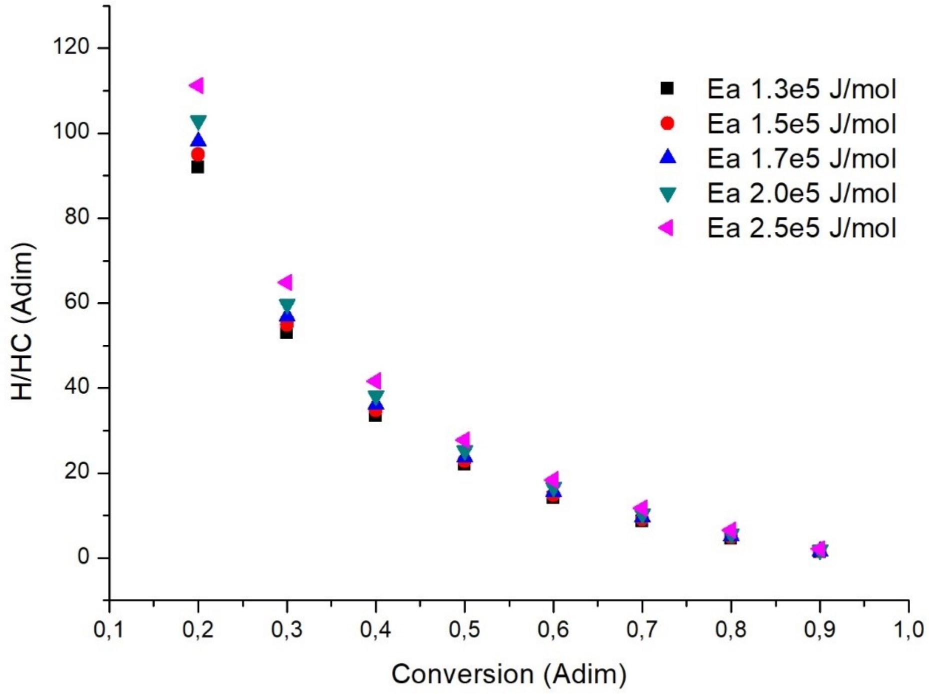

Figure A.1.Conversion for different H/HC ratios values and different activation energy levels.

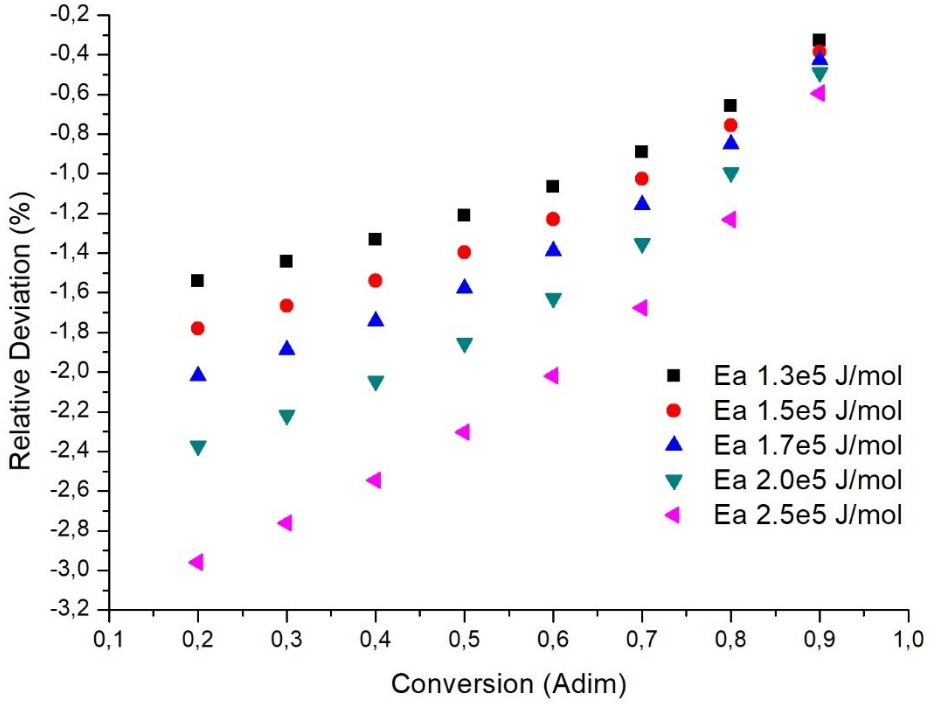

Figure A.2. Relative deviation for different H/HC ratios and different activation energy levels.

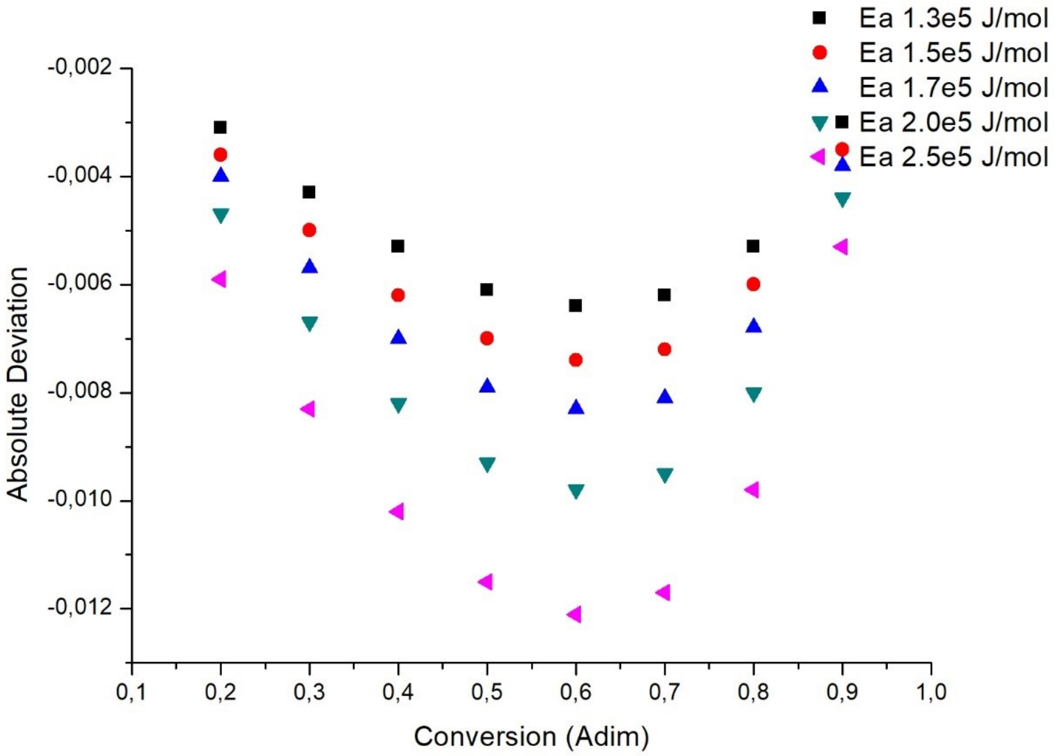

Figure A.3. Absolute deviation for different H/HC ratios and different activation energy levels.

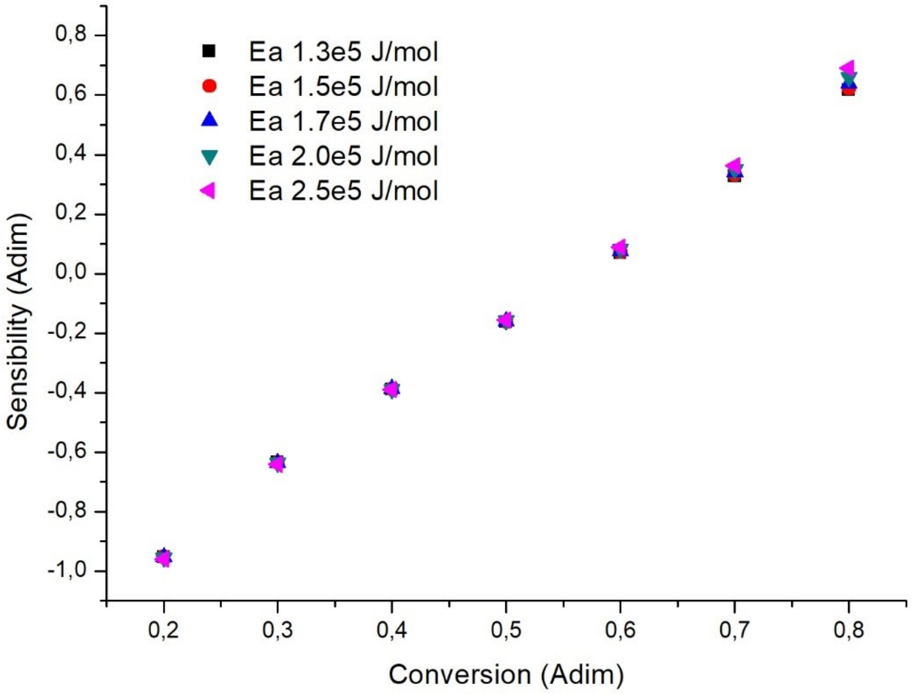

Figure A.4. Sensibility for different H/HC ratios and different activation energy levels.

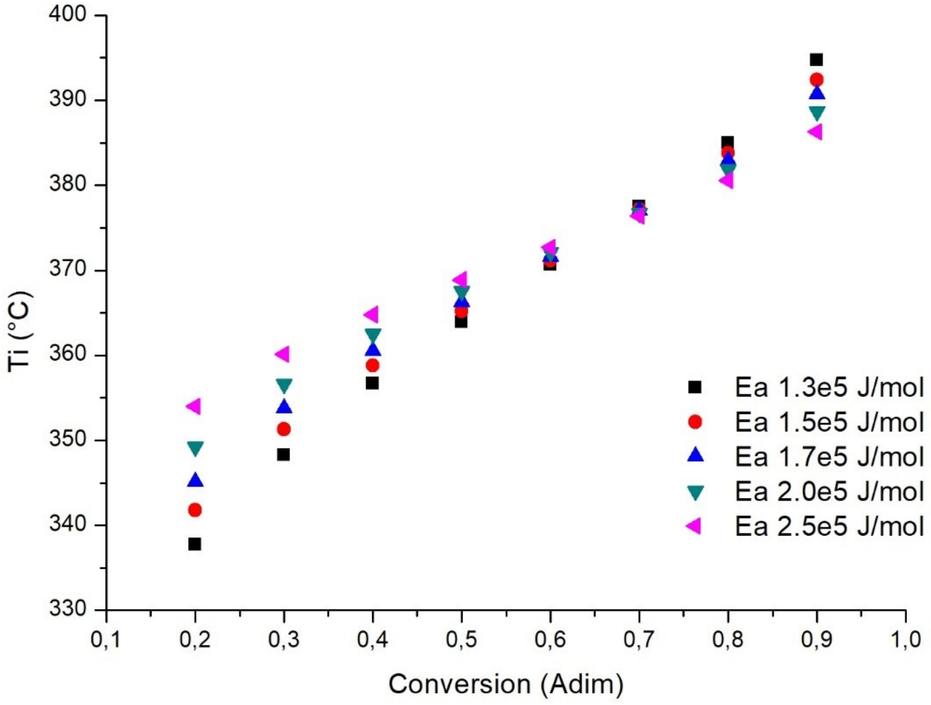

Figure A.5. Conversion for different temperature values and different activation energy levels.

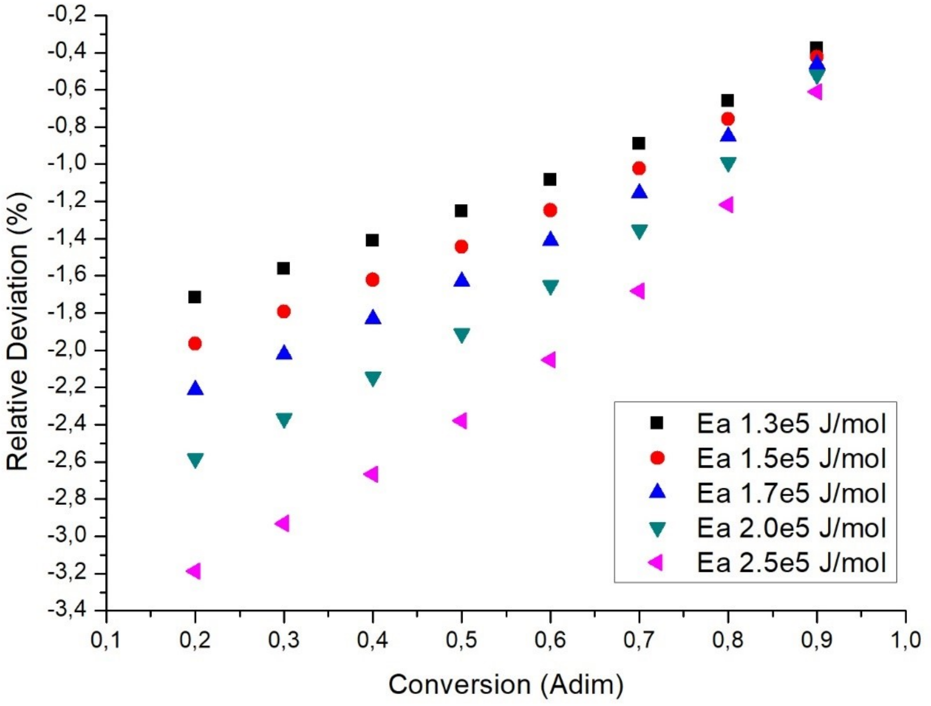

Figure A.6. Relative deviation for different temperature values and different activation energy levels.

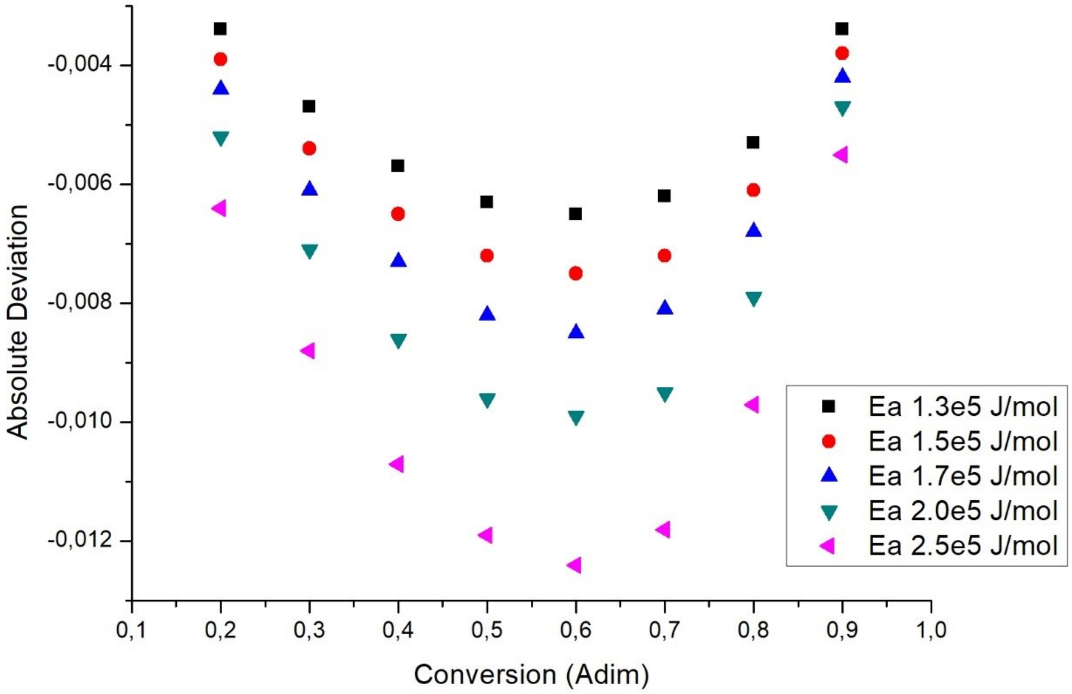

Figure A.7. Absolute deviation for different temperature values and different activation energy levels.

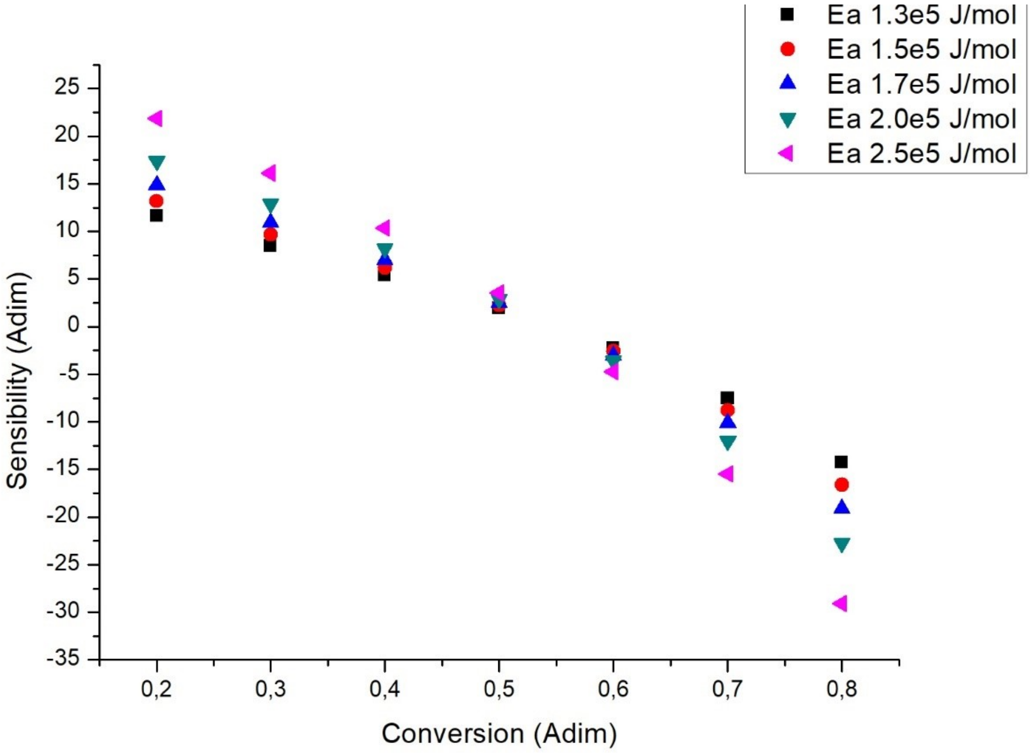

Figure A.8. Sensibility for different temperature values and different activation energy levels.

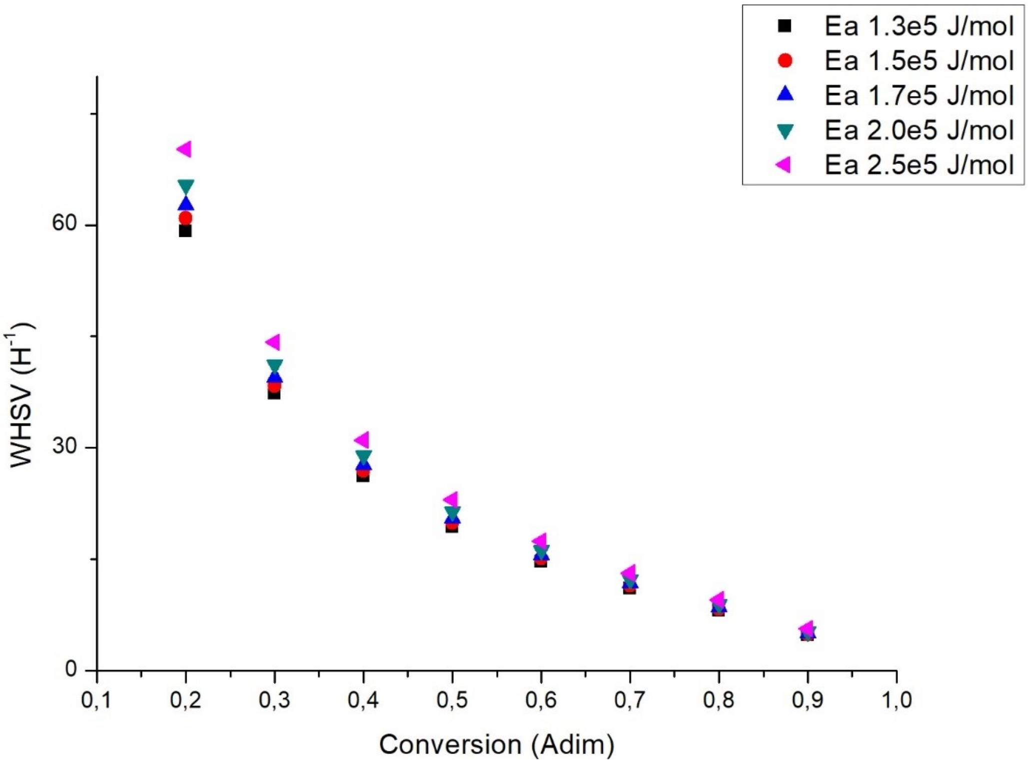

Figure A.9. Conversion for different WHSV values and different activation energy levels.

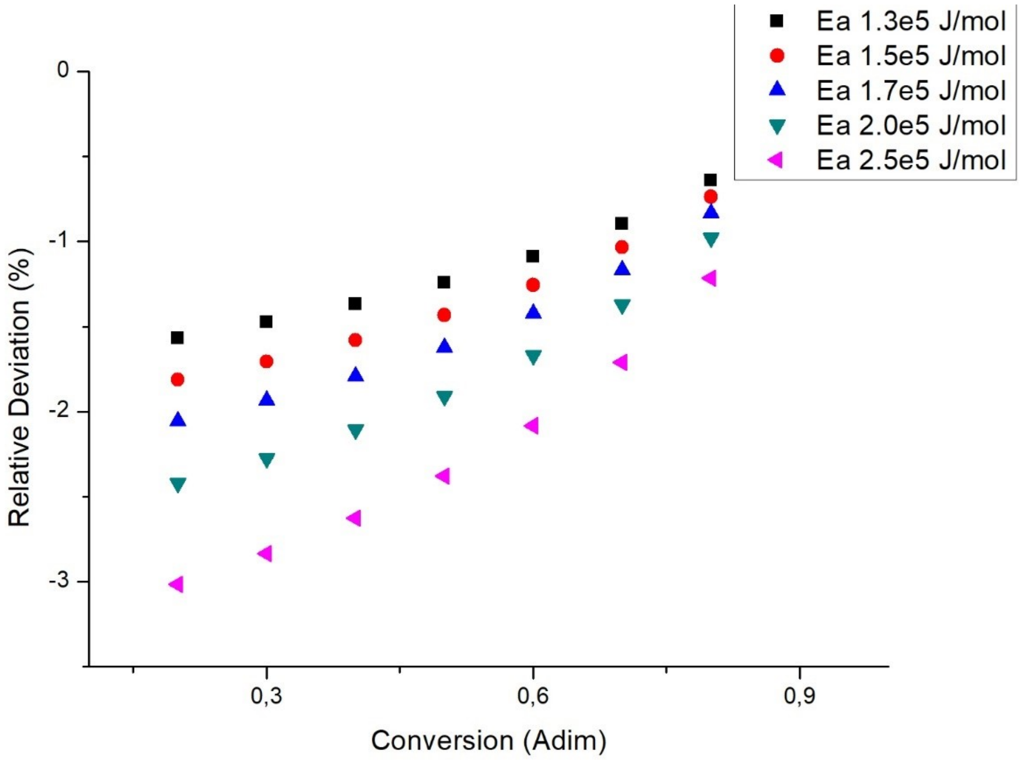

Figure A.10. Relative deviation for different WHSV values and different activation energy levels.

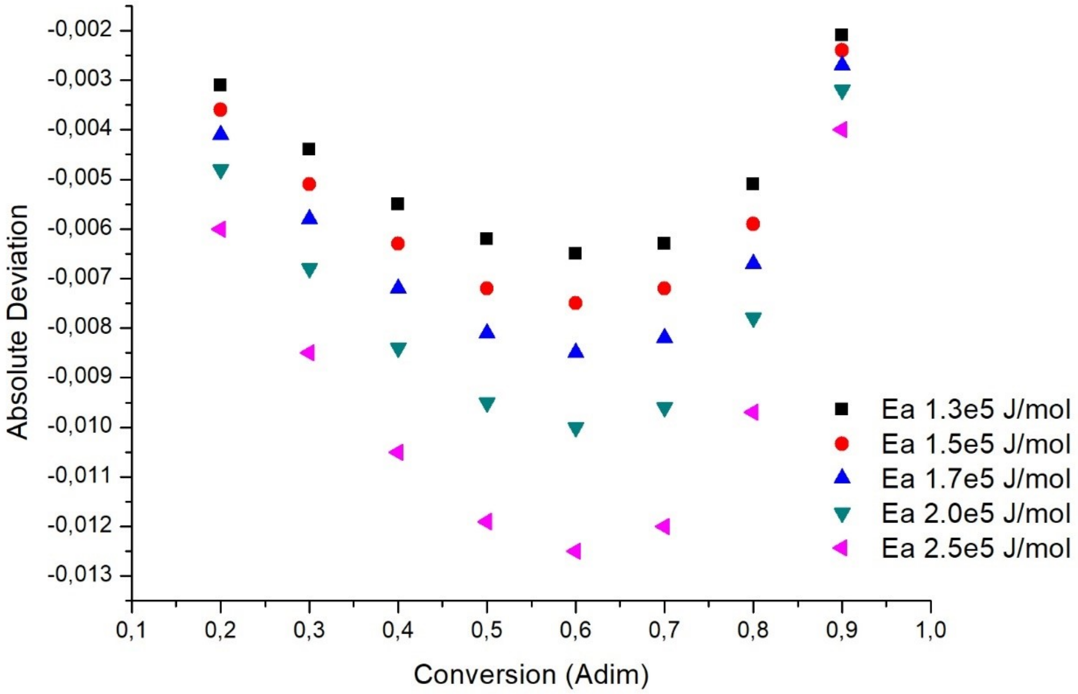

Figure A.11. Absolute deviation for different WHSV values and different activation energy levels.

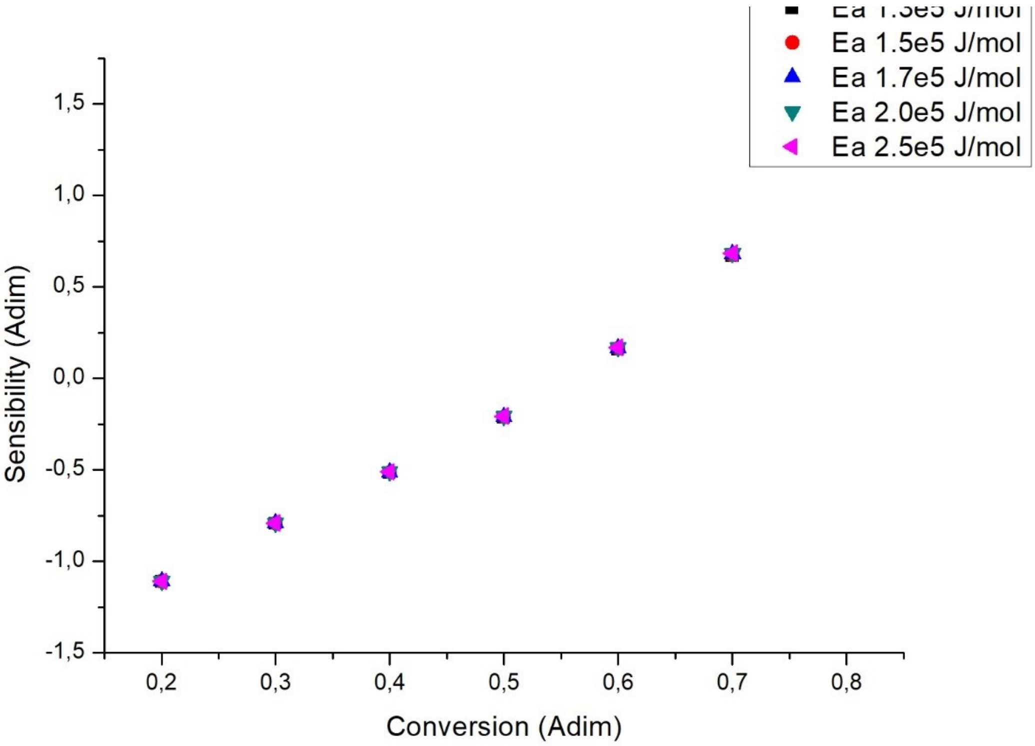

Figure A.12. Sensibility for different WHSV values and different activation energy levels.

- Pressure as PV

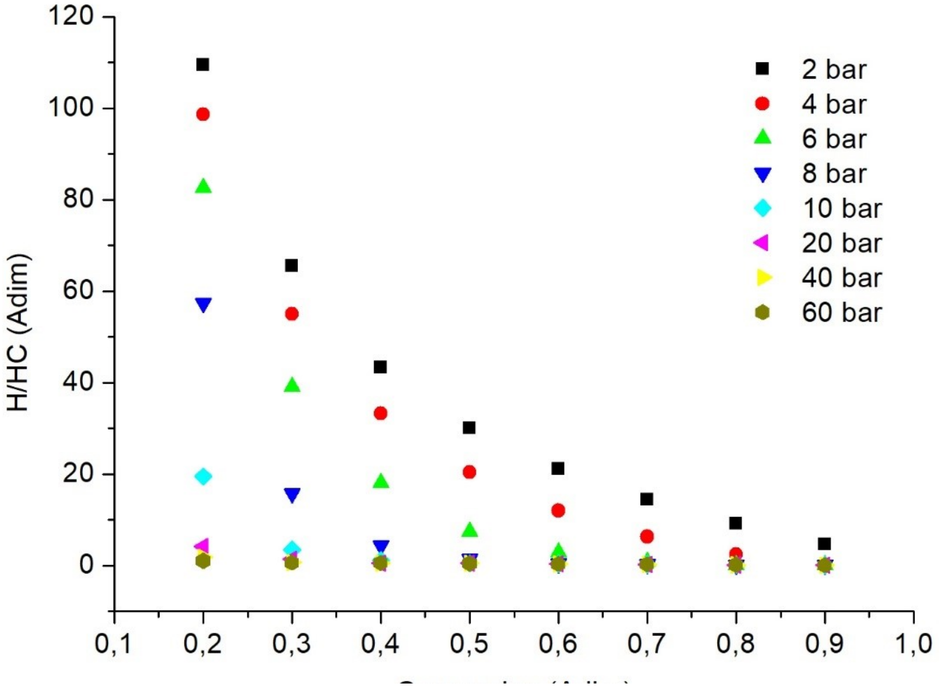

Figure A.13. Conversion for different H/HC ratios and different pressure levels.

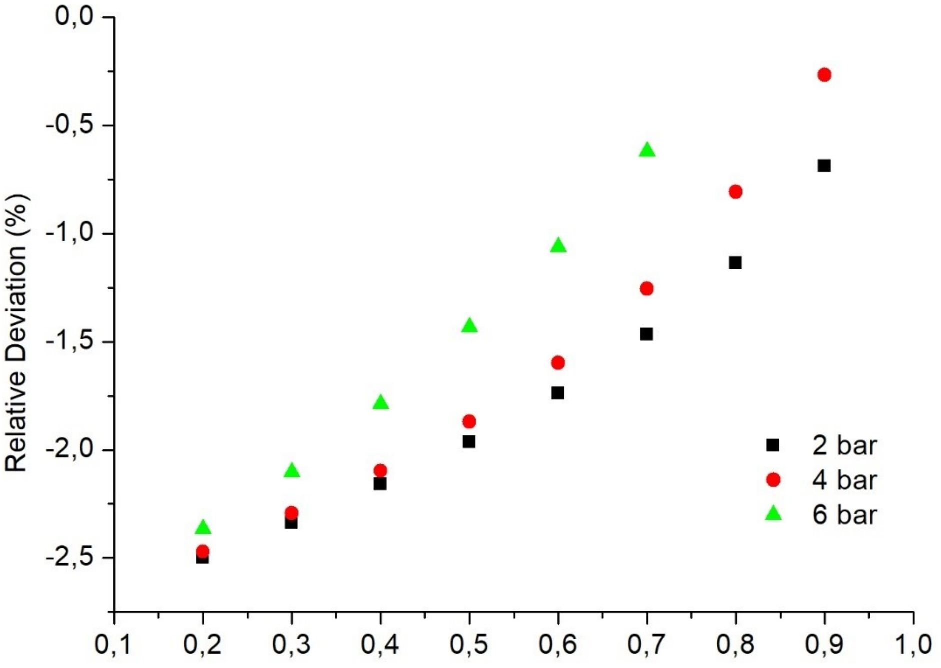

Figure A.14. Relative deviation for different H/HC ratios and different pressure levels.

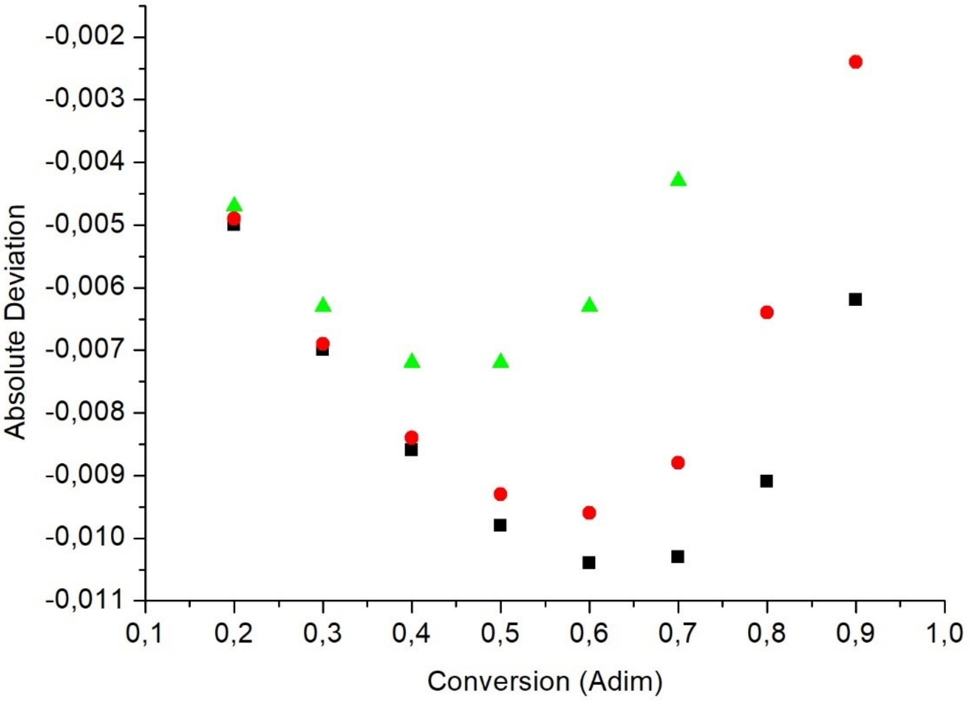

Figure A.15. Absolute deviation for different H/HC ratios and different pressure levels.

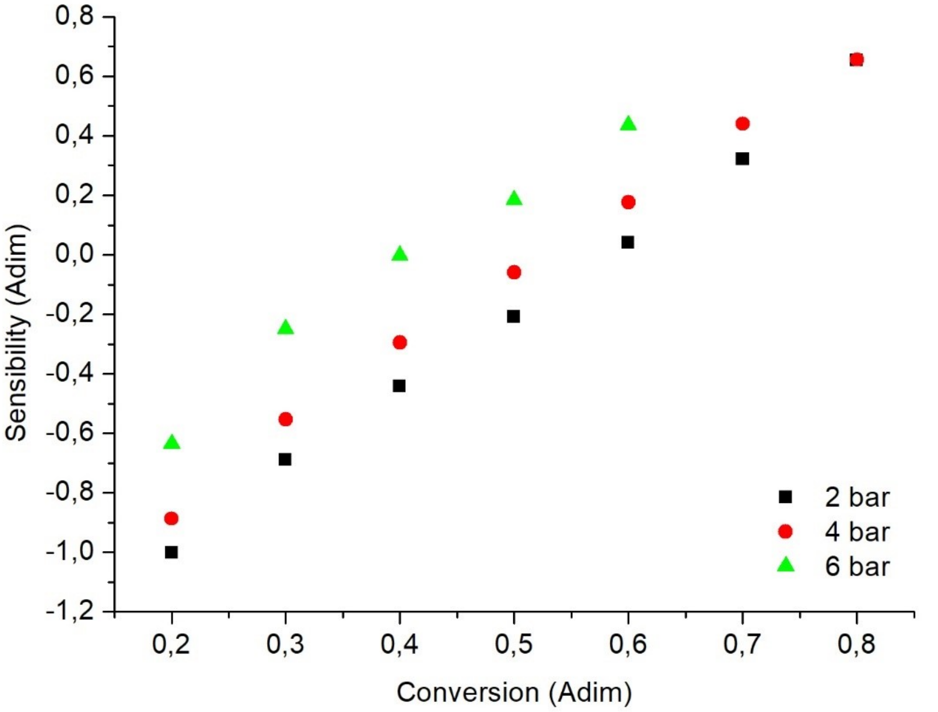

Figure A.16. Sensibility for different H/HC ratios and different pressure levels.

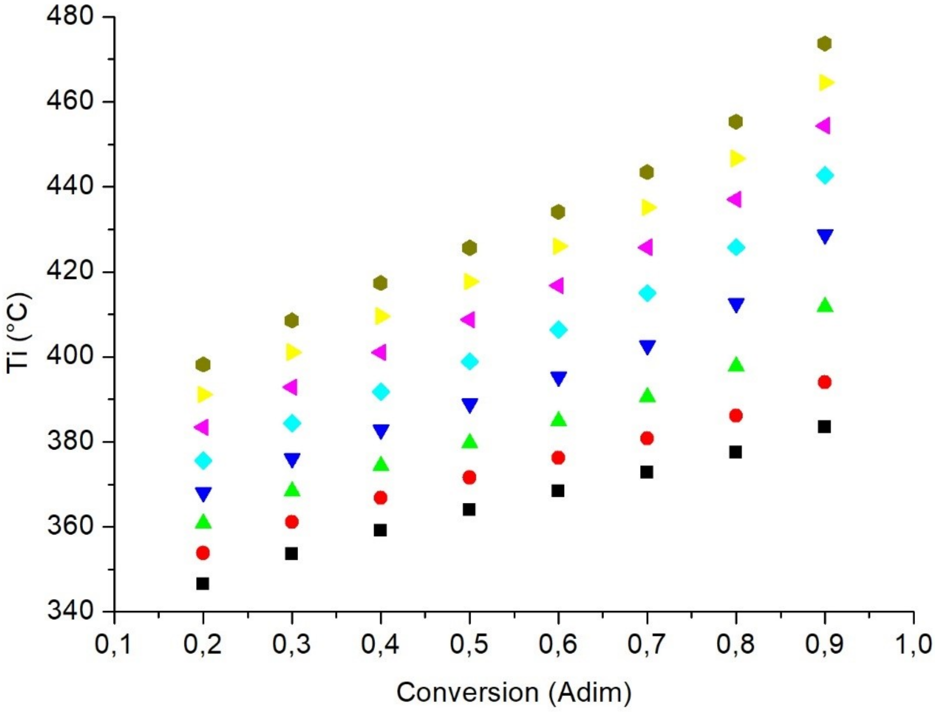

Figure A.17. Conversion for different temperature values and different pressure levels.

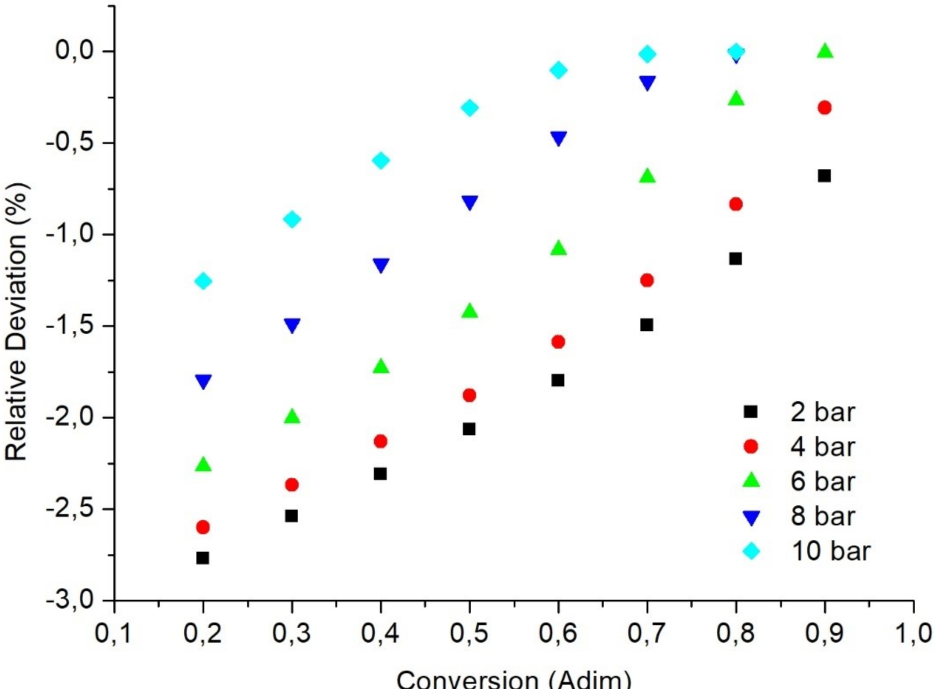

Figure A.18. Relative deviation for different temperature values and different pressure levels.

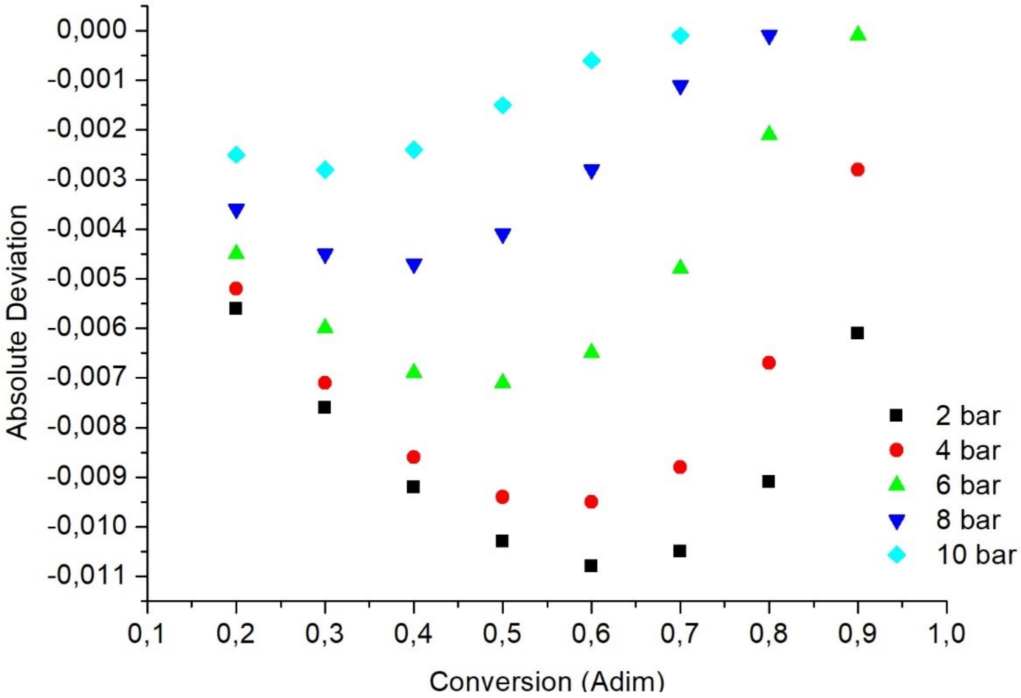

Figure A.19. Absolute deviation for different temperature values and different pressure levels.

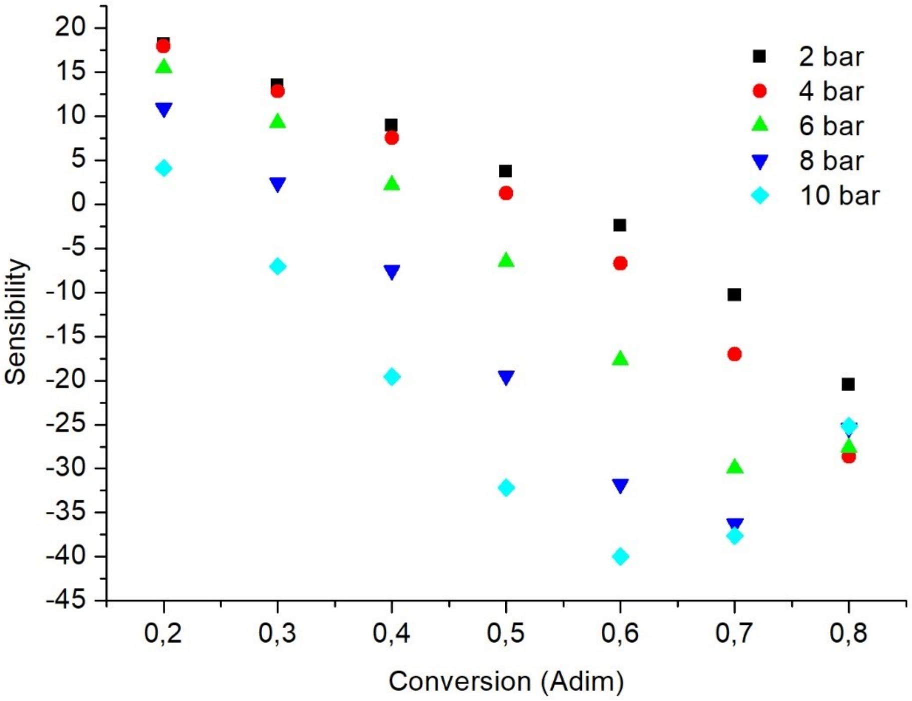

Figure A.20. Sensibility for different temperature values and different pressure levels.

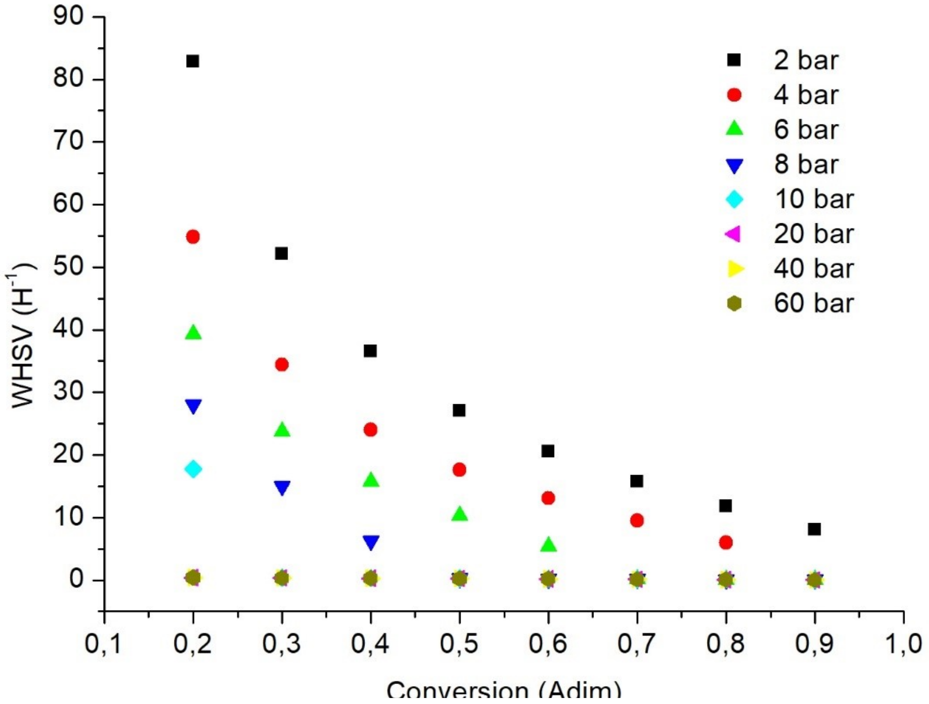

Figure A.21. Conversion for different WHSV values and different pressure levels.

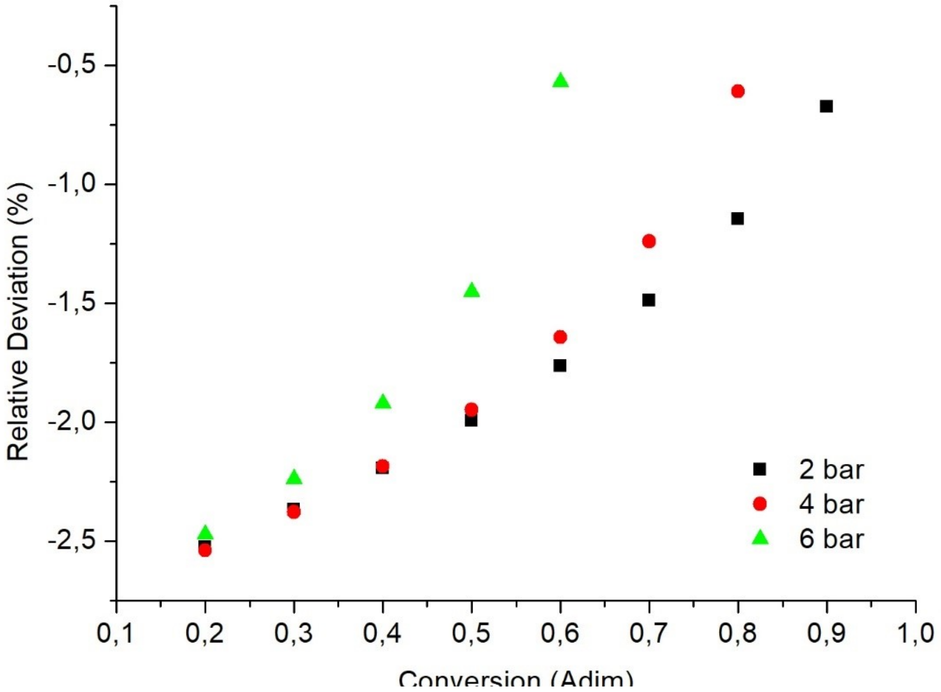

Figure A.22. Relative deviation for different WHSV values and different pressure levels.

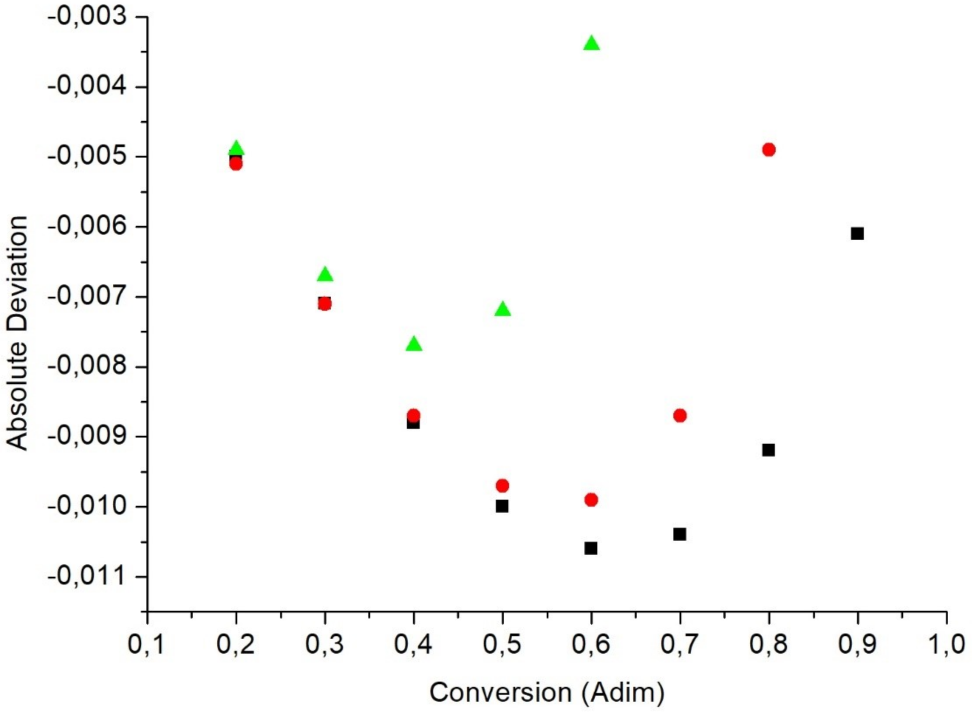

Figure A.23. Absolute deviation for different WHSV values and different pressure levels.

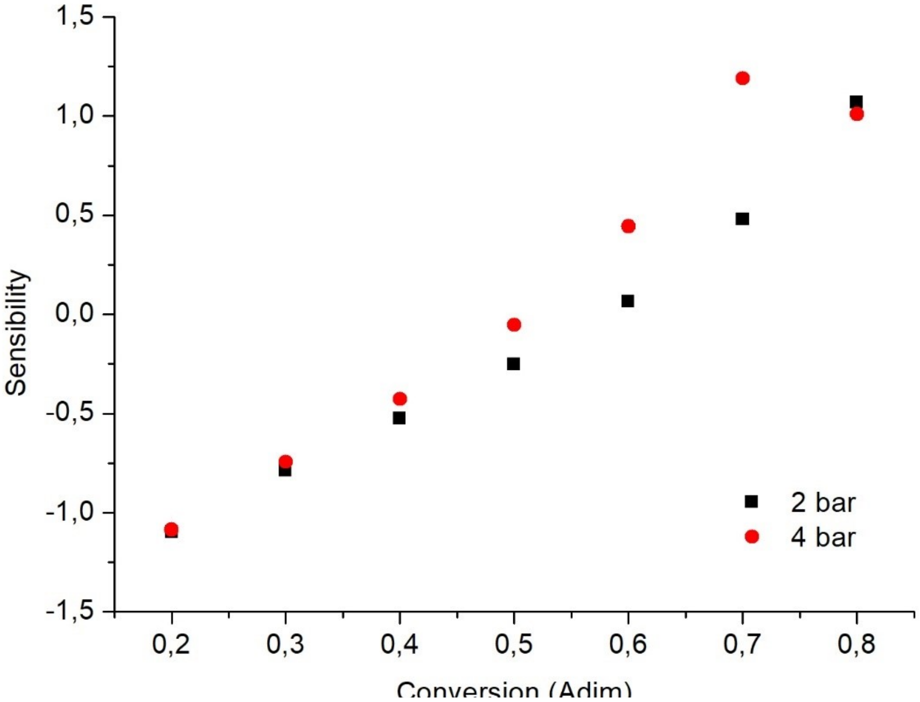

Figure A.24. Sensibility for different WHSV values and different pressure levels.

- Temperature as PV

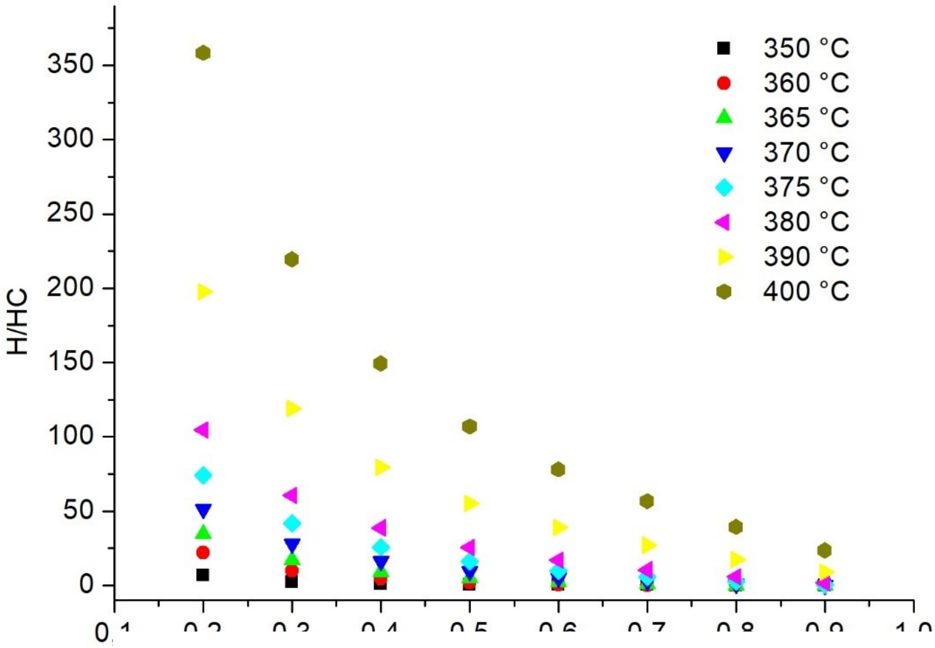

Figure A.25. Conversion for different H/HC ratios values and different temperature levels.

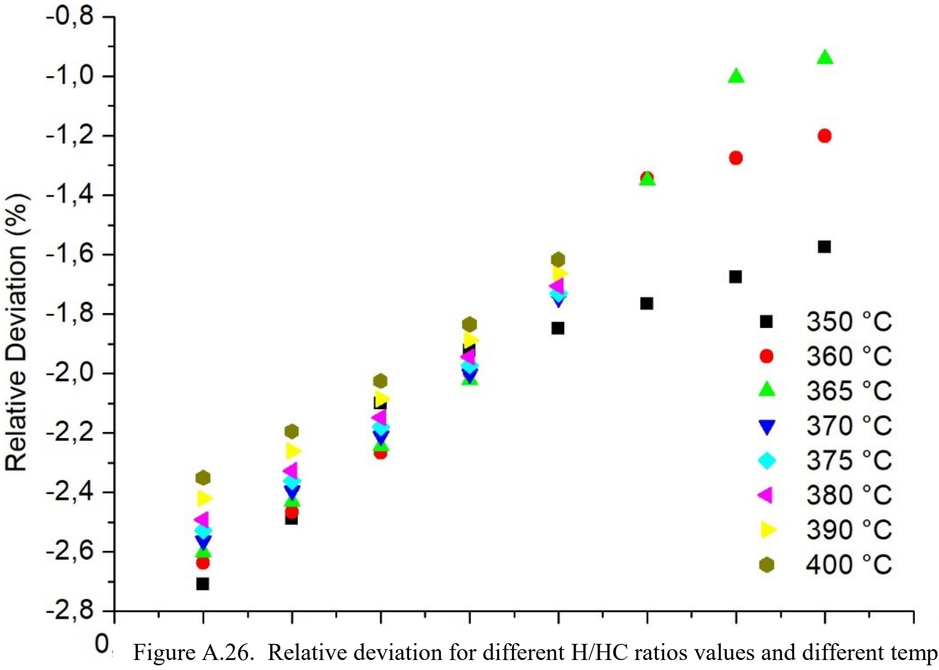

Figure A.26. Relative deviation for different H/HC ratios values and different temperature levels.

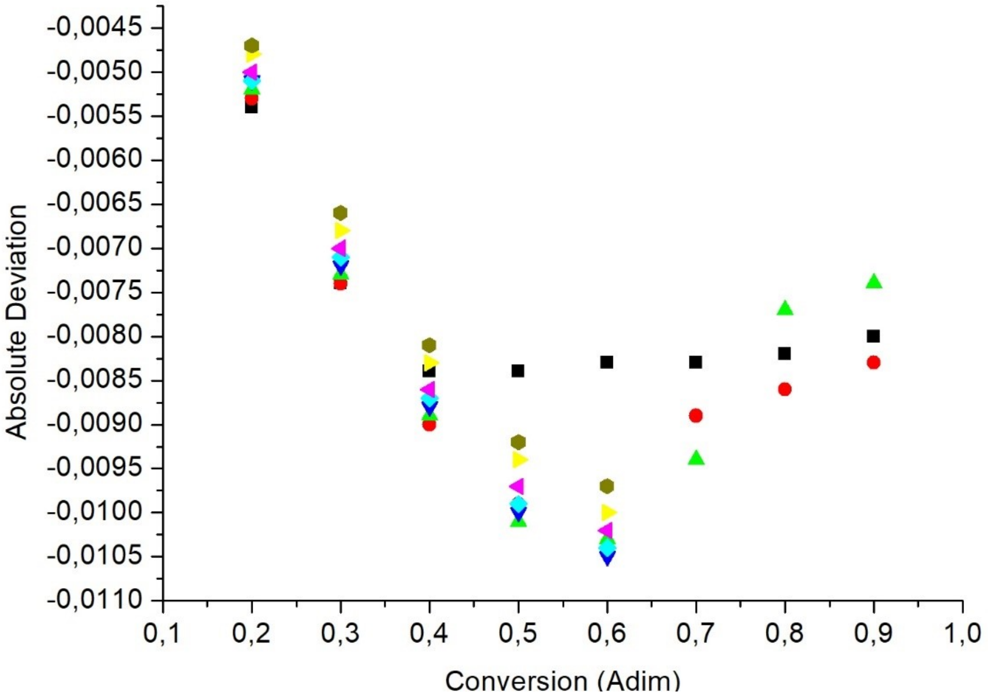

Figure A.27. Absolute deviation for different H/HC ratios values and different temperature levels.

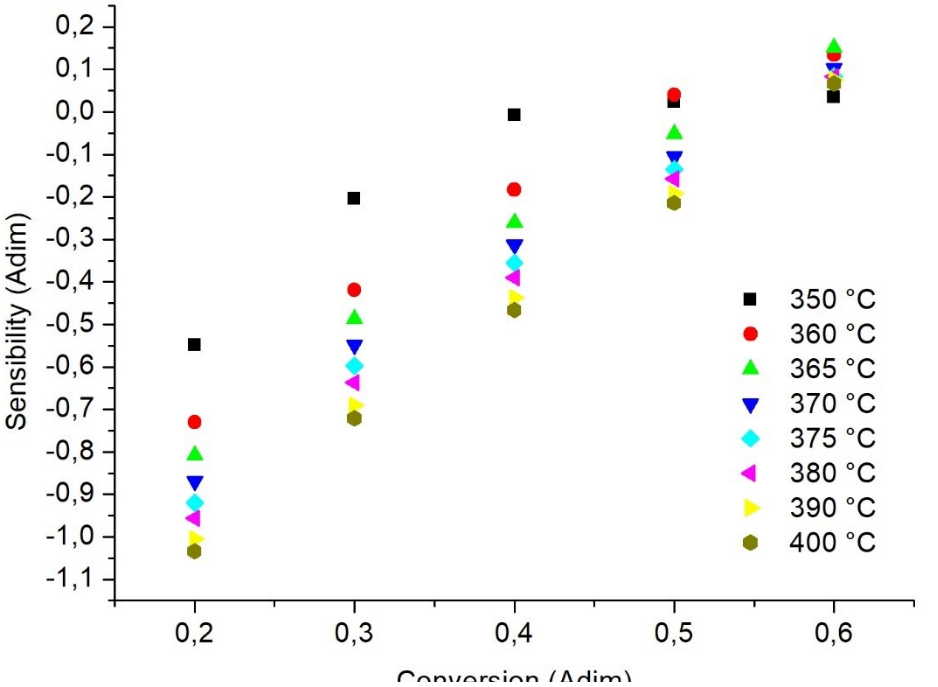

Figure A.28. Sensibility for different H/HC ratios values and different temperature levels.

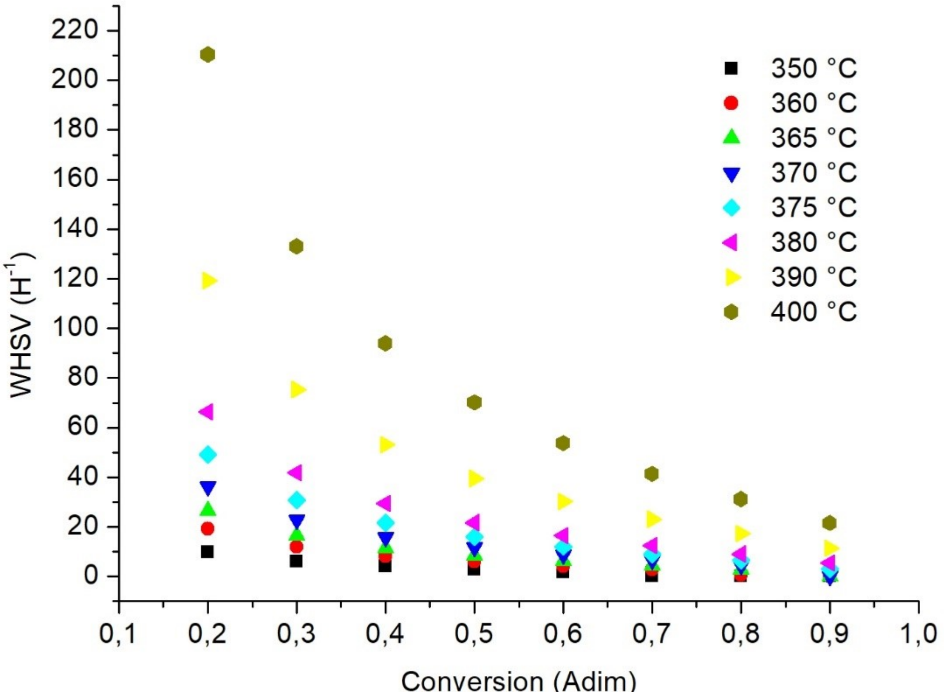

Figure A.29. Conversion for different WHSV values and different temperature levels.

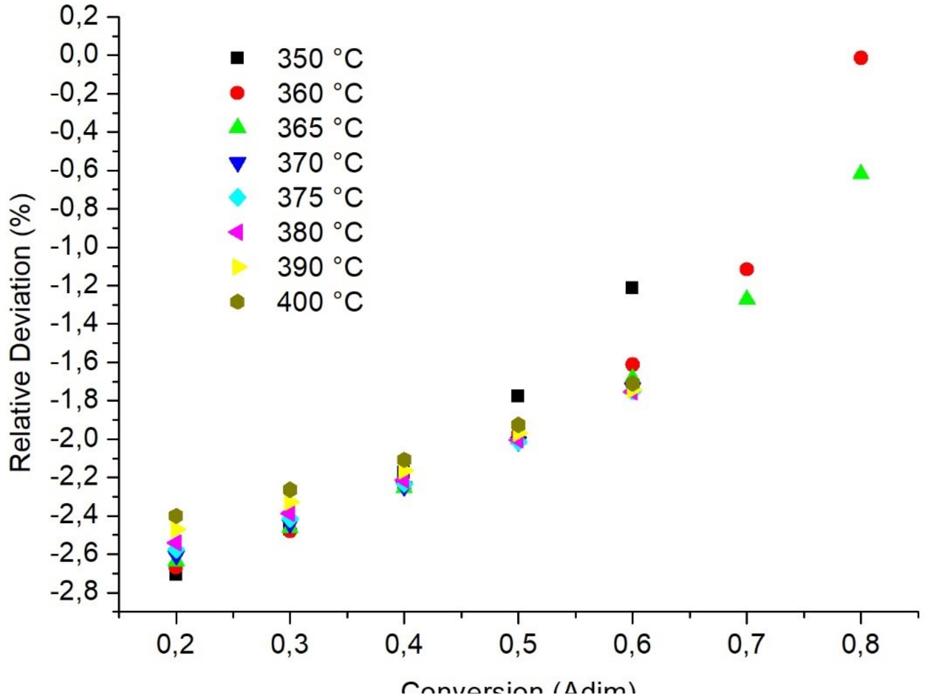

Figure A.30. Relative deviation for different WHSV values and different temperature levels.

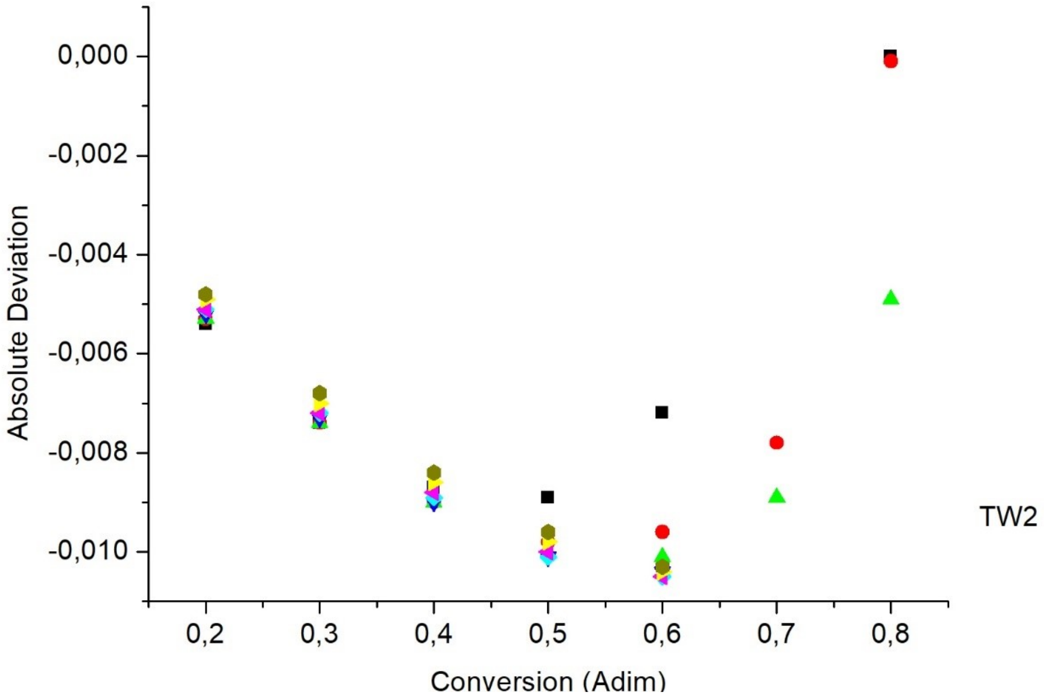

Figure A.31. Absolute deviation for different WHSV values and different temperature levels.

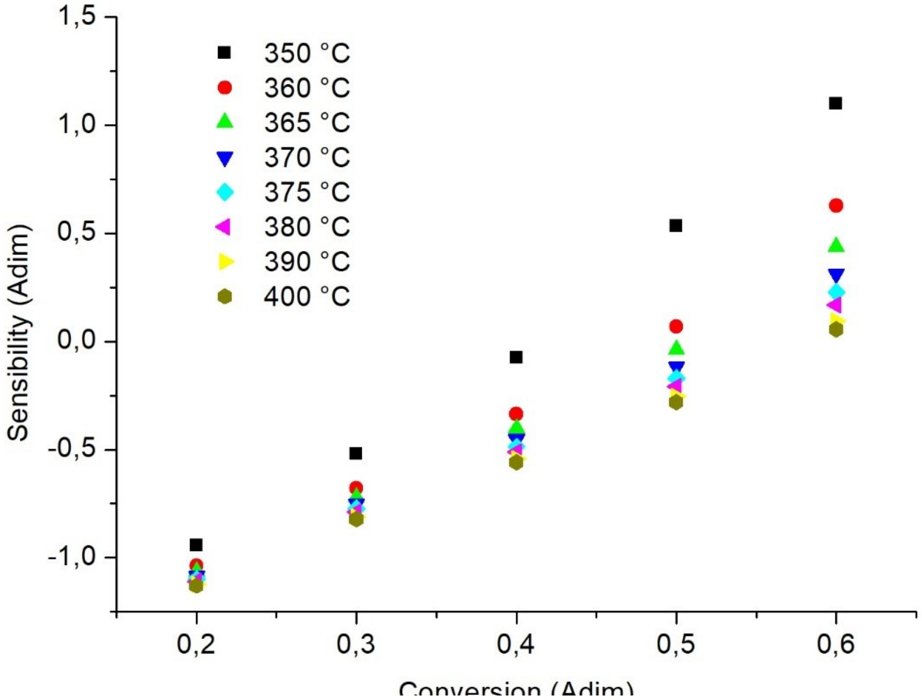

Figure A.32. Sensibility for different WHSV values and different temperature levels.

- WHSV as PV

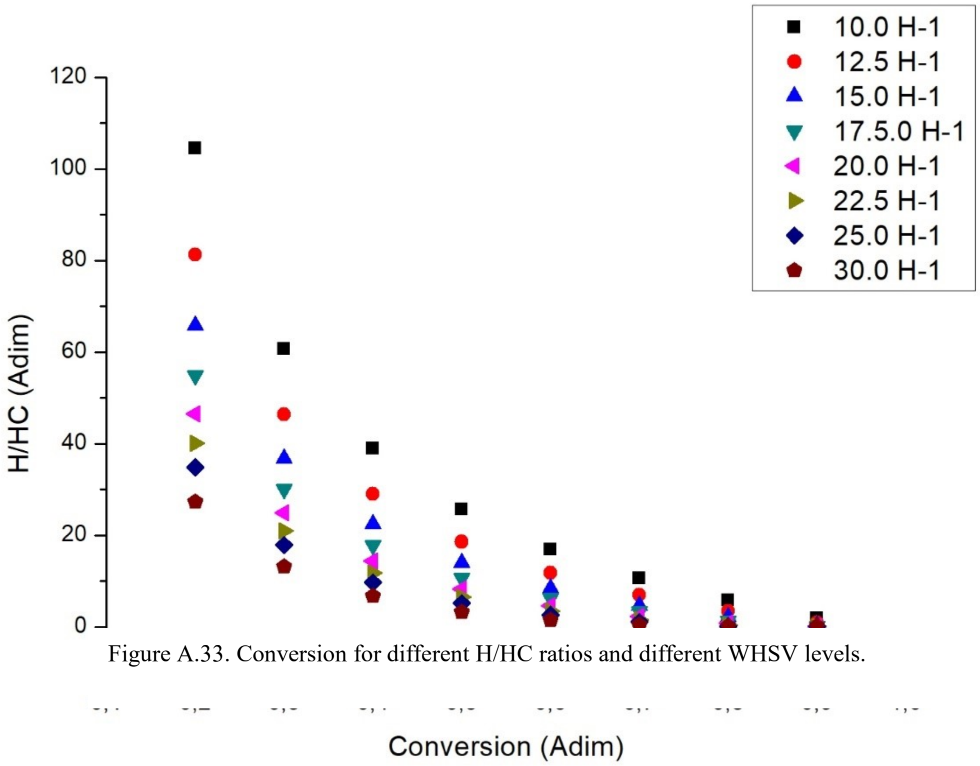

Figure A.33. Conversion for different H/HC ratios and different WHSV levels.

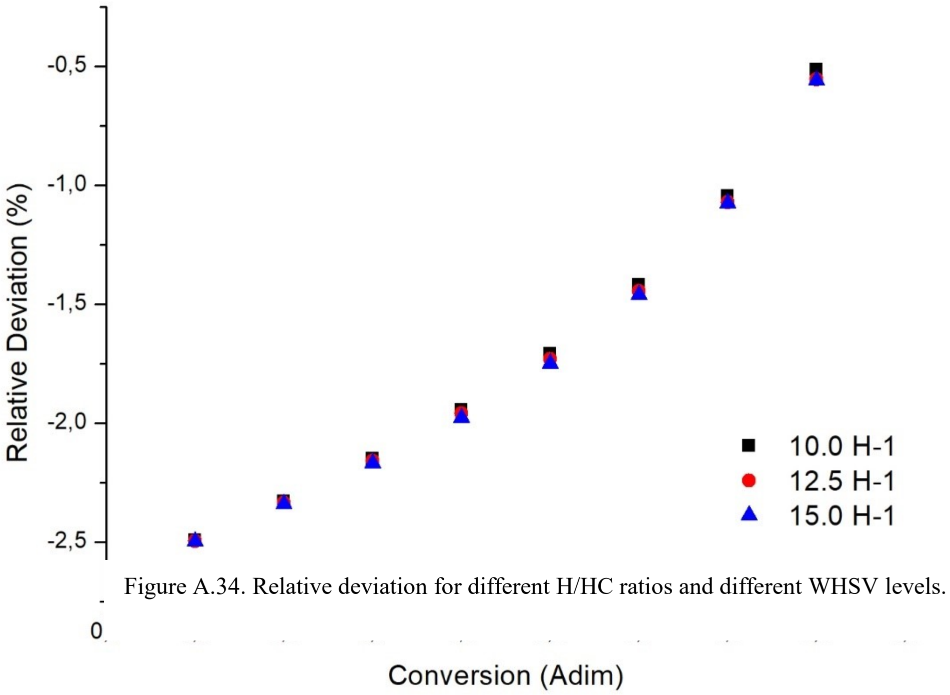

Figure A.34. Relative deviation for different H/HC ratios and different WHSV levels.

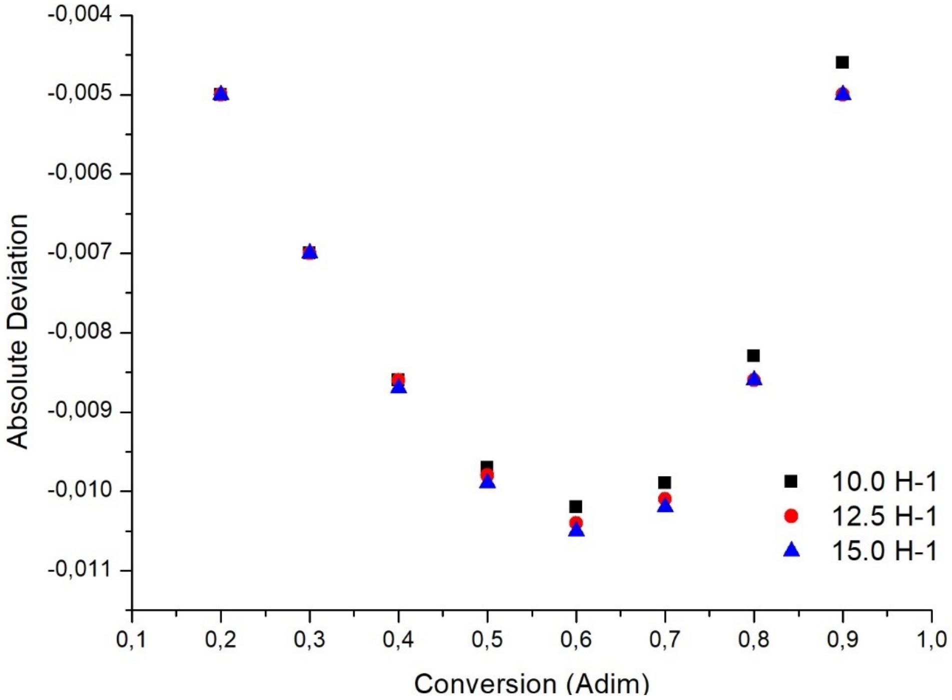

Figure A.35. Absolute deviation for different H/HC ratios and different WHSV levels.

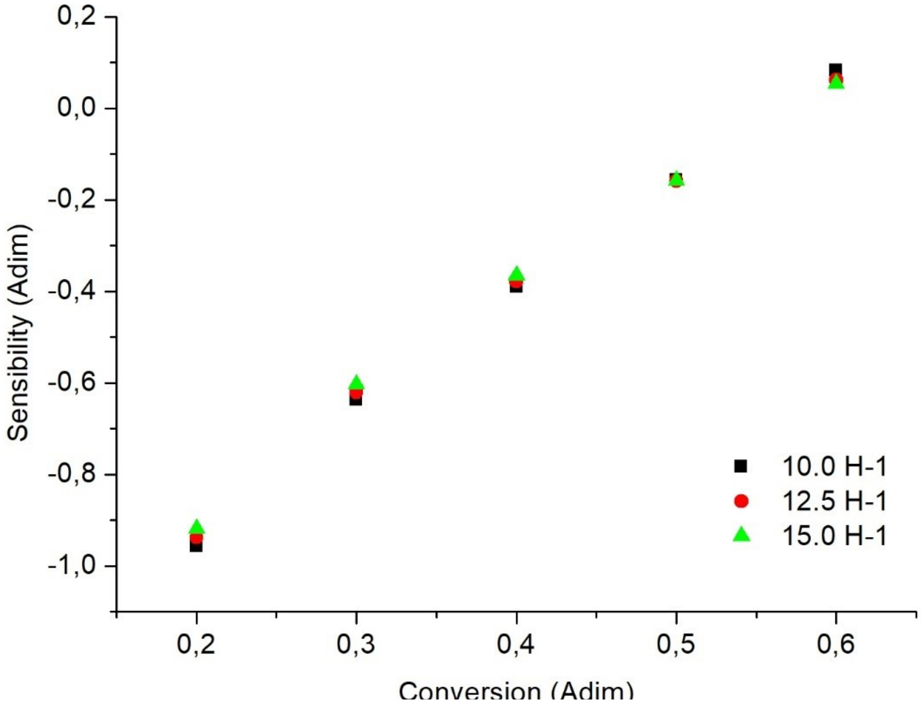

Figure A.36. Sensibility for different H/HC ratios and different WHSV levels.

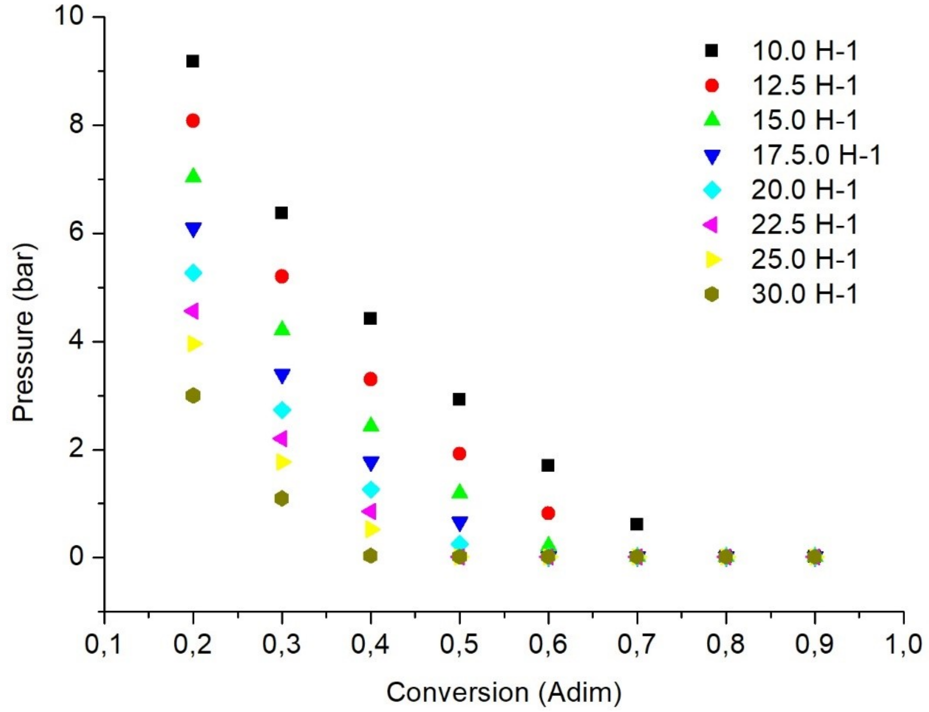

Figure A.37. Conversion for different pressure values and different WHSV levels.

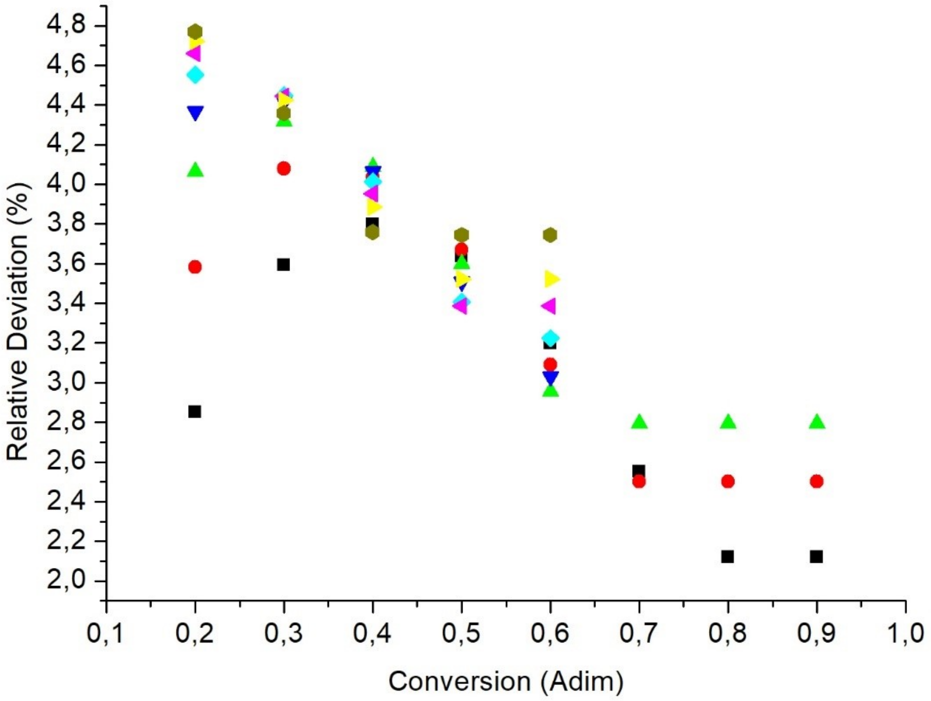

Figure A.38. Relative deviation for different pressure values and different WHSV levels.

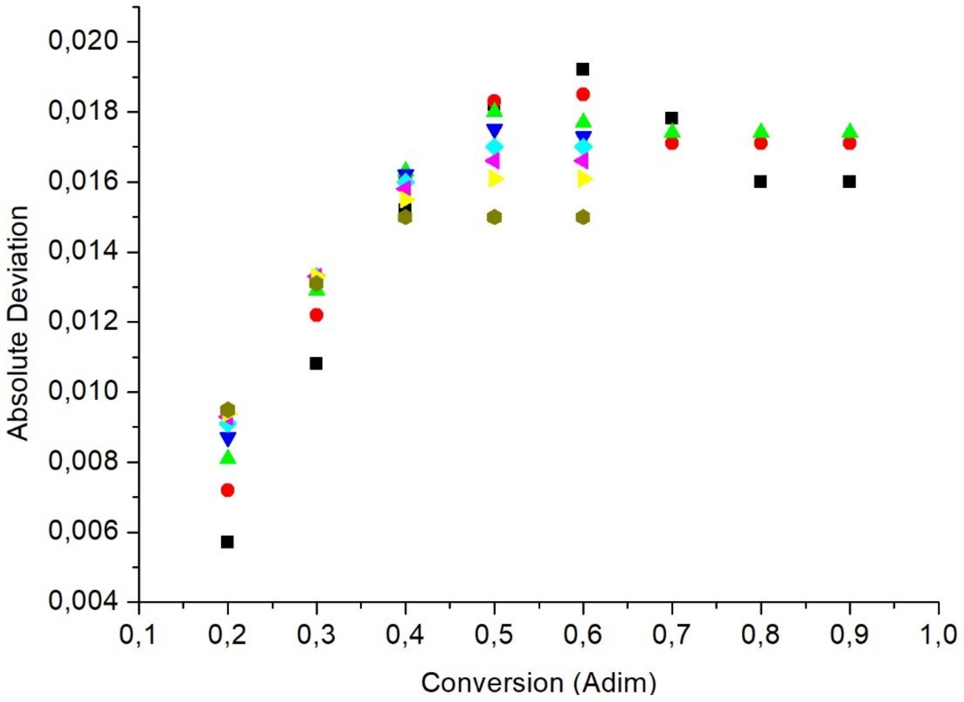

Figure A.39. Absolute deviation for different pressure values and different WHSV levels.

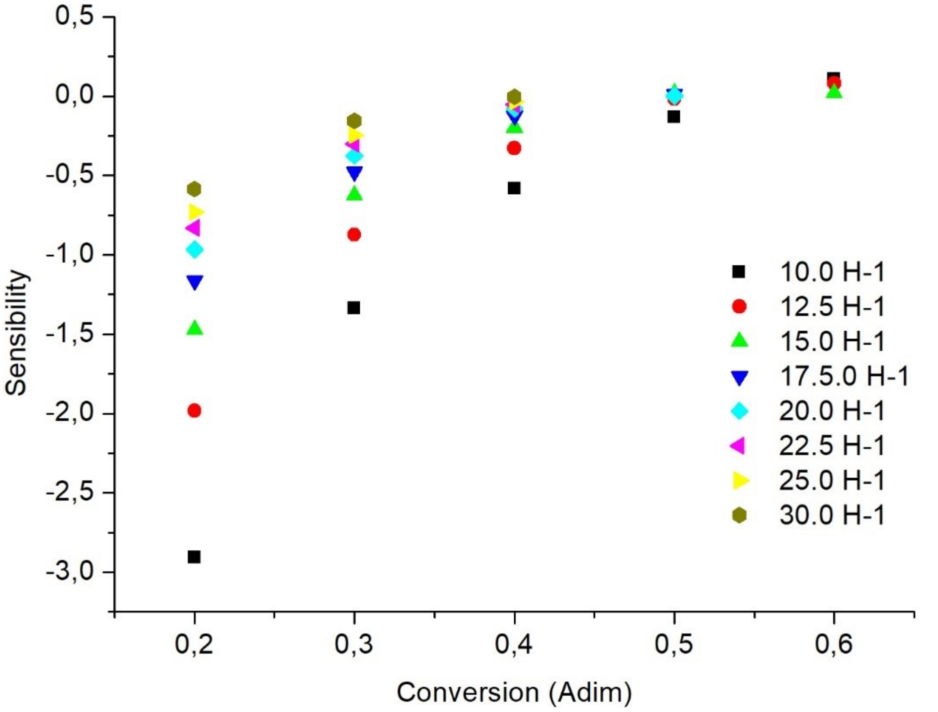

Figure A.40. Sensibility for different pressure values and different WHSV levels.

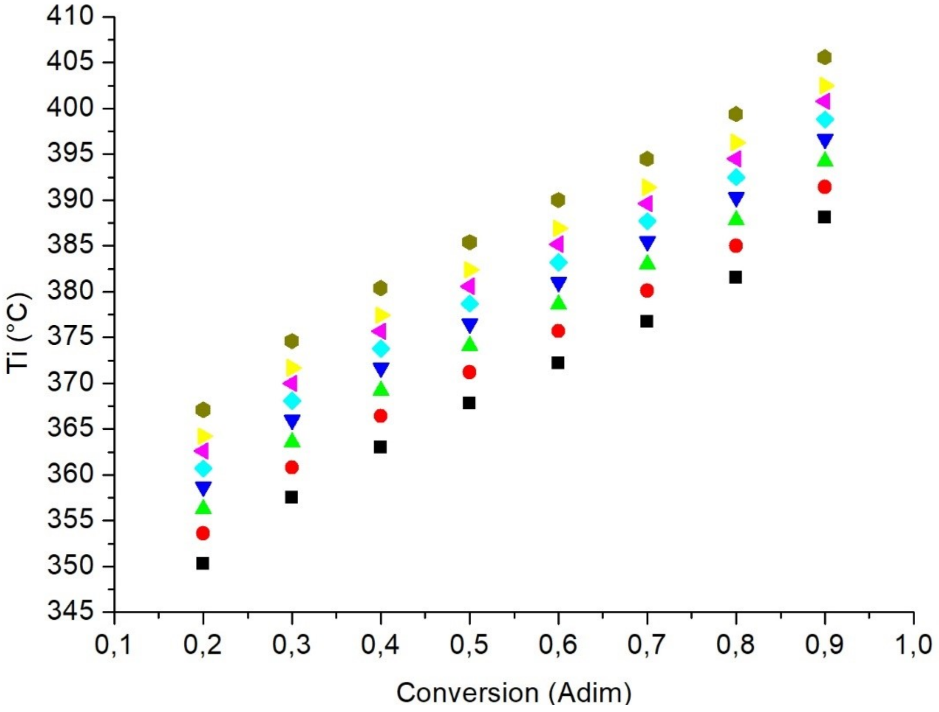

Figure A.41. Conversion for different temperature values and different WHSV levels.

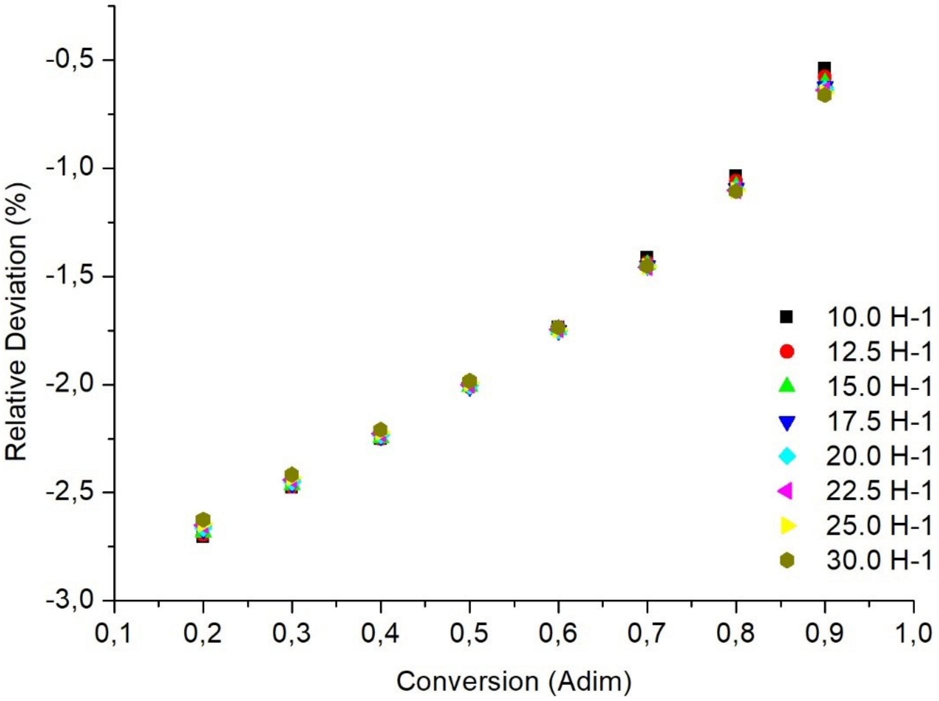

Figure A.42. Relative deviation for different temperature values and different WHSV levels.

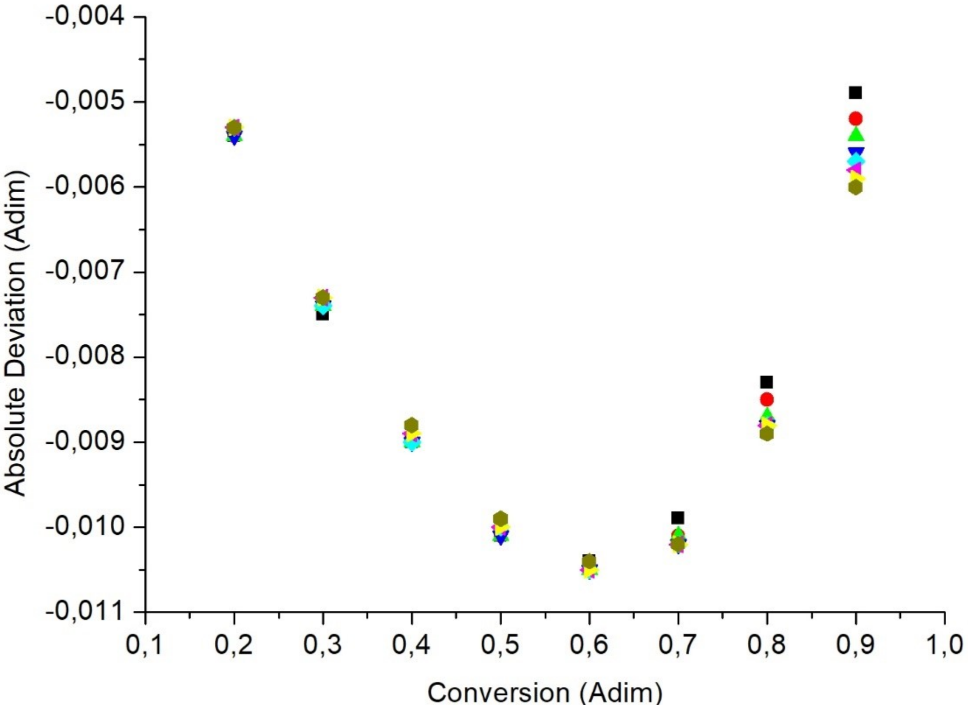

Figure A.43. Absolute deviation for different temperature values and different WHSV levels.

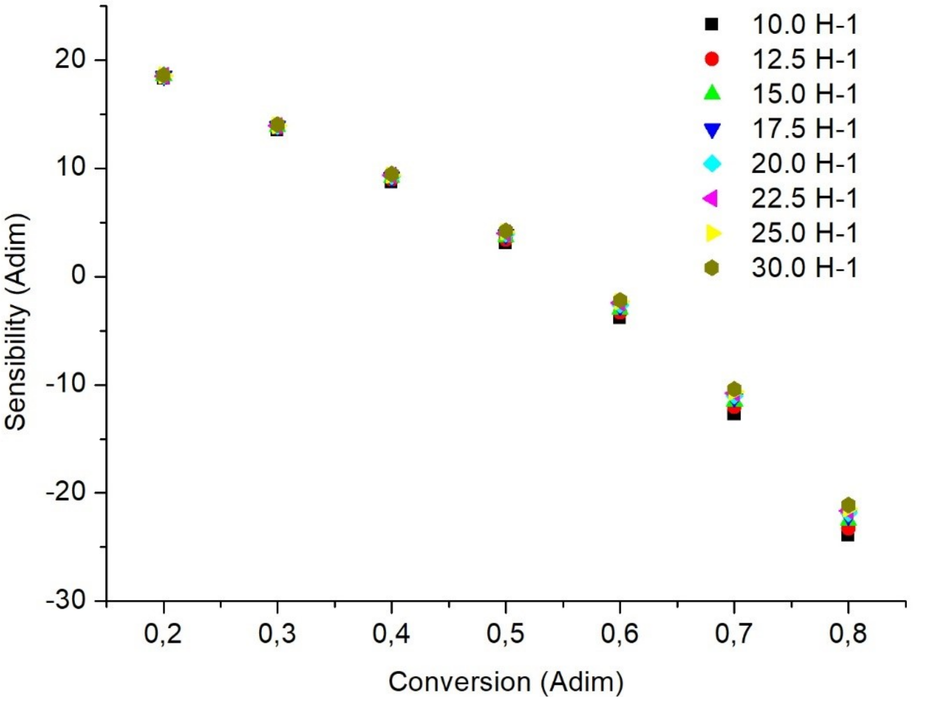

Figure A.44. Sensibility for different temperature values and different WHSV levels.

Appendix III: Zero-Deviation Function Results

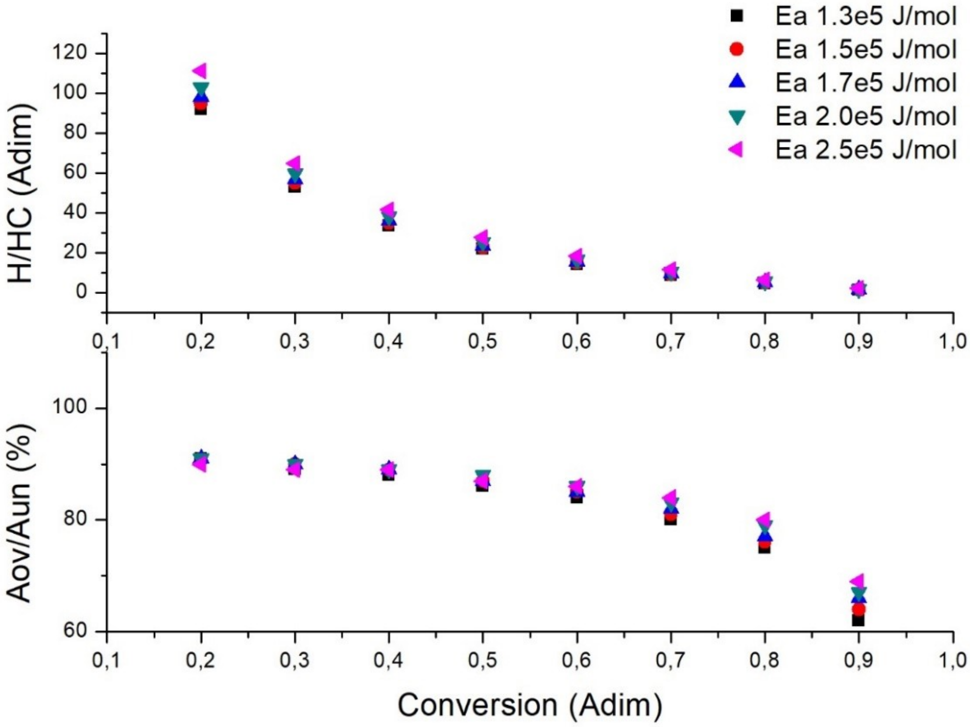

Figure A.45. (a)Conversion for different H/HC ratios and different activation energy levels. (b) Ratio of area values for the conditions evaluated in (a)

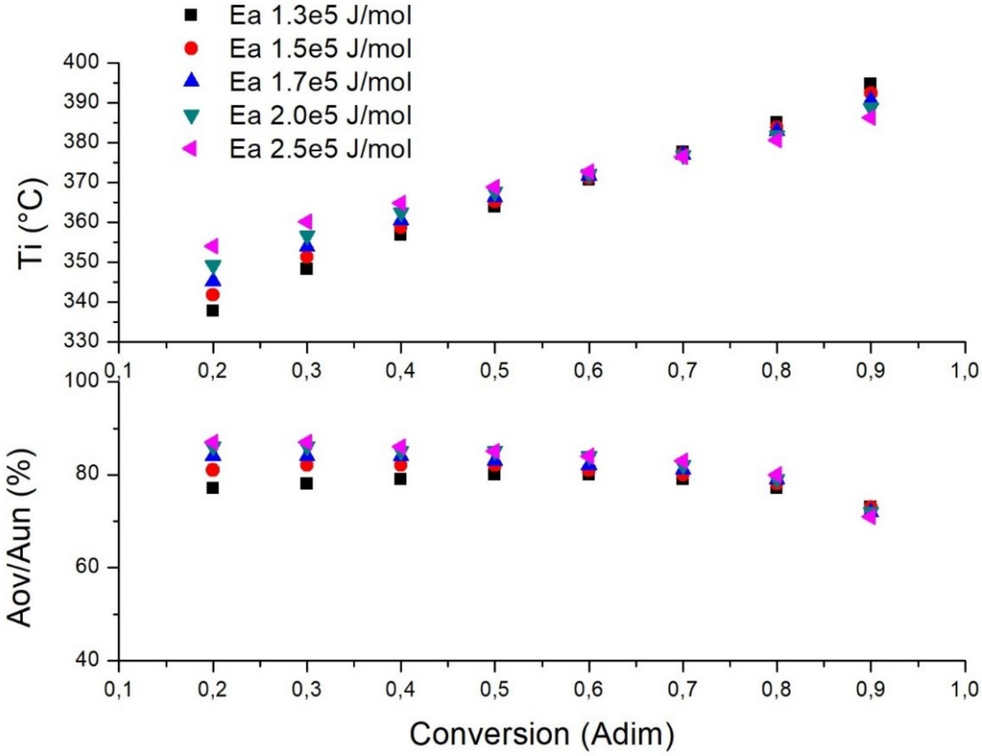

Figure A.46. (a)Conversion for different temperature values and different activation energy levels. (b) Ratio of area values for the conditions evaluated in (a)

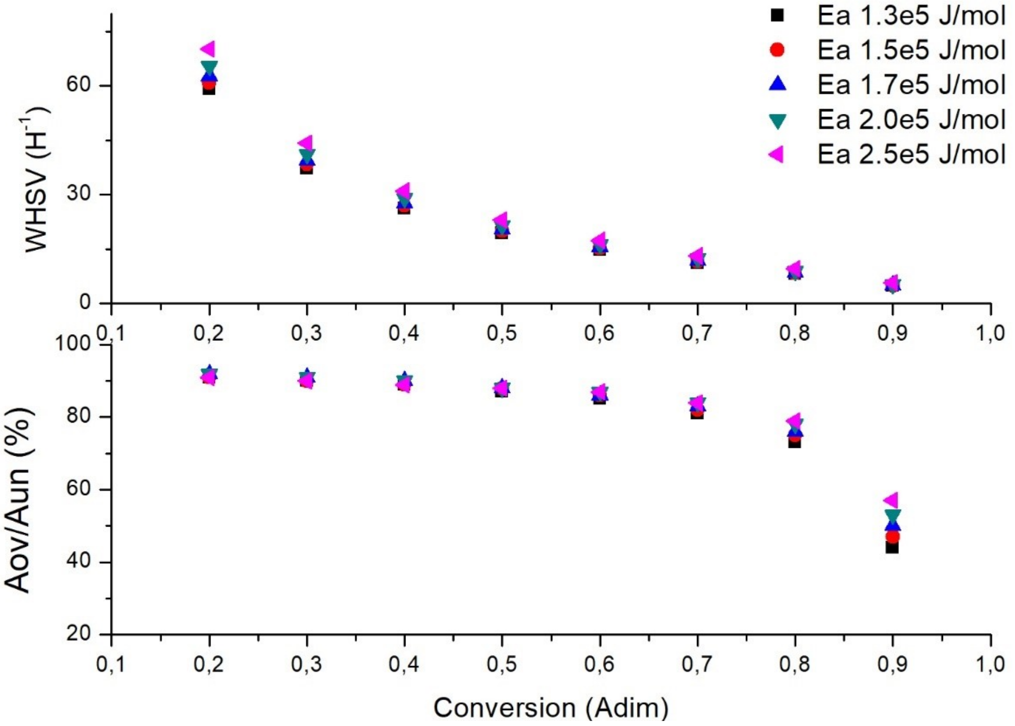

Figure A.47. (a)Conversion for different WHSV values and different activation energy levels. (b) Ratio of area values for the conditions evaluated in (a)

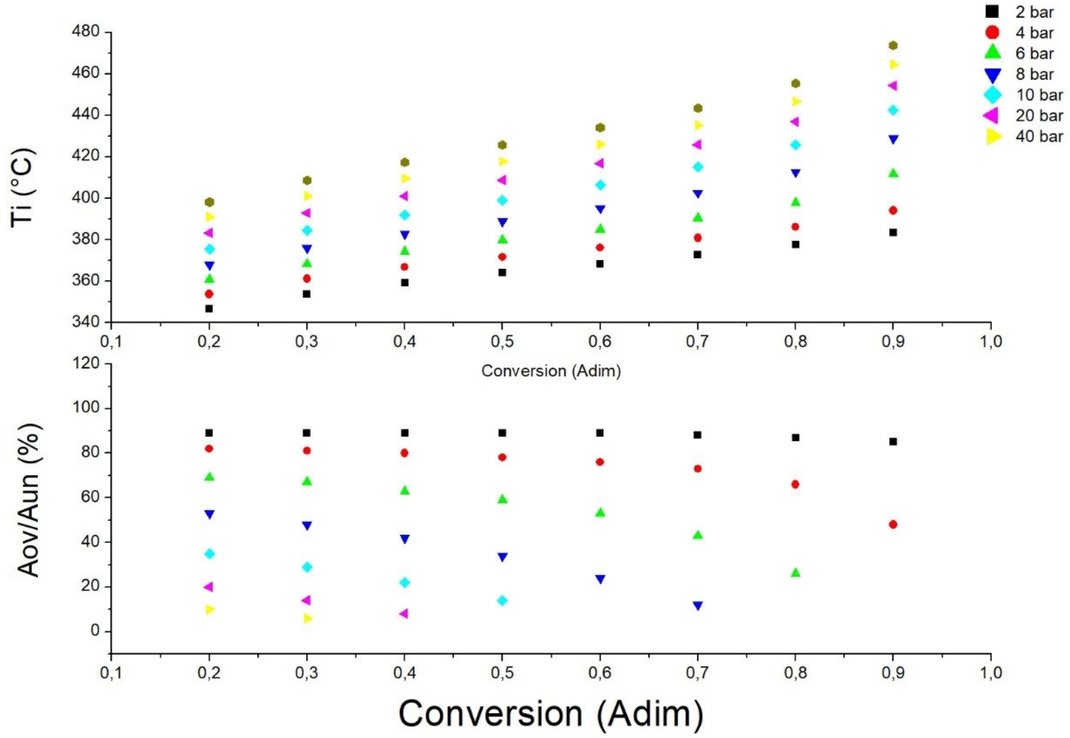

Figure A.48. (a)Conversion for different temperature values and different pressure levels (b) Ratio of area values for the conditions evaluated in (a)

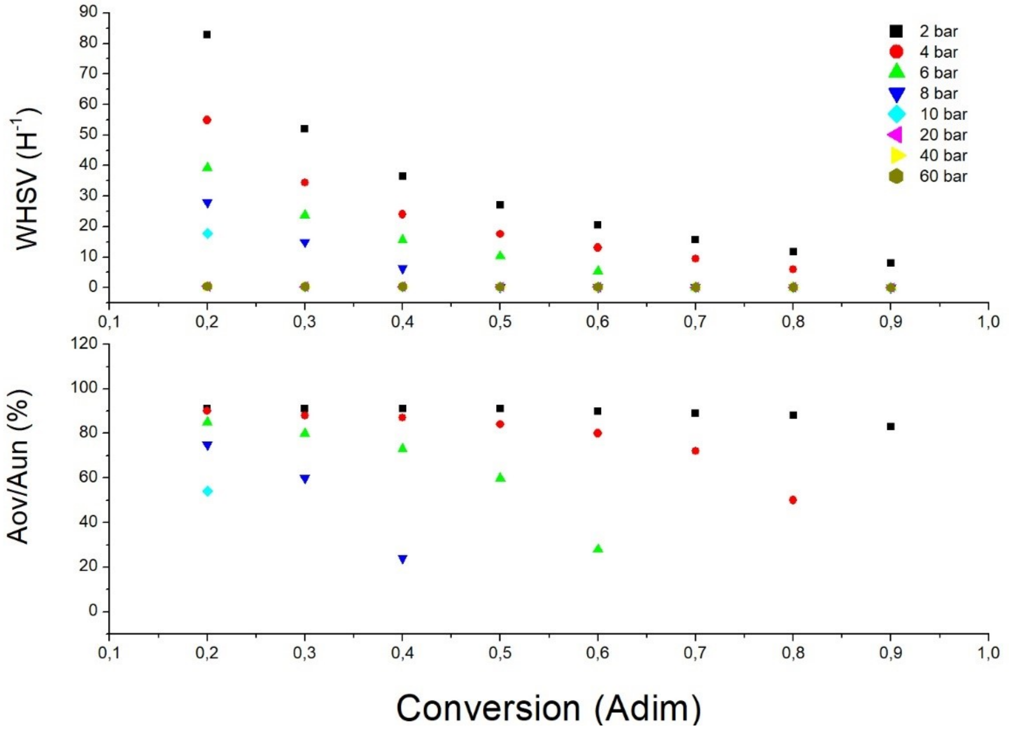

Figure A.49. (a)Conversion for different WHSV values and different pressure levels (b) Ratio of area values for the conditions evaluated in (a)

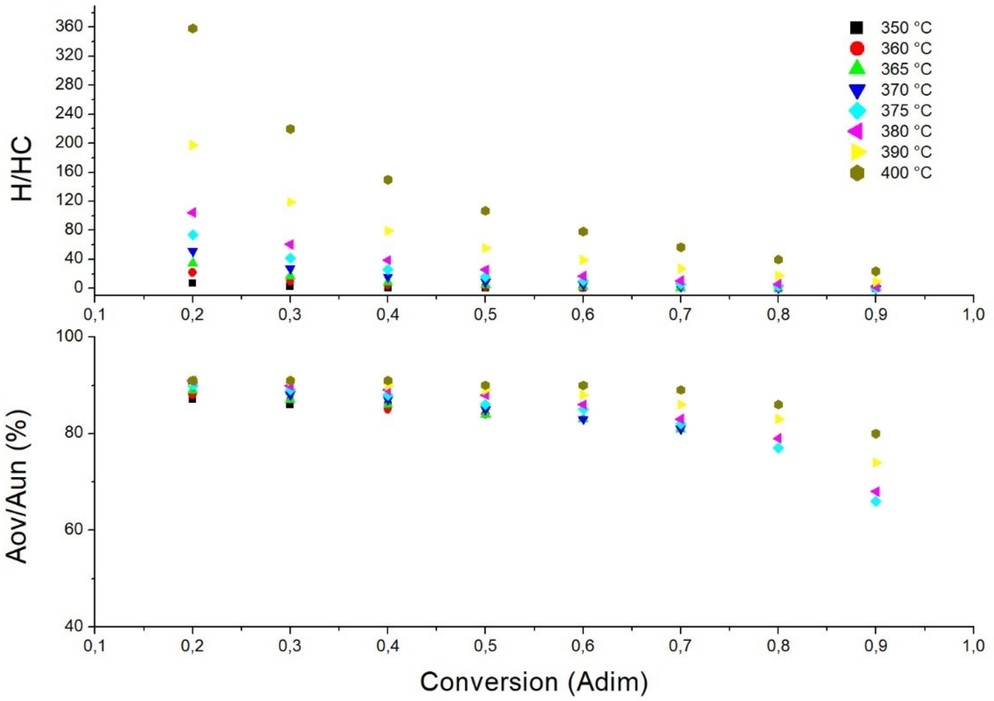

Figure A.50. (a)Conversion for different H/HC ratios and different temperature levels (b) Ratio of area values for the conditions evaluated in (a)

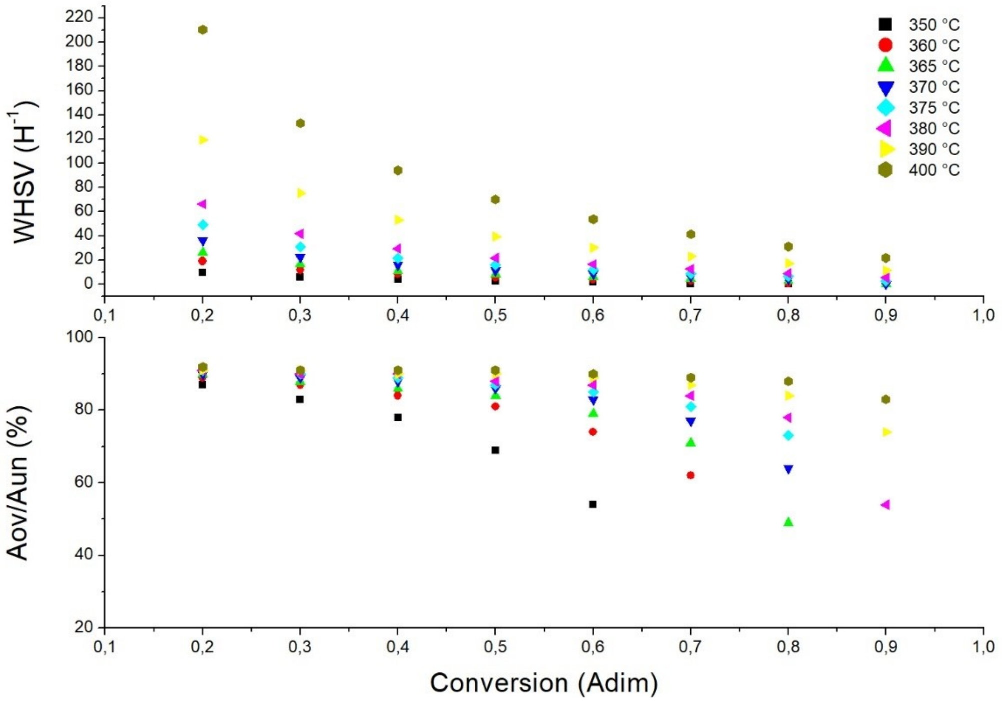

Figure A.51. (a)Conversion for different WHSV values and different temperature levels (b) Ratio of area values for the conditions evaluated in (a)

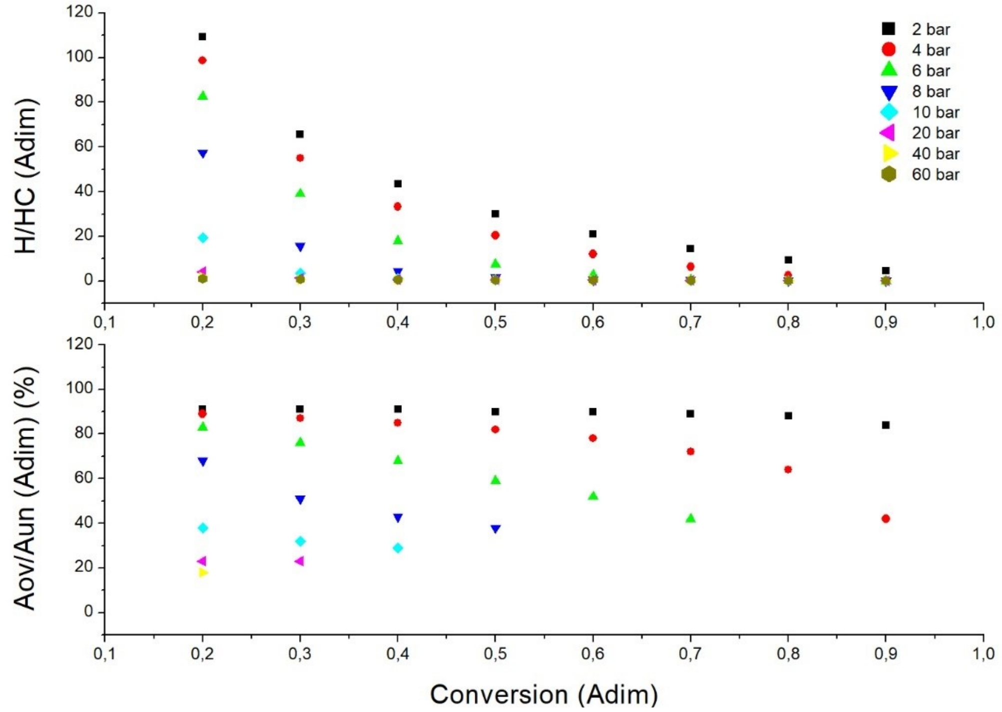

Figure A.52. . (a)Conversion for different H/HC ratios and different pressure levels (b) Ratio of area values for the conditions evaluated in (a)

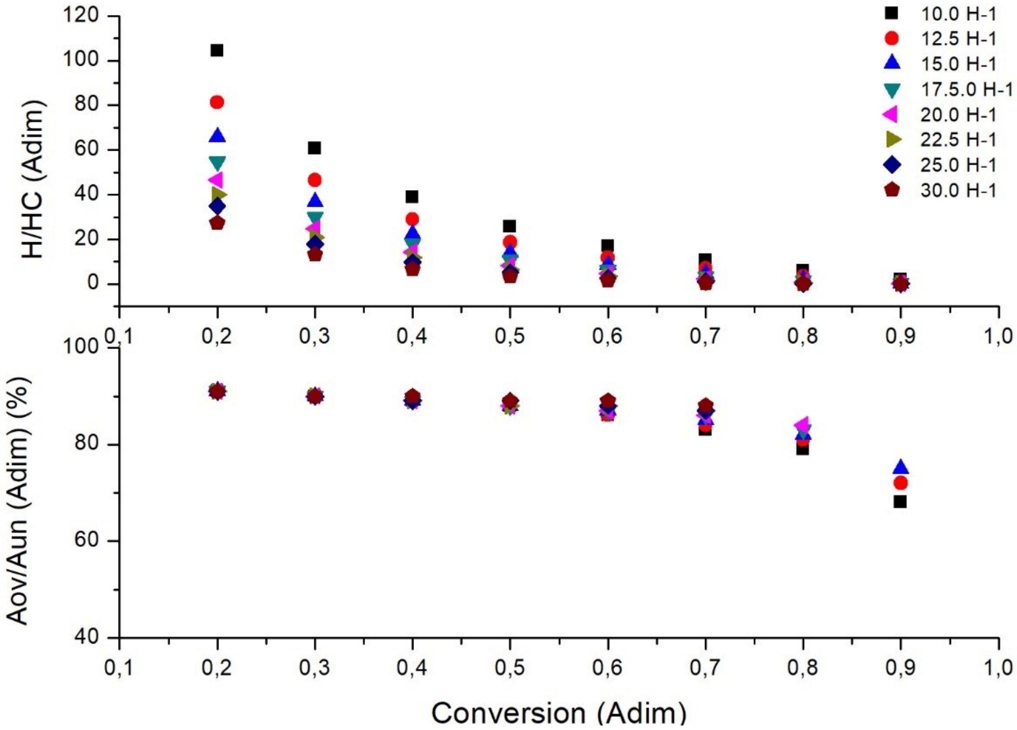

Figure A.53. (a)Conversion for different H/HC ratios and different WHSV levels (b) Ratio of area values for the conditions evaluated in (a)

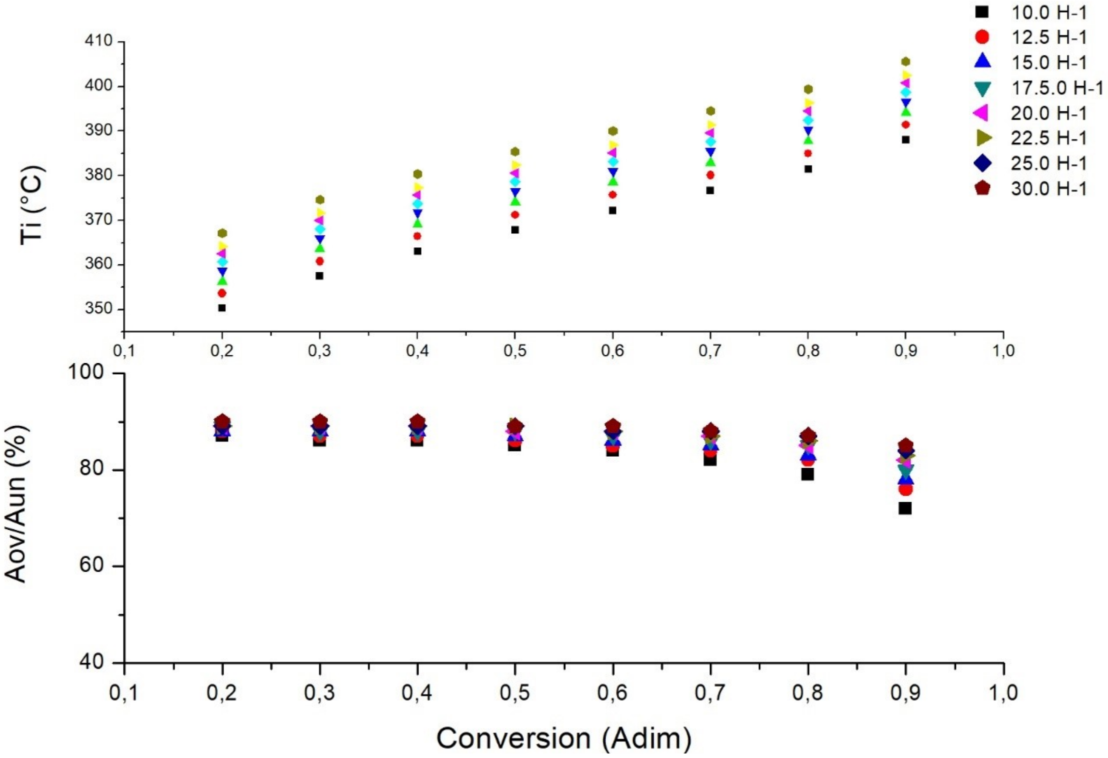

Figure A.54. (a)Conversion for different temperature values and different WHSV levels (b) Ratio of area values for the conditions evaluated in (a)

Appendix IV: Five Percent Deviation Function Results

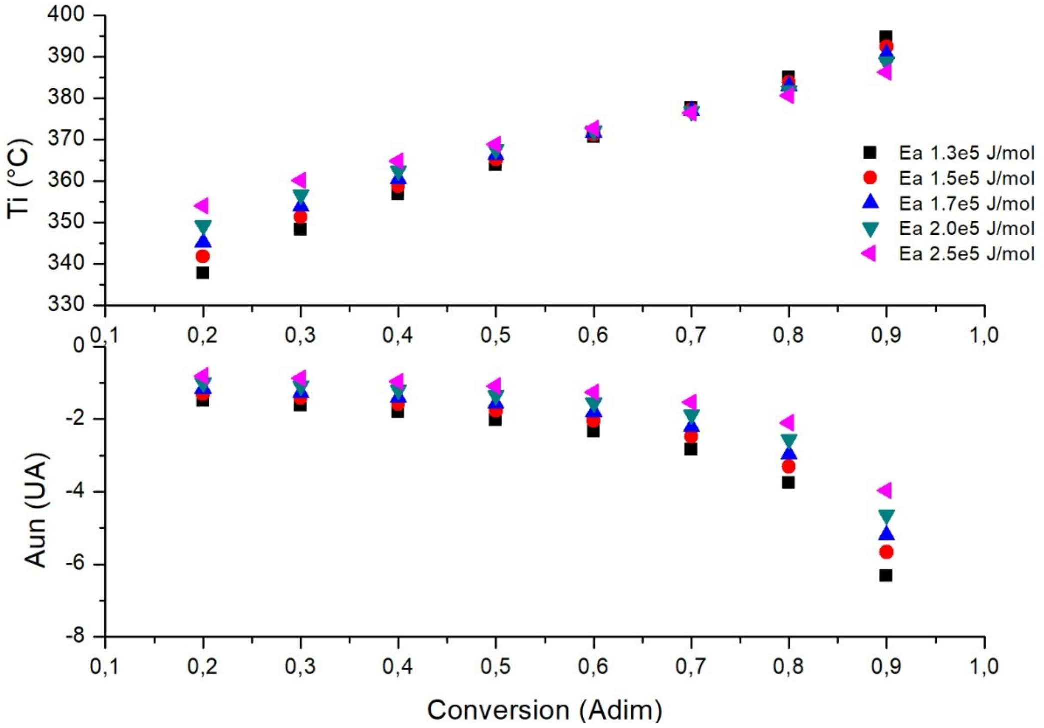

Figure A.55. a)Conversion for different temperature values and different activation energy levels (b) Undershoot area to obtain 5% of deviation with zero overshoot for the (a) conditions

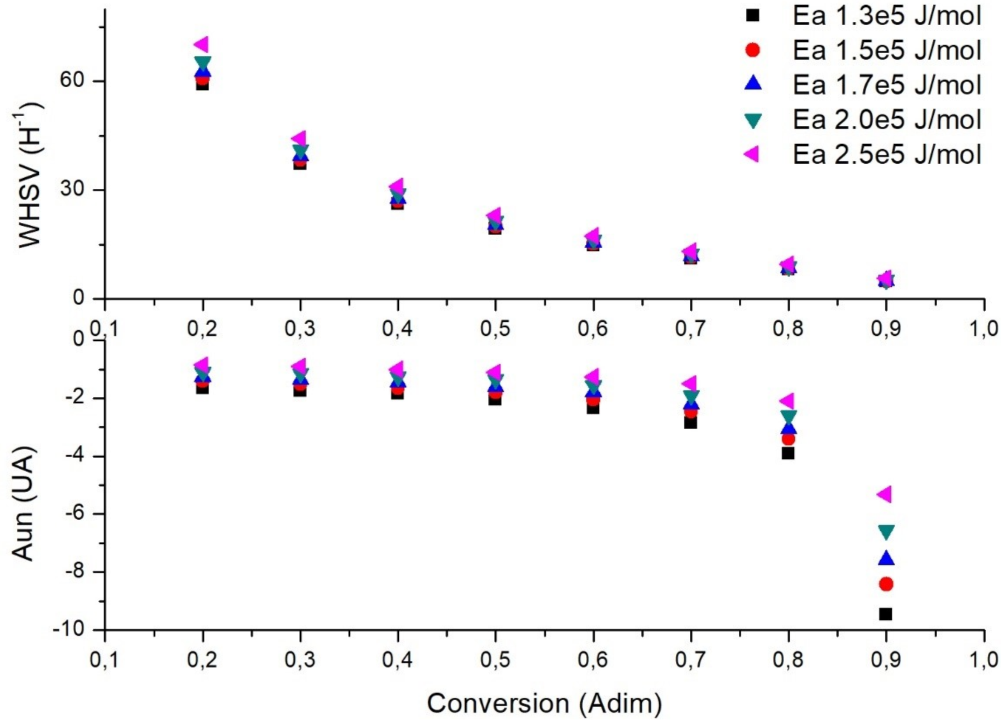

Figure A.56. (a)Conversion for different WHSV values and different activation energy levels (b) Undershoot area to obtain 5% of deviation with zero overshoot for the (a) conditions

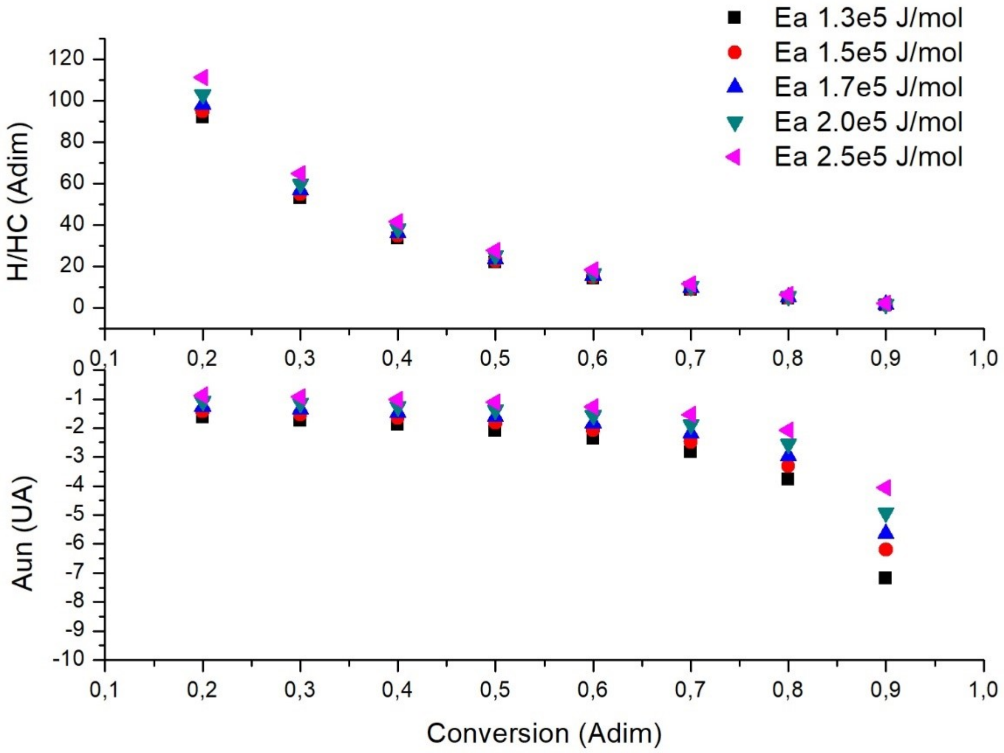

Figure A.57. (a)Conversion for different H/HC ratios and different activation energy levels (b) Undershoot area to obtain 5% of deviation with zero overshoot for the (a)

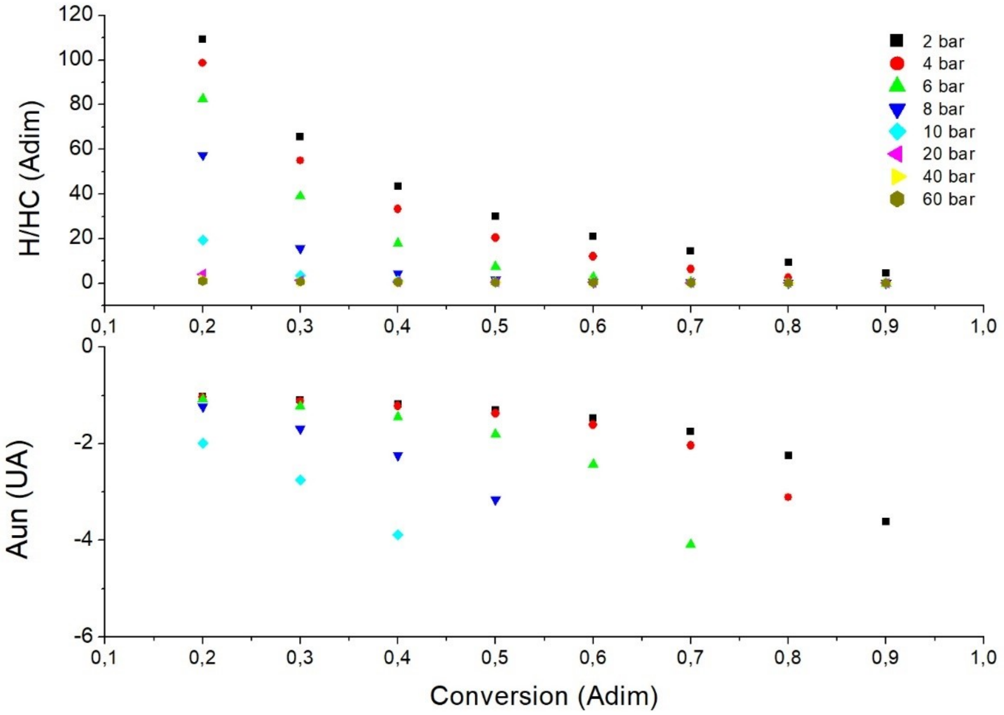

Figure A.58. (a)Conversion for different H/HC ratios and different pressure levels (b) Undershoot area to obtain 5% of deviation with zero overshoot for the (a)

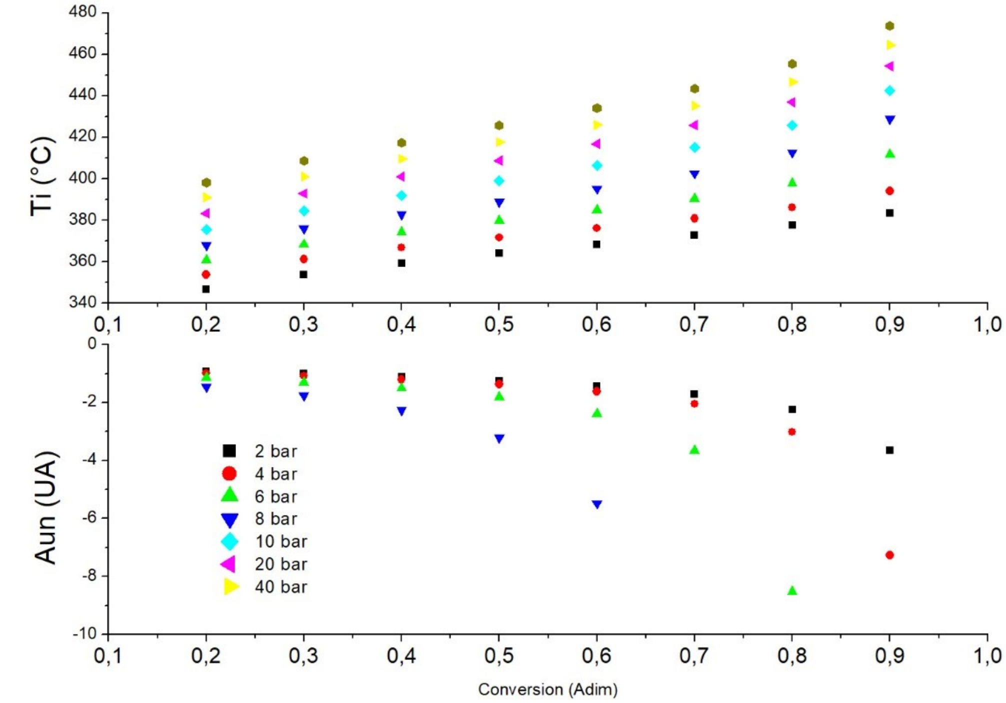

Figure A.59. (a)Conversion for different temperature and different pressure levels
(b) Undershoot area to obtain 5% of deviation with zero overshoot for the (a)

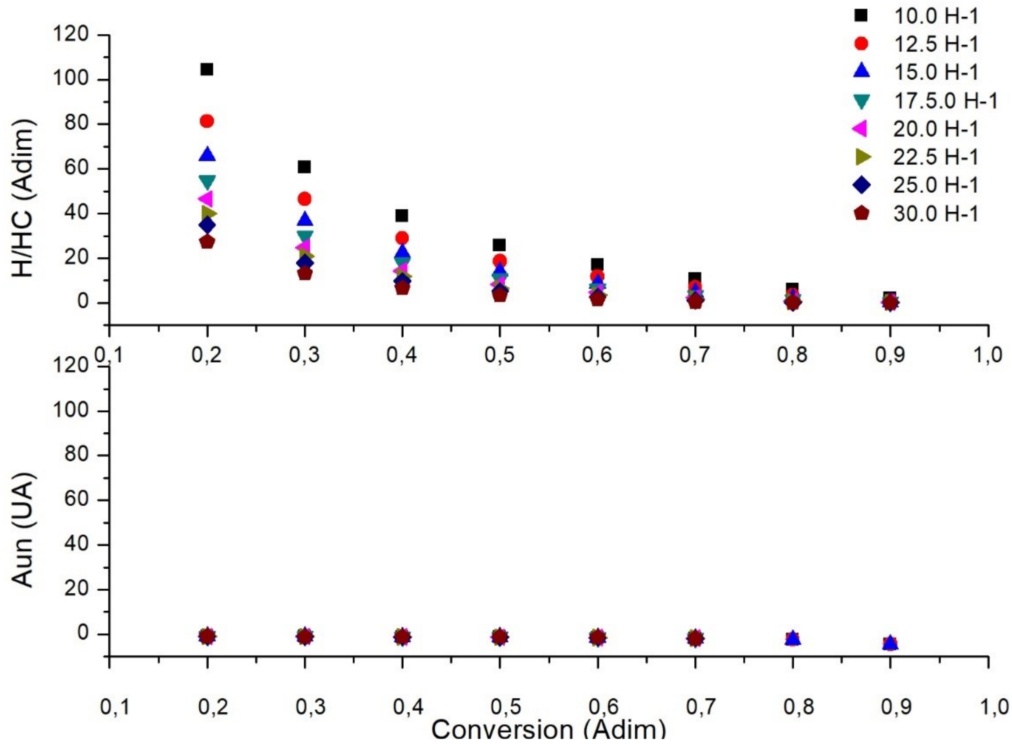

Figure A.60. (a)Conversion for different H/HC ratios and different WHSV levels
(b) Undershoot area to obtain 5% of deviation with zero overshoot for the (a)

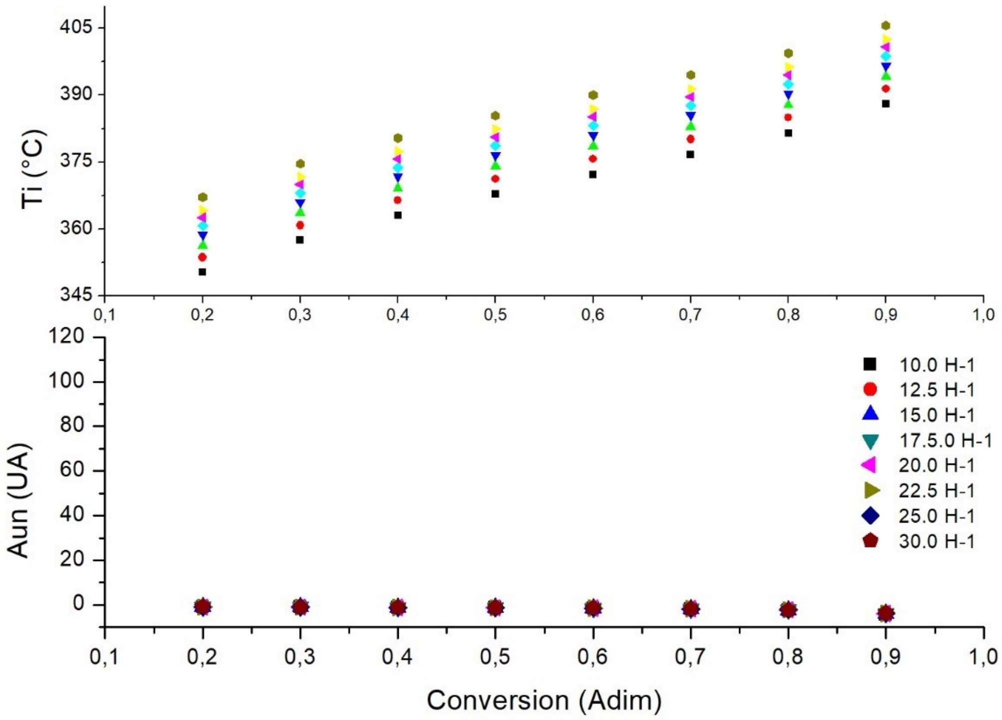

Figure A.61. (a)Conversion for different temperature values and different WHSV levels
(b) Undershoot area to obtain 5% of deviation with zero overshoot for the (a)

Appendix V: Contour Plots

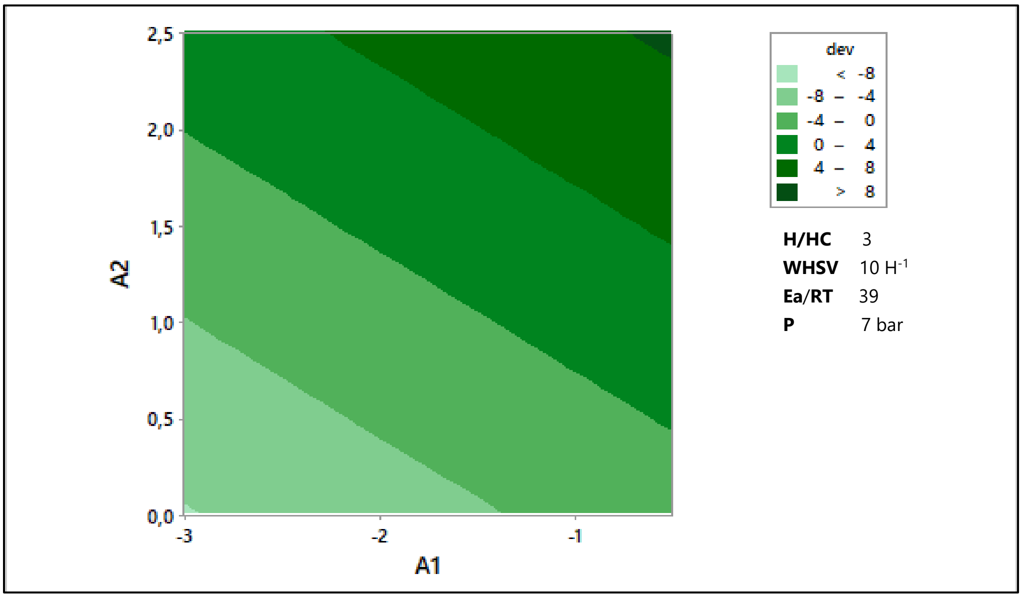

Figure A.62. Contour Plot for different areas

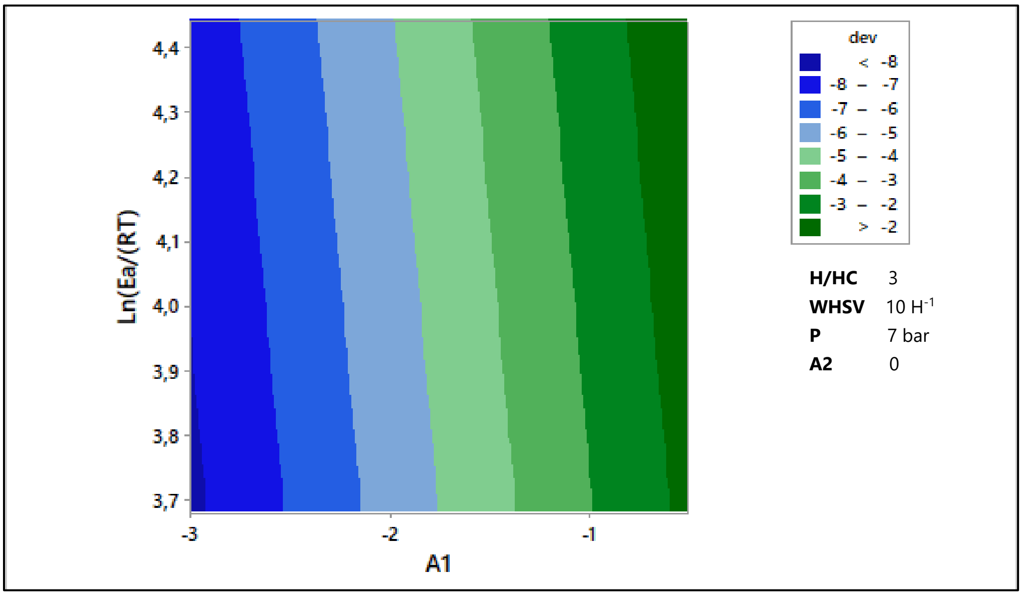

Figure A.62. Contour Plot for Temperature and the undershoot area, null overshoot

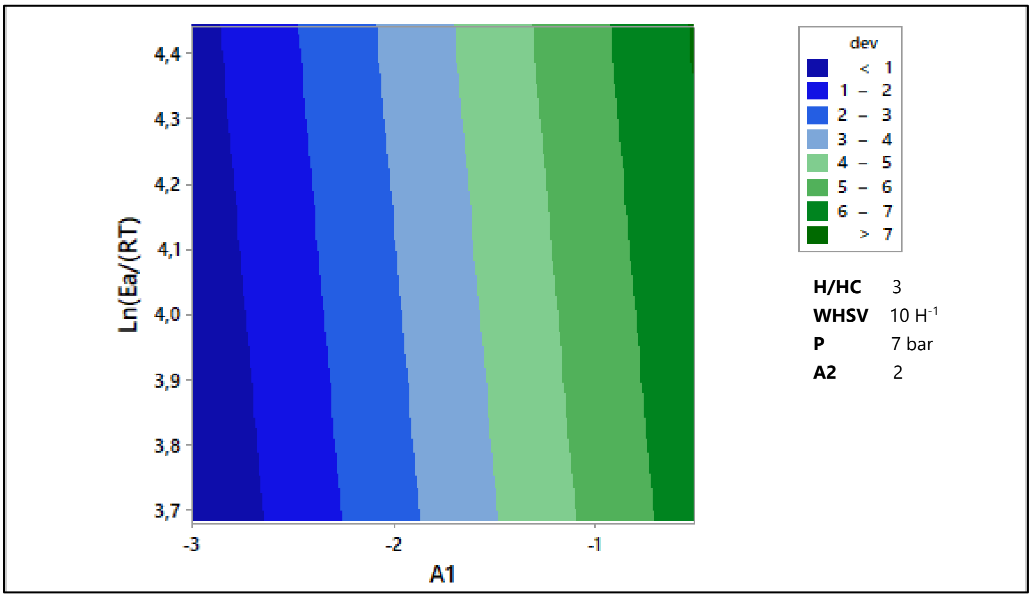

Figure A.63. Contour Plot for temperature and the undershoot area.

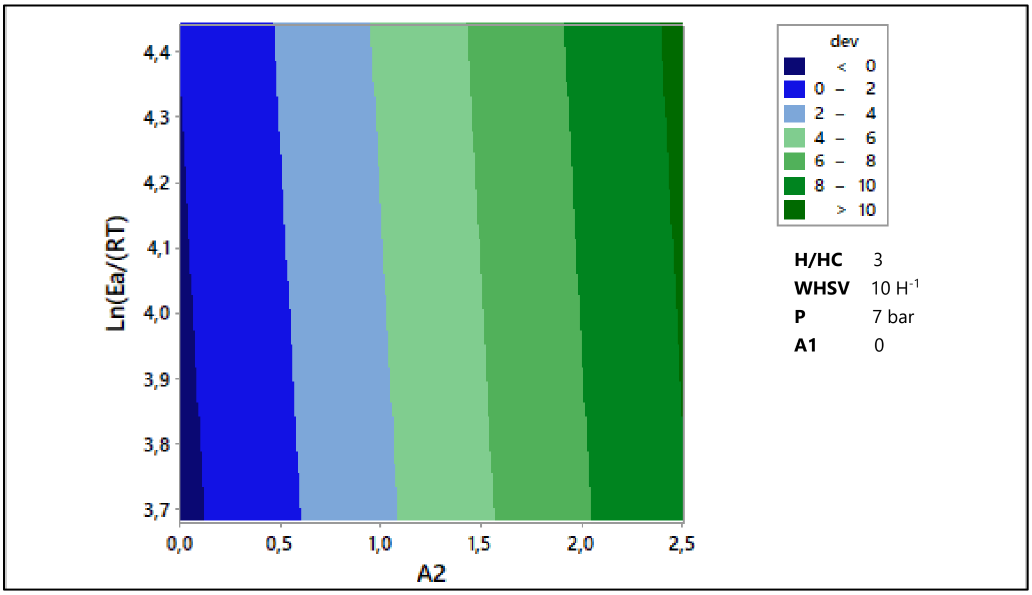

Figure A.64. Contour Plot for temperature and the overshoot area-null undershoot.

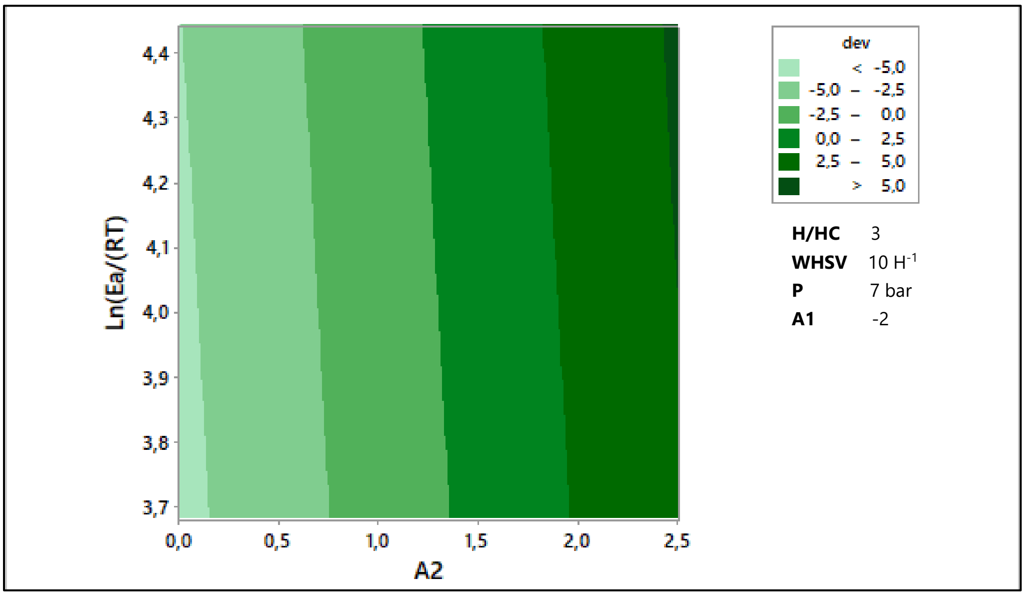

Figure A.65. Contour Plot for temperature and the undershoot area bis.

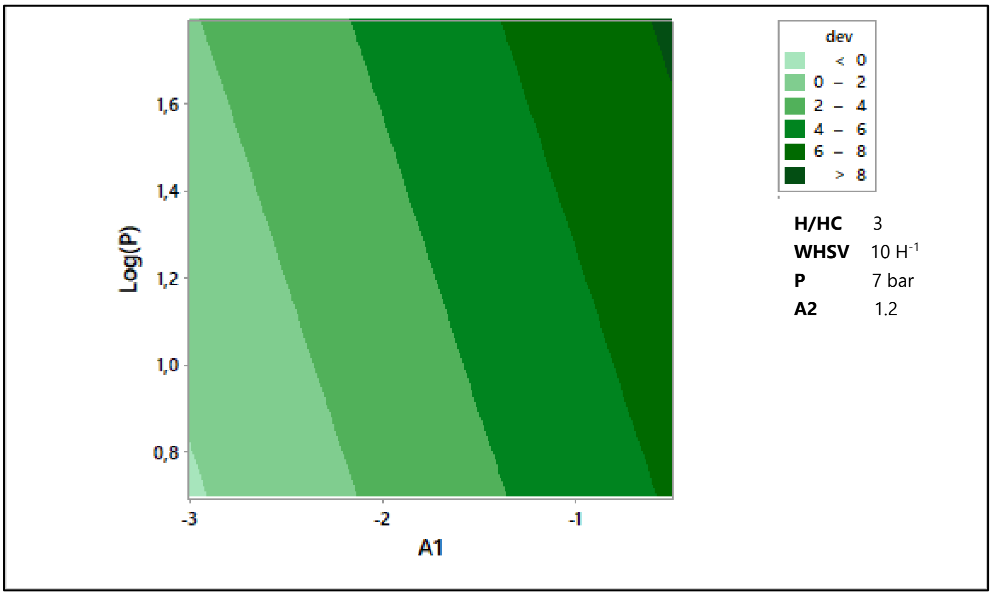

Figure A.66. Contour Plot for the pressure and the undershoot area.

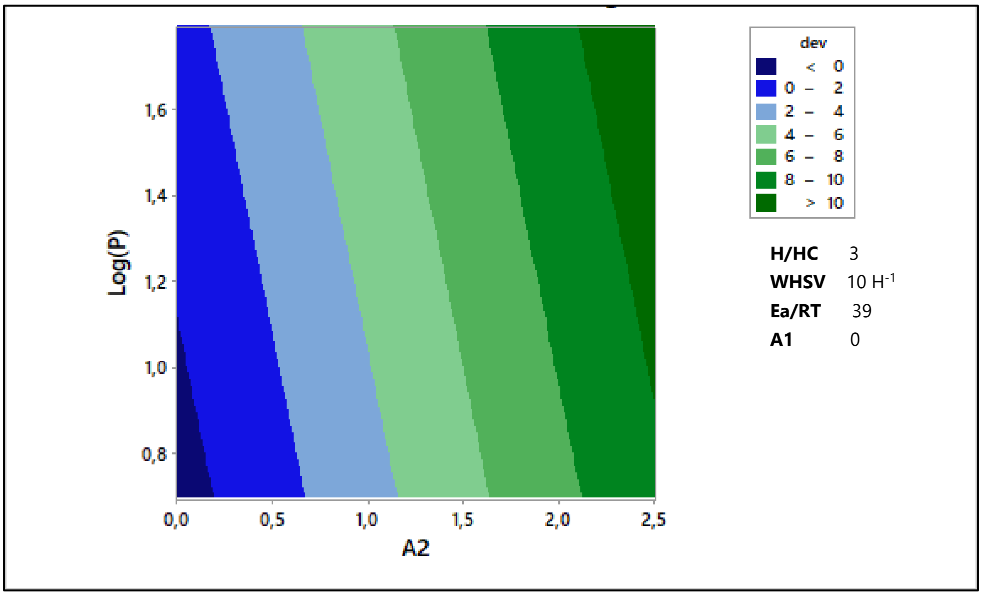

Figure A.67. Contour Plot for the pressure and the overshoot area-null undershoot.

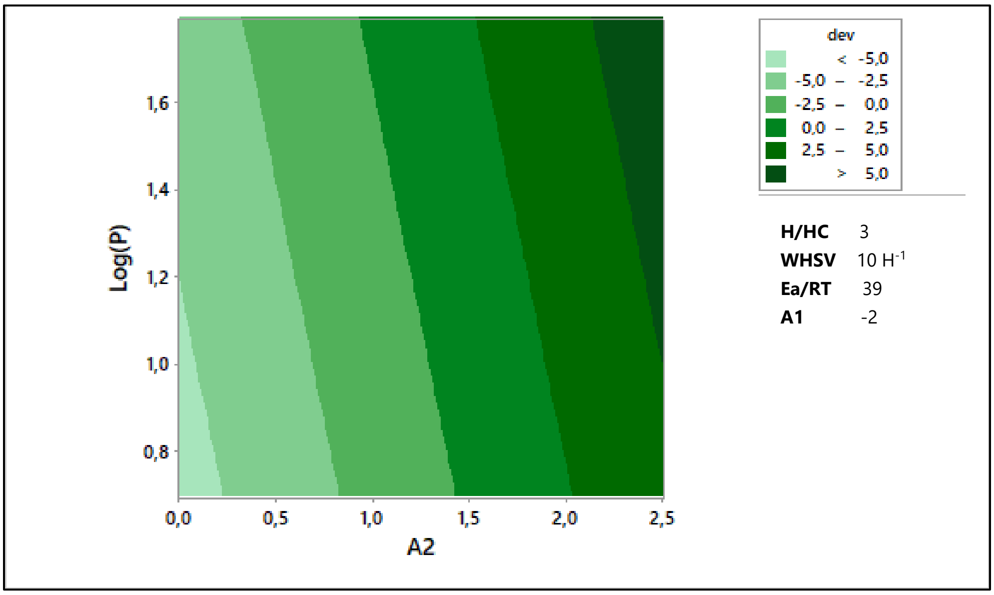

Figure A.68. Contour Plot for the pressure and the overshoot area bis.

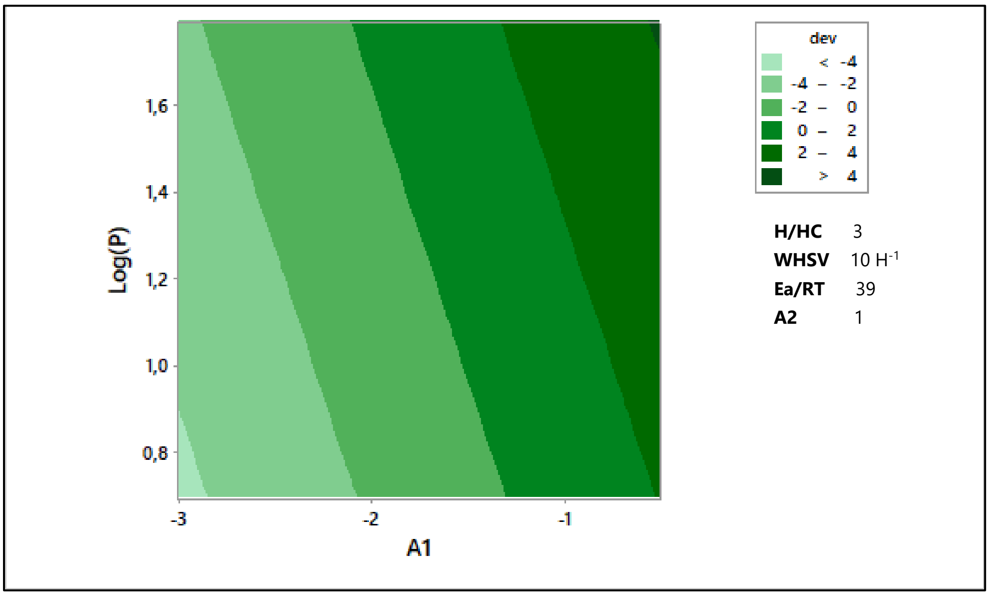

Figure A.69. Contour Plot for the pressure and the undershoot area bis .

Appendix V: Experimental Profiles Results

Table A.4: Experimental thermal profiles 1

380,00	381,51	379,69	378,93	379,21	380,56	381,08	380,48	379,46	379,14	378,94
	387,86	388,99	386,49	380,76	372,58	365,24	360,48	358,65	358,94	362,03
	390,39	394,55	395,29	392,04	386,47	376,71	368,97	363,97	362,04	362,21
	386,51	387,36	386,81	383,17	379,97	364,23	358,31	357,26	352,81	353,20
	381,44	381,89	382,44	380,79	377,22	375,09	360,72	355,46	353,47	349,44
	398,63	398,46	400,09	399,73	398,30	396,54	396,49	395,86	396,62	397,79
390,00	389,00	389,55	390,74	390,80	390,10	389,03	389,19	389,29	390,64	391,52
	388,73	389,24	390,21	389,23	388,10	383,84	381,11	380,31	380,14	381,05
	390,15	390,29	389,54	387,29	384,18	376,67	370,23	366,28	364,22	365,03
	392,91	394,31	394,80	393,58	390,02	388,54	376,00	371,31	368,26	367,13
	389,96	390,14	388,52	384,78	379,20	371,85	366,29	364,13	364,38	366,95
	389,58	389,85	388,44	385,07	379,92	372,66	367,23	364,45	363,86	366,09
	398,35	401,71	402,47	399,65	393,73	386,59	378,70	373,84	371,09	371,31
	404,85	408,80	409,59	405,28	398,54	389,70	381,57	376,63	374,47	374,37
	379,35	380,74	381,07	380,57	379,59	379,89	380,53	381,41	383,30	382,14
400,00	402,52	403,09	403,07	402,90	402,10	401,87	403,18	403,73	403,45	402,74
	400,55	401,29	400,36	399,07	399,08	399,68	399,48	401,18	400,92	401,46
	398,96	399,72	398,47	395,98	394,73	396,42	396,38	399,91	400,35	400,49
	399,26	400,22	397,80	396,02	394,87	393,59	395,19	398,98	400,35	400,47
	400,99	400,84	400,05	398,57	396,08	394,55	394,38	399,20	400,16	400,16
	402,60	402,88	401,02	398,95	396,47	395,37	397,05	399,71	400,28	400,25
	400,05	400,16	399,90	398,43	398,63	399,85	400,86	404,74	403,45	401,83
	400,11	395,94	390,38	386,73	383,54	382,87	383,89	386,03	391,10	395,87
	399,67	398,12	394,74	389,41	384,90	382,61	382,33	383,89	386,41	391,27
	399,96	398,20	394,20	388,26	381,13	374,93	374,83	379,42	386,98	393,90
	403,36	404,60	402,52	396,09	385,99	377,09	375,10	376,11	379,76	387,29
	405,28	405,05	400,95	394,42	387,78	380,50	376,30	375,56	376,64	380,51
	409,85	408,28	404,43	397,49	389,29	382,70	378,30	377,72	378,65	382,93
	407,44	406,44	402,18	395,67	388,13	381,64	377,83	376,68	378,16	382,67
	413,03	412,62	410,11	402,80	395,11	386,18	381,21	379,18	379,36	382,52

Table A.5: Experimental thermal profiles 2

380,00	1,51	-0,31	-1,07	-0,79	0,56	1,08	0,48	-0,54	-0,86	-1,06
	7,86	8,99	6,49	0,76	-7,42	-14,76	-19,52	-21,35	-21,06	-17,97
	10,39	14,55	15,29	12,04	6,47	-3,29	-11,03	-16,03	-17,96	-17,79
	6,51	7,36	6,81	3,17	-0,03	-15,77	-21,69	-22,74	-27,19	-26,80
	1,44	1,89	2,44	0,79	-2,78	-4,91	-19,28	-24,54	-26,53	-30,56
	18,63	18,46	20,09	19,73	18,30	16,54	16,49	15,86	16,62	17,79
390,00	-1,00	-0,45	0,74	0,80	0,10	-0,97	-0,81	-0,71	0,64	1,52
	-1,27	-0,76	0,21	-0,77	-1,90	-6,16	-8,89	-9,69	-9,86	-8,95
	0,15	0,29	-0,46	-2,71	-5,82	-13,33	-19,77	-23,72	-25,78	-24,97
	2,91	4,31	4,80	3,58	0,02	-1,46	-14,00	-18,69	-21,74	-22,87
	-0,04	0,14	-1,48	-5,22	-10,80	-18,15	-23,71	-25,87	-25,62	-23,05
	-0,42	-0,15	-1,56	-4,93	-10,08	-17,34	-22,77	-25,55	-26,14	-23,91
	8,35	11,71	12,47	9,65	3,73	-3,41	-11,30	-16,16	-18,91	-18,69
	14,85	18,80	19,59	15,28	8,54	-0,30	-8,43	-13,37	-15,53	-15,63
	-10,65	-9,26	-8,93	-9,43	-10,41	-10,11	-9,47	-8,59	-6,70	-7,86
400,00	2,52	3,09	3,07	2,90	2,10	1,87	3,18	3,73	3,45	2,74
	0,55	1,29	0,36	-0,93	-0,92	-0,32	-0,52	1,18	0,92	1,46
	-1,04	-0,28	-1,53	-4,02	-5,27	-3,58	-3,62	-0,09	0,35	0,49
	-0,74	0,22	-2,20	-3,98	-5,13	-6,41	-4,81	-1,02	0,35	0,47
	0,99	0,84	0,05	-1,43	-3,92	-5,45	-5,62	-0,80	0,16	0,16
	2,60	2,88	1,02	-1,05	-3,53	-4,63	-2,95	-0,29	0,28	0,25
	0,05	0,16	-0,10	-1,57	-1,37	-0,15	0,86	4,74	3,45	1,83
	0,11	-4,06	-9,62	-13,27	-16,46	-17,13	-16,11	-13,97	-8,90	-4,13
	-0,33	-1,88	-5,26	-10,59	-15,10	-17,39	-17,67	-16,11	-13,59	-8,73
	-0,04	-1,80	-5,80	-11,74	-18,87	-25,07	-25,17	-20,58	-13,02	-6,10
	3,36	4,60	2,52	-3,91	-14,01	-22,91	-24,90	-23,89	-20,24	-12,71
	5,28	5,05	0,95	-5,58	-12,22	-19,50	-23,70	-24,44	-23,36	-19,49
	9,85	8,28	4,43	-2,51	-10,71	-17,30	-21,70	-22,28	-21,35	-17,07
	7,44	6,44	2,18	-4,33	-11,87	-18,36	-22,17	-23,32	-21,84	-17,33
	13,03	12,62	10,11	2,80	-4,89	-13,82	-18,79	-20,82	-20,64	-17,48